

H24/3832

No Restrictions.

MONASH UNIVERSITY
THESIS ACCEPTED IN SATISFACTION OF THE
REQUIREMENTS FOR THE DEGREE OF
DOCTOR OF PHILOSOPHY

ON..... 26 April 2005.....
.....

Sec. Research Graduate School Committee

Under the Copyright Act 1968, this thesis must be used only under the normal conditions of scholarly fair dealing for the purposes of research, criticism or review. In particular no results or conclusions should be extracted from it, nor should it be copied or closely paraphrased in whole or in part without the written consent of the author. Proper written acknowledgement should be made for any assistance obtained from this thesis.

AN INVESTIGATION OF THE EFFECTS OF 2-BODY
INTERACTIONS IN AN EFFECTIVE MEDIUM THEORY

A THESIS SUBMITTED FOR THE DEGREE OF
DOCTOR OF PHILOSOPHY

By
Aris Alexopoulos
BSc (Hons)

Department of Physics,
Monash University,
Australia.

November 2004

© Copyright 2004

by

Aris Alexopoulos
BSc (Hons)

Contents

Abstract	v
Declaration	vi
Acknowledgements	vii
1 Introduction	1
2 Effective Medium Theory	4
2.1 Introduction	4
2.2 The development of EMT	4
2.3 Alternative formulations of EMT	11
2.3.1 Green's functions	11
2.3.2 Variational bounds	12
2.3.3 Density functional theory	13
3 Extensions to Effective Medium Theory	17
3.1 Introduction	17
3.2 n -body scattering	18
3.2.1 The T-matrix for a single sphere	20
3.2.2 The T matrix for two spheres	24
3.2.3 The T matrix for n spheres	26
3.3 Beyond the 1-body EMT: Other methods	29
4 Multipole Expansion Method	35
4.1 Introduction	35
4.2 Extending Jeffrey's solution to d -dimensions	37
4.2.1 Parallel field case	38

4.2.2	Perpendicular field case	40
4.2.3	Parallel flux integral	42
4.2.4	Perpendicular flux integral	43
4.3	Symmetrical bihyperspheres	45
4.4	Higher dimensions	48
5	Method of Images	50
5.1	Introduction	50
5.2	Image theory in d -dimensions	52
5.2.1	Neumann images of a point charge	52
5.2.2	First perpendicular dipole image	54
5.2.3	First parallel dipole image	56
5.3	Higher-order images	57
5.3.1	Perpendicular higher-order images	57
5.3.2	Parallel higher-order images	59
5.4	Perfect conductor limit	62
5.4.1	Point dipoles only approximation	62
5.4.2	Total dipole moments p_4 and p_5	63
5.5	Higher-order dipole moments for the perfect-conductor	64
5.5.1	Mapping of dipoles and charges	65
5.6	Potential difference between two hyperspheres	68
5.6.1	Dipole contributions	69
5.6.2	Dipole and charge contributions	71
5.7	Weak-scattering approximation	75
5.8	A useful algebraic approximation	76
6	Results and Beyond	79
6.1	Introduction	79
6.2	Results	80
6.3	Beyond	92

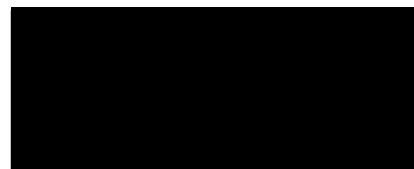
7	Appendices	95
7.1	Appendix A: Spherical harmonics shift formula 1	95
7.2	Appendix B: Spherical harmonics shift formula 2	96
7.3	Appendix C: Perpendicular flux formula	98
7.4	Appendix D: Neumann image theory in d dimensions	100
7.5	Appendix E: Point perpendicular dipole images	102
7.6	Appendix F: Point parallel dipole images	103
8	Publications and References	105

Abstract

Effective Medium Theory (EMT) deals with the interaction between a particle and its host medium, thus forming a composite structure that allows the determination of physical properties to be calculated such as the dielectric constant. While EMT has proven to be somewhat successful in determining first order effects, it fails to produce accurate results when we are interested in higher orders. If any improvement to the existing theory is to be made, it is important to consider the two-body terms that arise from such a binary system. With this in mind two methods are used to investigate the pair terms and to calculate the dielectric function: the multipole expansion method and the method of images.

In the case of the former we consider d -dimensional inclusions and use the multipole expansion method to calculate the coefficient κ of the second order term in the virial expansion for the dielectric function of a composite system. In the case of the latter we employ the method of images in a d -dimensional framework, to calculate κ for two hyperspheres in the presence of a uniform field. We employ extensions to image theory for classical charges and dipoles for dielectric spheres, which produce novel line charge and line dipole densities. The voltage between two hyperspheres is also investigated and comparison is made of the results for κ between the method of images and the multipole expansion method for arbitrary dimension. We also present numerical results that also allow us to compare convergence properties between the two methods.

This thesis contains no material accepted for the award of any other degree or diploma in any university. To the best of my knowledge, it contains no material published or written by another person, except where due reference is made in the text.



Aris Alexopoulos

Acknowledgements

I would like to thank my parents for their love and support and in particular my father who has been an inspiration to me as well as a friend. I also give thanks to my wonderful wife Stratoula for her kind support and understanding and love. I express my thank you to Tuck Choy and Andrew Smith for their help and support as well as the Australian government for its financial assistance in the form of an Australian Postgraduate Research Award (APRA).

List of Tables

- 6.1 The coefficient κ to seven significant figures is tabulated for $d = 1, 2, 3, 4$ for the perfect-conductor, $\alpha \rightarrow \infty$ 83
- 6.2 The coefficient κ to seven significant figures is tabulated for $d = 1, 2, 3, 4$ for the holes-limit, ie, when $\alpha \rightarrow 0$ 84
- 6.3 The table below shows values for $F_d(1)$ for the perfect conductor limit $\alpha \rightarrow \infty$ for $d = 2, 3, 4$. Note that for the case $d=1$, the result is 0. Also note that $F_d(1)$ is related to κ by $\kappa = d + F_d(1)$ 86
- 6.4 The table below shows values for \bar{p}_n for the perfect conductor limit using higher order dipole images in d -dimensions. Values up to $n = 23$ are shown for $d = 2, 3, 4$. Note that for the case $d=1$, the result is 0. One can see from the results below that the convergence towards the known values is much faster when compared to the multipole expansion method. Also note that $F_d(1)$ is related to κ by $\kappa = d + F_d(1)$. 87
- 6.5 $F_d(\beta)$ in the weak-scattering limit to the leading order β 88
- 6.6 Values obtained for ΔV showing very slow convergence for $d = 3$. The first four rows show convergence due to dipole-only interactions in eqn (5.62), while the last two rows include the image contributions also. 92

List of Figures

- 4.1 Twin spherical coordinates. We note that in d -dimensions there is a common azimuthal angle ϕ , around the line joining the two centres, and $p = d - 2$ polar angles. The two polar angles shown, θ_1 and θ_2 , have a special significance by virtue of the axial symmetry. 39
- 5.1 The Neumann image for a point charge Q outside a d -dimensional sphere. The origin is at the centre of the hypersphere, and the point image Q_K and the line image $\rho(z)$ are shown. 53
- 5.2 First image dipole $\mathbf{p}_2^{\perp 0}$ and line dipole $\bar{\rho}_2^{\perp}(z)$ as derived from the Neumann theory for the perpendicular configuration. The origin is at the centre of the hypersphere. 54
- 5.3 First image dipole $\mathbf{p}_2^{\parallel 0}$ and line charge $\rho_2^{\parallel 0}(z)$ and point charge Q_2 as derived from the Neumann theory for the parallel configuration. The origin is at the centre of the hypersphere. 55
- 5.4 Sequence of point-charge images for each generation up to \mathbf{p}_5^{\parallel} . The superscript j in Q_n^j refers to the image point b_{j-1} while n refers to the generation \mathbf{p}_n 64
- 5.5 Hyperspheres in the presence of an electric field \mathbf{E}_0 separated by the distance R . The radius of each hypersphere is a such that $\omega = a/R$ or $\bar{\omega} = R/a$ 69
- 6.1 Plot of κ vs $\log_{10}(\alpha)$ for $d = 2$. The result of Djordjević *et al.* (1996) is shown as the dashed curve and has a slightly different convergence to that of the multipole expansion method due to the different number of terms calculated. Here $\alpha = \epsilon_i/\epsilon_0$ is the ratio of the dielectric constant of the inclusions ($i = 1, 2$) to that of the host medium. 81

- 6.2 Plot of κ vs $\log_{10}(\alpha)$ for $d = 3$. The result using the multipole expansion method is compared to Jeffrey (1973), represented by the dots. Again $\alpha = \epsilon_i/\epsilon_0$ is the ratio of the dielectric constant of the inclusion to that of the host medium. 82
- 6.3 Plot of κ vs $\log_{10}(\alpha)$ for $d = 1, 2, 3, 4$. Again $\alpha = \epsilon_i/\epsilon_0$ has the same definition as in other figures. 82
- 6.4 Plot of κ vs $\log_{10}(\alpha)$ for $d = 1, 2, 3, 4$, comparing the third order result (dashed lines), eqn (6.7), and the multipole expansion method results eqn (6.4). Note that the discrepancy in the convergence is due to the number of terms calculated in each case, which does not coincide in this graph. 85
- 6.5 The graph of κ vs $\log_{10}(\alpha)$ for $d = 1, 2, 3, 4$. The weak-scattering limit eqn (6.10) is represented by the dashed curves and the solid curves represent the multipole expansion method eqn (6.4) 88
- 6.6 F_d vs d . The dashed line is eqn (6.11) and the solid line represents the weak-scattering limit eqn (6.9) 89
- 6.7 κ vs $\log_{10}(\alpha)$. The dashed lines come from eqn (6.11) and the solid lines are the result of the multipole expansion method. 90
- 6.8 The conductance $\sigma = \epsilon/\epsilon_0$ has been plotted for $d = 1, 2, 3, 4$ in the low volume fraction of inclusions c , for perfect-conducting inclusions. 90
- 6.9 The voltage between two inclusions is shown for $d = 2$. Three results are actually shown (i) the case of the image method derived here eqn (5.62), (ii) the case of Djordjević *et al.* (1996) and (iii) the approximation eqn (6.12). All curves are exact and so lie on top of each other. 91

6.10	The voltage between two inclusions is shown for $d = 3$. Three results are actually shown (i) the case of the image method derived here eqn (5.62) <i>without</i> the charge contributions (curve 1), (ii) the case of eqn (5.62) <i>with</i> the charge contributions (curve 2) and (iii) the approximation eqn (6.12) (curve 3). The inset shows the interval $\bar{\omega} \in [2, 2.5]$ so that the convergence can be better differentiated between each case.	93
7.1	Reoriented twin spherical coordinates. The two polar angles θ and θ' are equivalent to θ_1 and θ_2 of Fig 4.1	96
7.2	The electrostatic potential in d -dimensions.	101
7.3	Derivation of the image set $(\mathbf{p}_2^{0\perp}, \rho_2^\perp)$	102

CHAPTER 1

Introduction

For many years, various areas of scientific interest such as the dielectric properties of composites, hydrodynamics of suspensions, granular superconductors, optical properties, magnetoresistance, elasticity, sound propagation through porous media and so on, have been dealt by the principles of Effective Medium Theory (EMT). In some cases EMT turns out to be rather accurate and in other situations there is need for improvement of the theory. Essentially EMT is concerned with how a particle interacts with its surrounding medium. More specifically in the case of a composite material we may be interested to find out what the dielectric constant of the composite is, and one way to obtain it is via the study of how an inclusion or particle of dielectric constant ϵ_1 , interacts with its host material of dielectric constant ϵ_0 .¹ By averaging these one-body interactions over the medium, we can obtain the dielectric constant of the system to first order. In fact, in this thesis, we will be calculating the dielectric properties of a composite system (dielectric function), but we will consider going about it in ways that differ from the results of traditional EMT.

In Chapter 2 we will discuss some of the important aspects of the theory and some of the key ideas and concepts. Because EMT encompasses many areas of research, it is impossible to cover every aspect here. Nevertheless we will look at important theoretical developments that form the backbone of EMT such as those from Clausius-Mossotti, Maxwell-Garnett and Bruggeman. We will see that while these results are quite good to first order, when used to calculate second order effects they inevitably fail. We will briefly discuss the variational bounds method as a possible step forward to improving these results. Furthermore, these results

¹We will only be concerned with the static case and constant uniform fields and we will not study dynamical effects etc.

consider inclusions in two or three dimensions separately (discs, spheres). One of our goals is to consider inclusions of arbitrary shape, as well as a way to generalize the above approximations. Towards this end we will look at the powerful Green's function formulation and point out that we can derive the results due to Bruggeman and Maxwell-Garnett respectively. At this point we need to correct the results of the latter to second-order by studying two-body interactions.

In Chapter 3 we will investigate higher order terms that need to be included if we are to make extensions to EMT and include two-body effects. One way to do this is to look at multiple scattering and in particular we begin by formulating the one-body T matrix of a sphere ($d=3$). We then extend the results to two-bodies and then generalize to n bodies. It is worth noting that by the use of these scattering equations one can derive the Bruggeman and Maxwell-Garnett approximations even though we will not do so here. We will also look at an alternative approach to multiple scattering in the form of competing interactions, an approach that is not utilized to its fullest by researchers and we shall investigate two-body extensions to Maxwell-Garnett and Bruggeman and obtain a slowly convergent approximation in the low density limit, up to $O(\eta_1)$, (refer to section). At this stage, we investigate methods that will allow us to calculate second-order effects and generalize our results by writing them in a d -dimensional form. The two different approaches that we use are in agreement with each other and in the appropriate limits we obtain the results of others for the dielectric function ϵ .

Specifically in Chapter 4, by averaging over pairs of *hyperspheres*, we obtain the dielectric function for a binary mixture containing such inclusions up to order c^2 , where c is the volume fraction of inclusions. The procedure is based on multipole expansions for the potential of two spheres in a uniform field and is a generalization of the method of Jeffrey (1973) to d -dimensional space. Numerical results are also obtained for the second-order coefficient κ in the low c expansion of the dielectric constant for arbitrary d . These results verify earlier known results, as well as showing the dependence of κ on dimensionality, which is particularly simple as $d \rightarrow 1$ and as $d \rightarrow \infty$.

In Chapter 5, we use the method of images to once again obtain the solution of two *hyperspheres* in d dimensions in a uniform field, so that we can study the $O(c^2)$ coefficient κ using this alternative approach. We employ extensions to image theory for classical charges and dipoles for dielectric spheres, which produce novel line charge and line dipole densities. The voltage between two hyperspheres is also investigated and comparison is made of the results for κ between the method of images and the multipole expansion method for arbitrary dimension. We demonstrate by numerical results that the former has superior convergence properties than the latter, even though it is computationally less convenient, but even so it leads to useful analytic results in the weak scattering limit. Some simple approximations for various limits are also obtained that can be useful in the search for a method to resum complicated terms appearing in the calculations. In the perfect conducting limit, we obtain equations that allow us to generalize the complicated mapping of the point dipoles and charges to any order n , subject to computational power.

Finally, in Chapter 6 we present details of numerical results and analyze them graphically while we discuss some of the implications and we then consider extensions to the existing work that could be carried out in the future.

CHAPTER 2

Effective Medium Theory

2.1 Introduction

This Chapter is concerned with Effective Medium Theory (EMT), a very powerful method for determining certain properties of materials. One such property of interest in this thesis is the calculation of the dielectric function for a composite system. EMT is a 1-body approach, ie, it relies on the interaction of an inclusion with its host medium. Ultimately we will be interested in improving EMT methods by including 2-body interactions with the host medium. We begin by discussing the theories that essentially form the backbone of EMT, but which are by no means the only theories that can be used. We will highlight the main ideas in some of these theories that are the foundation of a very exciting area of physics. Our discussion of such pioneering work will not embrace dynamical considerations amongst other things, however the underlying principles are essentially the same in almost all other cases except that the symbolic nature of the mathematics changes. A full background of some of the developments outlined in this and the next chapter can be found in the book by Choy (1999).

2.2 The development of EMT

The central concept of this thesis is the study of particles inside a medium. More specifically we want to obtain the dielectric function ϵ for a 2-body composite system, however before doing so, the core idea that forms the backbone of EMT needs to be emphasised. For an inclusion and a host medium experiencing a field we need to solve Maxwell's equations, see Kittel (1971), Ashcroft and Mermin (1976), Reitz and Milford (1970) and Jackson (1975). The interesting aspect is that we require knowledge of the field in the local sense, but the problem is that for the dimensions

in question the description can be microscopic, mesoscopic or macroscopic. The concept of the local field was investigated by Lorentz (1870) while he was developing his views on macroscopic electrodynamics. Lorentz was able to show how to compute the local field \mathbf{E}_{local} by considering a cubic crystal made up of identical particles. The local field turns out to be ¹

$$\mathbf{E}_{local} = \mathbf{E} + \frac{1}{3\epsilon_0} \mathbf{P}, \quad (2.1)$$

for a polarisation \mathbf{P} and a uniform \mathbf{E} . More precisely, the field acting on a particle in a medium is called the local field \mathbf{E}_{local} . This field is not the microscopic field \mathbf{E}_{micro} , nor the averaged field \mathbf{E} . It is the part of \mathbf{E}_{micro} that is due to the external sources and to all the particles except the one under consideration. Of course just like most theories, Lorentz's formulation has had its fair share of criticisms, see Landauer (1978), Cohen *et al.* (1973), that have brought about the need to improve the relation between microscopic and macroscopic parameters. An early attempt to relate macroscopic parameters with those at the microscopic level has produced the Clausius-Mossotti formula. The basic idea is to find a connection between the dipole moment of a molecule and the local electric field. For instance a macroscopic property such as the dielectric constant ϵ can be connected to a microscopic property such as the molecular polarisability α . In such an event we can examine what the dielectric equation of state looks like if we suppose that a dielectric medium is made up of identical molecules that develop a dipole moment

$$\mathbf{p} = \alpha \epsilon_0 \mathbf{E}, \quad (2.2)$$

when placed in an electric field \mathbf{E} . If we assume that N is the number density of such molecules then the polarisation of the medium is

$$\mathbf{P} = N\mathbf{p} = N\alpha\epsilon_0\mathbf{E}, \quad (2.3)$$

or

$$\mathbf{P} = \epsilon_0 \mathbf{E} \frac{N_A \rho M \alpha}{M}, \quad (2.4)$$

¹or $\mathbf{E}_{local} = \mathbf{E} + \frac{4\pi}{3} \mathbf{P}$.

where ρ_M is the mass density, N_A is Avogadro's number and M is the molecular weight. An interesting question arises as to how we relate the electric field experienced by an individual molecule to the average electric field in the medium. Surprisingly this is not an easy question to answer since it is expected that the electric field varies strongly inside the dielectric when we consider atomic length scales. In order to answer the question we can suppose that the dielectric is polarised with a mean electric field \mathbf{E}_0 which is uniform on macroscopic length scales and directed along the z -axis. Next we consider any molecule which constitutes the dielectric and draw a sphere around the molecule of radius a . The imaginary sphere is to merely establish a boundary between the microscopic and macroscopic range of phenomena affecting the molecule. Furthermore, the dielectric outside the sphere is considered to be a continuous medium and the dielectric inside the sphere as a collection of polarised molecules. Then there is a polarisation surface charge of magnitude (Kittel (1974), Ashcroft and Mermin (1976)):

$$\sigma_{pol} = -P \cos(\theta) \quad (2.5)$$

on the inside of the sphere, where (r, θ, ϕ) are spherical coordinates, and $\mathbf{P} = P\hat{z} = \epsilon_0(\epsilon - 1)\mathbf{E}_0\hat{z}$ is the uniform polarisation of the dielectric. The magnitude of the electric field E_z at the molecule due to the surface charge is

$$E_z = -\frac{1}{4\pi\epsilon_0} \int \frac{\sigma_{pol} \cos(\theta)}{a^2} (2\pi a^2 \sin(\theta)) d\theta, \quad (2.6)$$

and upon integrating from $[0, \pi]$ we obtain

$$\begin{aligned} E_z &= \frac{P}{2\epsilon_0} \int_0^\pi \cos^2(\theta) \sin(\theta) d\theta \\ &= \frac{P}{3\epsilon_0}. \end{aligned} \quad (2.7)$$

Following the same procedure we find that the electric fields for the other coordinates are zero, ie, $E_\theta = E_\phi = 0$. Therefore the field at the molecule due to the surface charges on the sphere becomes

$$\mathbf{E} = \frac{\mathbf{P}}{3\epsilon_0}. \quad (2.8)$$

The field due to the individual molecules within the sphere is obtained by summing over the dipole fields of these molecules. The electric field at a distance r from a

dipole \mathbf{p} is

$$\mathbf{E} = -\frac{1}{4\pi\epsilon_0} \left(\frac{\mathbf{p}}{r^3} - \frac{3(\mathbf{p} \cdot \mathbf{r})\mathbf{r}}{r^5} \right). \quad (2.9)$$

The assumption here is that the dipole moment of each molecule within the sphere is the same and that the molecules are evenly distributed throughout the sphere. This implies that the electric field E_z experienced by the molecule as it interacts with all the other molecules within the sphere is

$$\begin{aligned} E_z &= -\frac{1}{4\pi\epsilon_0} \sum_{\text{mols}} \left(\frac{p_z}{r^3} - \frac{3(p_x x_z + p_y y_z + p_z z^2)}{r^5} \right) \\ &= 0. \end{aligned} \quad (2.10)$$

Thus, the electric field at the molecule due to the other molecules within the sphere vanishes and the net electric field experienced by an individual molecule is

$$\mathbf{E} = \mathbf{E}_0 + \frac{\mathbf{P}}{3\epsilon_0}. \quad (2.11)$$

Equation (2.11) tells us that the electric field of a molecule is larger than the average electric field \mathbf{E}_0 in the dielectric. This effect can be attributed to the long range interactions of the molecule with the other molecules in the medium. From the analysis so far and the result $\mathbf{P} = \epsilon_0(\epsilon - 1)\mathbf{E}_0$ we obtain

$$\frac{\epsilon - 1}{\epsilon + 2} = \frac{N_A \rho_M \alpha}{3M}, \quad (2.12)$$

which is the Clausius-Mossotti relation that works pretty well for various dielectric liquids and gases. Looking at (2.12), we see that the original goal we had in mind has been achieved, ie, we have found a connection between macroscopic and microscopic parameters ϵ and α respectively, see Kittel (1974), Ashcroft and Mermin (1976) and its relation to the formula by Böttcher (1952). All that is required in using (2.12) is to evaluate the molecular polarisability α . There have been efforts to obtain α by using semi-classical methods such as spring models for atomic systems for example. However, the fact that α is a microscopic parameter, signifies that the most appropriate method would be to use a full quantum mechanical analysis (Pauling and Wilson (1935), Landau and Lifshitz (1991) and Landau *et al.* (1984)).

The evaluation of α is a persistent problem and it is one of the issues that forms the basis of the Maxwell-Garnett theory, which can be viewed as an extension of the

Clausius-Mossotti theory that deals with composite systems. The key ingredient here is to determine α , but if we are happy enough to approximate it using the classical approach where the molecule (inclusion) has spherical geometry, we obtain (Reitz and Milford (1970), Choy (1999))

$$\alpha = \left(\frac{\epsilon_1 - 1}{\epsilon_1 + 2} \right) a^3, \quad (2.13)$$

where the inclusion has dielectric constant ϵ_1 and radius a . Of course the polarisability can also be obtained by the use of non-spherical geometry such as ellipsoids for instance, but the method involves elliptic integrals, see Stoner (1945), Osborne (1945). Fortunately for spheres, we can make use of the Clausius-Mossotti equation derived above and upon substitution of α we have

$$\left(\frac{\epsilon - 1}{\epsilon + 2} \right) = \eta_1 \left(\frac{\epsilon_1 - 1}{\epsilon_1 + 2} \right), \quad (2.14)$$

where all constant parameters have been absorbed in the volume fraction of inclusions η_1^2 . Equation (2.14) implies that we can study a composite medium with dielectric constant ϵ_0 which contains inclusions with dielectric constant ϵ_1 of volume fraction η_1

$$\left(\frac{\epsilon - \epsilon_0}{\epsilon + 2\epsilon_0} \right) = \eta_1 \left(\frac{\epsilon_1 - \epsilon_0}{\epsilon_1 + 2\epsilon_0} \right), \quad (2.15)$$

or

$$\epsilon = \epsilon_0 + \frac{3\eta_1\gamma_1}{1 - \eta_1\gamma_1} \epsilon_0, \quad (2.16)$$

with

$$\gamma_1 = \frac{\epsilon_1 - \epsilon_0}{\epsilon_1 + 2\epsilon_0}. \quad (2.17)$$

Alternatively we can represent the same composite with dielectric constant ϵ_1 and inclusions embedded with dielectric constant ϵ_0 and volume fraction η_0 as,

$$\left(\frac{\epsilon - \epsilon_1}{\epsilon + 2\epsilon_1} \right) = \eta_0 \left(\frac{\epsilon_0 - \epsilon_1}{\epsilon_0 + 2\epsilon_1} \right). \quad (2.18)$$

However equations (2.18) and (2.14) are not symmetric and generally will not give the same result when solving for ϵ by either method. More problems surface when

²Here the volume fraction of inclusions is written as η in order to follow early convention. Theories developed in more recent times denote this as c .

one attempts to generalise (2.14) to several components, Böttcher (1952):

$$\frac{\epsilon - \epsilon_0}{\epsilon + 2\epsilon_0} = \sum_i \eta_i \left(\frac{\epsilon_i - \epsilon_0}{\epsilon_i + 2\epsilon_0} \right). \quad (2.19)$$

Equation (2.19) becomes problematic because the assumption is that all elements in the composite are acted upon by the same Lorentz field. In order to avoid this issue any successful formulation must exclude the Lorentz field. The Maxwell-Garnett theory was advanced by the work of Bruggeman (1935) who made major improvements by analysing the symmetrical properties of a composite medium. To understand Bruggeman's idea, we consider a composite host of dielectric constant ϵ with a spherical inclusion of radius a embedded in it whose dielectric constant is ϵ_1 . Far from the vicinity of the inclusion the field is assumed to be constant, but as we get closer to the inclusion the field varies. The fields outside and inside the inclusion become respectively (see Reitz and Milford (1970), Landau *et al.* (1984) and Choy (1999)),

$$\mathbf{E}_{outside} = (E_0 + 2\frac{C_1}{r^3}) \cos \theta \hat{r} + (-E_0 + \frac{C_1}{r^3}) \sin \theta \hat{\theta}, \quad (2.20)$$

$$\mathbf{E}_{inside} = -A_1 \cos \theta \hat{r} + A_1 \sin \theta \hat{\theta}, \quad (2.21)$$

where

$$C_1 = \left(\frac{\epsilon_1 - \epsilon}{\epsilon_1 + 2\epsilon} \right) a^3 E_0, \quad A_1 = -\left(\frac{3\epsilon}{\epsilon_1 + 2\epsilon} \right) E_0. \quad (2.22)$$

Bruggeman considered the flux deviation $\Delta\Phi_1$ for a spherical inclusion which can be calculated as, (Choy (1999)),

$$\Delta\Phi_1 = 2\pi \left(\int_0^a dr r D - \int_0^a dr r \epsilon E_0 \right) = 2\pi a^2 \epsilon E_0 \left(\frac{\epsilon_1 - \epsilon}{\epsilon_1 + 2\epsilon} \right), \quad (2.23)$$

that uses the hypothesis that there should be zero average flux deviations,

$$\eta_1 \Delta\Phi_1 + \eta_2 \Delta\Phi_2 = 0. \quad (2.24)$$

If Bruggeman's hypothesis is correct and (2.23) gives the required results, then it must be assumed that the flux deviations are due to single particle polarisations in an effective medium. Equation (2.22) can now be used to show that

$$\eta_1 \left(\frac{\epsilon_1 - \epsilon}{\epsilon_1 + 2\epsilon} \right) + \eta_2 \left(\frac{\epsilon_2 - \epsilon}{\epsilon_2 + 2\epsilon} \right) = 0, \quad (2.25)$$

which is a widely used expression that can be extended to any number of particles very easily

$$\sum_i \eta_i \left(\frac{\epsilon_i - \epsilon}{\epsilon_i + 2\epsilon} \right) = 0. \quad (2.26)$$

The importance of the Bruggeman formula warrants further investigation of its properties and behaviour at certain limits. For more details see the book by Choy (1999), Kirkpatrick (1971,1973), Davidson and Tinkham (1976) and Shante and Kirkpatrick (1971). Suffice to say that in the context of obtaining the dielectric function, in which we are interested in this thesis, we can get a feel for the behaviour of these formulae if we look at the superconducting limit $\epsilon \rightarrow \infty$. The Maxwell-Garnett formula gives the dielectric function as

$$\epsilon = 1 + \frac{\eta}{\frac{1}{3}(1 - \eta)} = 1 + 3\eta + 3\eta^2 + \dots, \quad (2.27)$$

while the Bruggeman formula gives

$$\epsilon = \frac{1}{(1 - 3\eta)} = 1 + 3\eta + (3\eta)^2 + \dots \quad (2.28)$$

We can see immediately that the coefficient of η^2 , where η is the low volume fraction of inclusions, is either underestimated or overestimated.³ In fact the correct expansion for $d = 3$ gives the coefficient of η^2 as 4.51 as obtained by a large series of slowly convergent terms first obtained by Jeffrey (1973), so that

$$\epsilon = 1 + 3\eta + 4.51\eta^2 + \dots \quad (2.29)$$

Djordjević *et al.* (1996) obtained the correct expansion for a 2-dimensional inclusion as

$$\epsilon = 1 + 2\eta + 2.744989676\eta^2 + \dots, \quad (2.30)$$

by the use of image theory as opposed to Jeffrey's multipole expansion method. These results have been obtained as limits in a more generalised d -dimensional framework by Choy, Alexopoulos and Thorpe (1998a,1998b). Thus depending on their use, theories such as that of Bruggeman must be applied with caution. Fortunately, there are alternative derivations that can be quite useful as a check. In the next section we will mention some of these.

³These expressions calculate the dielectric function for a spherical inclusion.

2.3 Alternative formulations of EMT

The theories that have been discussed in the previous sections are not the only ones to describe the properties of a medium. Rather they can be thought of as being simply the most widely used. However these theories as mentioned previously have certain limitations and care must be exercised when using them. Many other theories have been developed that are very useful notwithstanding the fact that they are mathematically and computationally more involved. While these theories are quite numerous, and therefore impossible to cover extensively in this thesis, we will mention some of these with the knowledge that they share the same underlying physics in most cases with each other.

2.3.1 Green's functions

One method of studying an effective medium problem is by the use of Green's functions. Since the method is extremely powerful when it comes to boundary value problems, e.g., as is the case of the inclusion shape and interface with the surrounding medium, we can use it to study the properties of a composite medium. As previously stated, it can also be used to check the validity of other theories such as those of Maxwell-Garnett and Bruggeman, (Stroud (1975)). Since we are dealing with an ensemble of inclusions in an inhomogeneous material of volume V that is bound by a surface S , we can calculate the ensemble average $\epsilon(\mathbf{x})$, (Khincin (1949), Hadjipanayis and Siegel (1994)), as

$$\epsilon(\mathbf{x}) = \frac{1}{V} \int_V \epsilon(\mathbf{x}) d\mathbf{x}, \quad V \rightarrow \infty. \quad (2.31)$$

In fact we are interested in calculating a tensor for the effective dielectric $\underline{\epsilon}$ for an external electric field \mathbf{E}_0 . The boundary conditions for this problem and its solution allow us to obtain $\underline{\epsilon}$

$$\underline{\epsilon} = \epsilon_0 + \langle \chi(\mathbf{x}) \rangle, \quad (2.32)$$

where the tensor $\chi(\mathbf{x})$ is defined as

$$\chi(\mathbf{x})\mathbf{E}_0 = \delta\epsilon(\mathbf{x})\mathbf{E}(\mathbf{x}) \quad (2.33)$$

that satisfies the integral equation ⁴

$$\chi(\mathbf{x}) = \delta\epsilon(\mathbf{x}) + \delta\epsilon(\mathbf{x}) \int_V \tilde{\mathbf{G}}(\mathbf{x}, \mathbf{x}') \chi(\mathbf{x}') d\mathbf{x}' . \quad (2.34)$$

The problem now is that (2.34) is generally difficult to solve for the Green's function but using the choice of

$$\langle \chi(\mathbf{x}) \rangle = 0 , \quad (2.35)$$

gives the expected solution $\underline{\epsilon} = \epsilon_0$. In fact we find that. (see Choy (1999), Kinoshita and Mura (1971), Stroud (1975), Moon (1996), Landau *et al.* (1984)), we obtain the self-consistent equation for $\underline{\epsilon}$,

$$\langle (1 - \delta\epsilon_i \Gamma_i)^{-1} \delta\epsilon_i \rangle = 0 , \quad (2.36)$$

which is essentially the same as Bruggeman's equation for a binary system of spherical inclusions. More precisely we obtain $\underline{\epsilon}$ directly as

$$\underline{\epsilon} = \epsilon_0 + \langle ((1 - \delta\epsilon_i \Gamma_i)^{-1}) \rangle^{-1} \langle (1 - \delta\epsilon_i \Gamma_i)^{-1} \delta\epsilon_i \rangle , \quad (2.37)$$

where the depolarisation tensor is given as

$$\Gamma_i^{\alpha\beta} = - \int_{S'} dS' \frac{\partial G(\mathbf{x}, \mathbf{x}')}{\partial x_\alpha} \mathbf{n}'_\beta . \quad (2.38)$$

It is interesting to note that (2.37) is the alternative form to the Maxwell-Garnett equation when ϵ_0 is chosen as the host medium. Thus we have obtained the Bruggeman and Maxwell-Garnett theories using the Green's functions technique by making a suitable choice for ϵ_0 which has led to the effective dielectric function $\underline{\epsilon}$.

2.3.2 Variational bounds

One other method that has been adapted to the study of composite systems is the variational bounds technique. From this technique, see Arthurs (1980) and Sewell (1992), a specific case can be derived that has come to be known as the Hashin-Shtrikman bounds method (Hashin and Shtrikman (1962a,1962b,1962c)). The effective dielectric of a medium can be obtained in terms of an integral formulation

⁴For a detailed mathematical derivation of these results see the book by Choy (1999).

of a cost functional. However the bounds derived are proportional to what ansatz is used for the polarisation fields of the system. If for a 2-inclusion system we know the volume fraction of one of these inclusions, the bounds obtained give the best possible solutions (Hashin (1968)).⁵ The bounds are derived as

$$\left\langle \frac{1}{\varepsilon(\mathbf{x})} \right\rangle < \varepsilon_e < \langle \varepsilon(\mathbf{x}) \rangle, \quad (2.39)$$

where

$$\langle \varepsilon(\mathbf{x}) \rangle = \sum_i^m \eta_i \varepsilon_i, \quad (2.40)$$

and we are considering an m -component composite and dielectric constant ε_i for a given i component and volume fraction η_i . These bounds have in fact been known for a very long time (Wiener (1912)), and have been reformulated throughout the years to cater for different properties, eg, thermal conductivity (Woodside and Messner (1961)) and for transport phenomena (Bergman (1976)). Hashin and Shtrikman (1962a) have used these variational bounds to derive the 2-body composite formula

$$\varepsilon_1 + \frac{\varepsilon_1 \eta_2}{\frac{\varepsilon_1}{(\varepsilon_2 - \varepsilon_1)} + \frac{\eta_1}{3}} < \varepsilon_e < \varepsilon_2 + \frac{\varepsilon_2 \eta_1}{\frac{\varepsilon_2}{(\varepsilon_1 - \varepsilon_2)} + \frac{\eta_2}{3}}. \quad (2.41)$$

Equation (2.41) tells us that the effective dielectric constant must lie between these two bounds which are related to the Maxwell-Garnett expressions. The application of the variational bounds technique can be used extensively in many other areas such as the concentric shell model, but we will not investigate these areas any further here.

2.3.3 Density functional theory

Since we are dealing with the effects of an ensemble of particles embedded in a host medium, we can consider the concept of density in order to gain an insight to the behaviour of such systems. This density based formulism is in fact what we commonly refer to as density functional theory (DFT) and is so diverse that it is equally applied successfully to both quantum and classical systems. In the case of quantum length scales, the central concept of DFT involves a one-particle

⁵See the work done by Choy (1997) using the complementary variational approach on superconductors.

Schrödinger like Kohn-Sham (1965) equation, while in the case of a classical system DFT consists amongst other things of Boltzmann type distributions. Here of course we are interested in a DFT pertaining to a composite system so we recall from previous sections, see in particular the Clausius-Mossotti relation, that our goal has been the connection of macroscopic (c) and microscopic (α) parameters. For a more accurate solution we require a quantum mechanical description of the molecular polarisability α . Fortunately, DFT can prove useful in this pursuit because in a mesoscopic regime that involves atomic length scales, it uses the single-inclusion number density as the only basic variable. In fact we can consider the effective interaction and correlation effects of a two-particle system and depending on the type of problem we are concerned with, the inter-particle interactions can be obtained through a microscopic DFT calculation or by simple model potentials, eg, hard-sphere or the Lennard-Jones approach. In the case of a two-component system we can write down the grand potential $\Omega[\rho_\alpha, \rho_\beta]$ as, see Henderson (1992) and deGennes (1992,1999),

$$\Omega[\rho_\alpha, \rho_\beta] = F_{ex}[\rho_\alpha, \rho_\beta] + \frac{1}{\beta_0} \sum_\nu \int \rho_\nu(\mathbf{r}) [\ln(\rho_\nu(\mathbf{r})\Lambda_\nu^3) - 1] d\mathbf{r} + \sum_\nu \int [v_\nu(\mathbf{r}) - \mu_\nu] \rho_\nu(\mathbf{r}) d\mathbf{r}, \quad (2.42)$$

where $F_{ex}[\rho_\alpha, \rho_\beta]$ is the excess free energy, ρ_α and ρ_β are the inclusion densities, $\beta_0 = 1/k_B T$ is the inverse temperature, μ is the chemical potential and Λ is the thermal de-Broglie wavelength. If we were next to minimise (2.42) we would obtain an Euler-Lagrange equation so that

$$\rho_\nu(\mathbf{r}) = \rho_\nu^0 \exp \left[-\beta_0 v_\nu(\mathbf{r}) + c_\nu^{(1)}(\mathbf{r}; [\rho_\alpha, \rho_\beta]) - \bar{c}_\nu^{(1)}(\rho_\alpha^0, \rho_\beta^0) \right], \quad (2.43)$$

for $\nu = \alpha, \beta$ and where $\rho_{\alpha, \beta}^0$ correspond to the bulk phase of the component densities. Here also, the bulk is represented by \bar{c} and the direct correlation function which describes the extra contribution to the effective potential via the inter-inclusion interactions, is given by

$$c_\nu^{(1)}(\mathbf{r}; [\rho_\alpha, \rho_\beta]) = -\beta_0 \frac{\delta F_{ex}[\rho_\alpha, \rho_\beta]}{\delta \rho_\nu(\mathbf{r})}. \quad (2.44)$$

For a two-inclusion system for which we are interested here, the second-order inclusion interactions are an extension of (2.44) and we write them as

$$c_{\nu\nu'}^{(2)}(\mathbf{r}_1, \mathbf{r}_2; [\rho_\alpha, \rho_\beta]) = -\beta_0 \frac{\delta^2 F_{\text{ex}}[\rho_\alpha, \rho_\beta]}{\delta \rho_\nu(\mathbf{r}_1) \delta \rho_{\nu'}(\mathbf{r}_2)}. \quad (2.45)$$

Looking at the first-order contributions as given by the functional derivative in (2.44), we may wonder how we obtain a solution if these first-order interactions in an inhomogeneous density distribution are not known. Fortunately for such a case, we can consider a Taylor expansion of the functional in powers of the density inhomogeneity $\Delta \rho_\nu(\mathbf{r})$, thus

$$c_\nu^{(1)}(\mathbf{r}; [\rho_\alpha, \rho_\beta]) = \bar{c}_\nu^{(1)}(\rho_\alpha^0, \rho_\beta^0) + c_\nu^{(2)}(\mathbf{r}) + c_\nu^{(n)}(\mathbf{r}), \quad (2.46)$$

where $c_\nu^{(2)}(\mathbf{r})$ are the contributions from a two-body system and $c_\nu^{(n)}(\mathbf{r})$ are the contributions for higher orders (many-body interactions). This means that the density equation (2.43) can now be re-written as

$$\rho(\mathbf{r}) = \rho_\nu^0 \exp \left[-\beta_0 v_\nu(\mathbf{r}) + \sum_{\nu'} \int c_{\nu\nu'}^{(2)}(\mathbf{r}_1, \mathbf{r}_2; [\rho_\alpha^0, \rho_\beta^0]) \Delta \rho_{\nu'}(\mathbf{r}_2) d\mathbf{r}_2 + c_\nu^{(n)}(\mathbf{r}) \right], \quad (2.47)$$

where $\nu = \alpha, \beta$ for a two-component system and we have included the second-order contributions

$$c_\nu^{(2)}(\mathbf{r}) = \sum_{\nu'} \int c_{\nu\nu'}^{(2)}(\mathbf{r}_1, \mathbf{r}_2; [\rho_\alpha^0, \rho_\beta^0]) \Delta \rho_{\nu'}(\mathbf{r}_2) d\mathbf{r}_2, \quad (2.48)$$

where the Taylor expansion has been made via $\Delta \rho_\nu(\mathbf{r}) = \rho_\nu(\mathbf{r}) - \rho_\nu^0$. It would be interesting to relate the work that is to be presented in later Chapters for the two-body problem with (2.48) and to thus try and rederive the results in a DFT framework. Either way these second-order interactions can be modelled by some pair potential scheme and so in most cases this is straightforward but the difficulty arises when we consider higher order terms $c_\nu^{(n)}(\mathbf{r})$. If we do not have knowledge of the latter we may run into convergence problems, however, efforts have been made in order to arrive at some valid approximations by Choudhury and Ghosh (1999) in terms of two-body terms and by Rickayzen and Augousti (1984) by considering a two-component generalisation of the one-body component result. We will not pursue the ideas of DFT here any further, suffice to say that the power of DFT in describing

particle interactions in a medium can be applied to the problem of calculating the effective dielectric ϵ if we are prepared to make the appropriate modifications to the general theory.

CHAPTER 3

Extensions to Effective Medium Theory

3.1 Introduction

So far we have investigated some aspects of effective medium theory that allow us to determine amongst other things the dielectric property of a medium. However, the various methods used focus on the 1-body problem, ie, on how an inclusion¹ interacts with the host medium. Ultimately we would like to consider 2-body contributions and we have to extend some of the ideas pertaining to current EMT. It is important to understand that any way forward requires the study of scattering effects of the inclusions embedded in a host medium. There are numerous techniques to describe scattering from inclusions such as the T-matrix method, CPA, Green's functions-that can involve the dynamical case (Papas (1998)), and variational bounds methods to name only a few. The underlying theme is that all of these approaches have an electromagnetic basis, as opposed say to the geometrical optics based techniques, because the size of the scatters are on the same scale as the wavelength λ . Two approaches can be made in order to solve such problems: (i) by solving the full vector fields, which numerically at least are extremely difficult to solve or (ii) solving by the use of approximation techniques, eg, by the theory of scattering due to Mie (1908)² or the concentric sphere model (Kerker *et al.* (1978)). Both of these approximations are limited to spherical inclusions. Scattering from an arbitrarily inhomogeneous particle almost always requires numerical techniques, which necessitate large computational resources, especially for systems that are more than a few wavelengths in dimension. The T-matrix method (Waterman (1965)) is a formulation that is used for spheroids and particles described by

¹Everywhere in this thesis, the terms inclusion, particle, grain and so on have equivalent meaning unless otherwise stated. Furthermore they have classical dimensions.

²This is in fact the 1-body Mie theory.

Chebyshev polynomials. In what follows below, we shall study some of the methods that can be used to investigate multiparticle scattering which might contribute to the improvement of existing EMT. In particular we will dwell longest on one such method: the T-matrix technique.

3.2 n -body scattering

The study of multiple scattering is vital in the pursuit of an extension to existing 1 - *body* EMT. An understanding of two or more body effects are not only of interest in the area of composite materials, but in numerous problems associated with pressure waves in disperse systems, scattering of light waves off environmental objects such as clouds, and in acoustic scattering to name only a few areas. In modelling a system with multiple inclusions, it is typical to assume that the scatterers are spherical in nature because of the ease with which one can parametrise large and complicated systems using spheroid geometry. For instance, dust particles, droplets or bubbles are modelled as having spherical appearance with excellent results, see Gumerov *et al.* (1988), Duraiswami and Prosperetti (1995). Given that spherical geometries can be very good approximations for studying the properties of composite materials too, the next step is to consider not only the interaction between one-sphere with its surrounding medium, but two and ideally n -spheres. If this is achieved, it puts us in a better position to re-examine one-body EMT as we try to incorporate at the very least 2-sphere interactions to improve current EMT theories. The question now arises as to what methodology might be used in order to compute n -sphere interactions. Evidently this can be a matter of convenience since one technique might be superior to the next but the common denominator is that even 2-body interactions are not a trivial matter to compute as we shall see later. The problem of computing scattering effects of n -spherical inclusions, with specified impedance boundary conditions at their surfaces, can be addressed via numerical techniques for example. Some of the well known numerical methods are those such as the boundary element methods (BEM), finite element methods (FEM) and finite difference methods (FDM). Even while these numerical methods

have their advantages, they are all hampered by the same deficiency related to the necessity of discretisation of either the boundary surfaces or of the complete space. The process of discretisation introduces a particular size or length scale of the surface or spatial element. For consistent and accurate numerical results, the change of the discretisation length must not interfere with computation. If the latter is to be achieved, the length scale or size should be much smaller than the wavelength λ . For higher frequencies this leads to the use of very fine surface or spatial meshes. Discretisation methods require the solution of very large linear systems that are very costly in terms of CPU time and memory. This is evident in the use of boundary element methods (BEM) whose solutions involve dense interinfluence matrices while even larger but sparse matrices are required when finite-element/finite-difference methods (FEM/FDM) are used.

One way around this problem is to consider a semi-analytical approach such as the T-matrix method, see Waterman and Truell (1961), Varadan and Varadan (1980), Mishchenko *et al.* (1996) and Chew *et al.* (1990). The T-matrix method characterises the scattering properties of the inclusions by considering the coefficients of the local expansion of the incident wave centred at the inclusions and transforms them into the coefficients of an outgoing (scattered) wave. We are reminded that for non-spherical inclusions, ie, inclusions of complex shape and boundary conditions the solutions can be obtained either numerically or by analytical/semi-analytical techniques, after translating any complex shape into one of a simpler geometry (such as a sphere). In what follows we shall approach the interaction of inclusions in a material from the point of view of the T-matrix method for spherical scatterers because for an arbitrary incident field the solutions can be obtained analytically. It appears to be the most appropriate way to extend 1-body interactions to n -bodies (see Bergman and Stroud (1980), Chew *et al.* (1990)). Before even considering the many-body problem, it is sensible to proceed cautiously with the analysis of two-body interactions. Early attempts have been made towards this end in the context of hydrodynamics but the results were rather disappointing which was to be expected given that the efforts were *ad hoc* (Bedeaux (1987), Choy (1995)). Other

studies dedicated to 2-spheres have been made by Marnevskaia (1969), Gaunaud and Huang (1994) and Gaunaud *et al.* (1995) using representations of the translation coefficients via the Clebsch-Gordan coefficients or $3-j$ Wigner symbols (Epton and Dembart (1995), Koc *et al.* (1999)). Even though this method achieves an exact computation of the T-matrix elements, it is time consuming and thus only practical for a small number of spheres³. The computational time that it takes to calculate a system of n -spheres can be reduced by several orders of magnitude if the computation of the translation coefficients could be performed more efficiently (Bunning and Lo (1971)). Bunning and Lo (1971) applied recursive computation of these coefficients for the case where the sphere centres are located on a line. This is always true for two spheres and is a special case for three or more spheres. Everything that we have discussed thus far propagates the notion that the T-matrix underpins the drive for an improved EMT. For this reason, we will consider the T-matrix more closely and derive the 1-sphere, 2-sphere and n -sphere cases in the next section.

3.2.1 The T-matrix for a single sphere

The T-matrix approach discussed so far involves finding the relationship between an incident wave scattering off the inclusion (sphere) expanded in the form of orthogonal eigenfunctions

$$E_0 = \sum_n^{\infty} a_n \phi_n^{(0)}, \quad (3.1)$$

where a_n are the expansion coefficients for the incident wave. Furthermore, the scattered wave is also expanded in terms of orthogonal eigenfunctions

$$E_{scat} = \sum_k^{\infty} b_k \phi_k^{(scat)}, \quad (3.2)$$

where b_k are the scattering wave's expansion coefficients and can be written as a matrix equation

$$b_k = \sum_n^{\infty} T_{kn} a_n, \quad (3.3)$$

or in the notation

$$\mathbf{B} = \mathbf{T}\mathbf{A}, \quad (3.4)$$

³We are only interested in examining 2-body effects anyway, so time constraints are minimal.

such that T_{kn} are the elements of the T-matrix. The flexibility of the T-matrix method means that for any scattering object of arbitrary shape both scalar or vector waves can be used. Strictly speaking, the geometry of the scatterers permits expansion of these waves as discrete series in terms of orthogonal eigenfunctions. Furthermore, we must take into account the fact that the behaviour of the scattering object to the incident wave must be linear and that the expansion series for the waves can be truncated at a finite number of terms. While in general the T-matrix is determined mathematically/computationally, it is also possible to obtain it from experimental measurements. Formulating the T-matrix depends on the physical characteristics of the inclusion, eg, size, geometry, composition and so on, and is independent of the incident field. These particulars allow the T-matrix to be calculated once only for a given inclusion and the same T-matrix can be used for repeated calculations. This is a very important property which places the T-matrix method at an advantage when compared to other methods of calculating scattering when recursive calculations are needed, (Mishchenko *et al.* (2000)). Mishchenko (1991) has shown that some cases are even more efficient if the waves are expanded in spherical functions because the averaging of scattering over various orientations of the inclusion compared to the direction of the incident wave can be performed analytically. Thus, in the case of spherical geometry the eigenfunction expansions of the fields are made in terms of vector spherical wavefunctions, see Waterman (1971), Tsang *et al.* (1983) and Jackson (1975). These are well known vector spherical harmonics that are written in terms of transverse electric (TE) and transverse magnetic (TM) eigenfunctions

$$\begin{aligned} (TE) : \mathbf{E}_{l,m,n}^{(M)}(\mathbf{r}) &= \phi_{l,n}^{(m)}(r) \mathbf{X}_{l,m}(\Omega); \\ (TM) : \mathbf{E}_{l,m,n}^{(E)}(\mathbf{r}) &= \frac{i}{k [1 - u_{l,n}^{(E)} \vartheta_1(r)]} \left\{ \text{curl} \left[\phi_{l,n}^{(E)}(r) \mathbf{X}_{l,m}(\Omega) \right] \right\}, \end{aligned} \quad (3.5)$$

where the vector spherical harmonics are given by

$$\mathbf{X}_{l,m}(\Omega) = \frac{\hat{\mathbf{L}} Y_{l,m}}{\sqrt{l(l+1)}}, \quad (3.6)$$

where \hat{L} is the angular momentum operator and $Y_{l,m}$ are the scalar spherical harmonic functions (see Schiff (1949) and Jackson (1975)). These scalar functions can be written in the form of Bessel functions within ($r < a$) and outside ($r > a$) the sphere respectively:

$$\begin{aligned}\phi_{l,n}^{(F)}(r) &= A_{l,n}^{(F)} j_l \left(kr \sqrt{1 - u_{l,n}^{(F)}} \right), & \text{for } r < a \\ &= B_{l,n}^{(F)} h_l^{(1)}(kr), & \text{for } r > a.\end{aligned}\quad (3.7)$$

The eigenfunctions and coefficients are determined by the boundary conditions at $r = a$ by the use of the continuity of the scalar functions and their derivatives

$$\begin{aligned}\phi_{l,n}^{(M)}(r), & \quad \frac{d}{dr} \left(\phi_{l,n}^{(M)}(r) \right), \\ \phi_{l,n}^{(E)}(r), & \quad \frac{1}{1 - u_{l,n}^{(E)} \theta_1} \frac{d}{dr} \left(r \phi_{l,n}^{(E)}(r) \right).\end{aligned}\quad (3.8)$$

It follows that from the application of (3.8) that the eigenvalues are obtained from

$$\begin{aligned}\frac{x j_l'(x)}{j_l(x)} \Big|_{x=x_{l,n}^{(M)}} &= \frac{x h_l^{(1)'}(x)}{h_l^{(1)}(x)} \Big|_{x=ka}, \\ \frac{1}{x^2} \left(1 + \frac{x j_l'(x)}{j_l(x)} \right) \Big|_{x=x_{l,n}^{(E)}} &= \frac{1}{x^2} \left(1 + \frac{x h_l^{(1)'}(x)}{h_l^{(1)}(x)} \right) \Big|_{x=ka},\end{aligned}\quad (3.9)$$

where the eigenvalues are denoted as

$$x_{l,n}^{(F)} \equiv ka \sqrt{1 - u_{l,n}^{(F)}}. \quad (3.10)$$

The next step is to calculate the T-matrix but it is worth noticing that the so called T-matrix is calculated in almost all cases using the extended boundary condition, originally developed by Waterman (1971), whose method is generally referred to as the T-matrix method because of the strong link to the technique. While the incident and scattered fields are usually expanded in vector spherical harmonic wave functions, other sets of eigenfunctions such as cylindrical wavefunctions for scatterers of finite length in one dimension, Floquet expansions in the case of planar periodic scatterers can be used, especially for non-spherical geometries. In all of these cases the T-matrix formulation applies in the same way, (Bowman *et al.* (1987)). In what follows we consider the T-matrix analysis based on Chew *et al.* (1990) (see also

Mackowski (1991)). For a more detailed exposition of the method see the book by Choy (1999). We focus on the TE case whose scalar functions are based on those of Chew *et al.* (1990) and Choy (1999) for consistency. An analogous treatment can be made for the TM case. In essence the technique rests on the theory developed by Mie (1908) and Debye (1909), see also Stratton (1941) and Van de Hulst (1981), that deals with electromagnetic scattering solutions of plane waves by a sphere. In the case of the incident field this becomes

$$\mathbf{E}_0(\mathbf{r}) = \sum_{l,m} j_l(kr) \mathbf{X}_{l,m}(\Omega) \mathbf{e}_{l,m}, \quad (3.11)$$

where $\mathbf{e}_{l,m}$ are the familiar coefficients for the plane waves. The external field applied to a spherical inclusion embedded in a medium is the sum of the incident and scattered fields

$$\mathbf{E}_{ext}(\mathbf{r}) = \mathbf{E}_0(\mathbf{r}) + \mathbf{E}_{scatt}(\mathbf{r}), \quad (3.12)$$

where similarly to equ (3.11), the form of the scattered field is

$$\mathbf{E}_{scatt}(\mathbf{r}) = \sum_{l,m} h_l^{(1)}(kr) \mathbf{X}_{l,m}(\Omega) \mathbf{a}_{l,m}. \quad (3.13)$$

The internal field to the sphere is expanded as:

$$\mathbf{E}_{int}(\mathbf{r}) = \sum_{l,m} j_l(k_1 r) \mathbf{X}_{l,m}(\Omega) \mathbf{b}_{l,m}, \quad (3.14)$$

where

$$k = \frac{\omega}{c} \sqrt{\kappa_2}, \quad \text{and} \quad k_1 = k \sqrt{\kappa_1}. \quad (3.15)$$

In order to obtain the coefficients $\mathbf{e}_{l,m}$, $\mathbf{a}_{l,m}$, $\mathbf{b}_{l,m}$ it is convenient to rewrite all previous equations in matrix notation (Choy (1999)):

$$\begin{aligned} \mathbf{E}_0 &= \hat{\mathbf{X}}^{(T)}(\Omega) \hat{\mathbf{j}}(kr) \mathbf{e}, \\ \mathbf{E}_{scatt} &= \hat{\mathbf{X}}^{(T)}(\Omega) \hat{\mathbf{h}}(kr) \mathbf{a}, \\ \mathbf{E}_{int} &= \hat{\mathbf{X}}^{(T)}(\Omega) \hat{\mathbf{j}}(k_1 r) \mathbf{b}, \end{aligned} \quad (3.16)$$

where $\hat{\mathbf{X}}(\Omega)$ is a column vector and the superscript (T) is the transpose, $\hat{\mathbf{j}}$ and $\hat{\mathbf{h}}$ are diagonal matrices containing the spherical Bessel functions, and \mathbf{e} , \mathbf{a} , \mathbf{b} are column

vectors containing the $e_{l,m}$, $a_{l,m}$, $b_{l,m}$ coefficients as elements. By the use of the boundary conditions (3.8), we can determine the unknowns,

$$\begin{aligned}\hat{X}^{(T)}(\Omega) [\hat{\mathbf{j}}(ka)\mathbf{e} + \hat{\mathbf{h}}(ka)\mathbf{a}] &= \hat{X}^{(T)}(\Omega)\hat{\mathbf{j}}(k_1a)\mathbf{b}, \\ k\hat{X}^{(T)}(\Omega) [\hat{\mathbf{j}}'(ka)\mathbf{e} + \hat{\mathbf{h}}'(ka)\mathbf{a}] &= k_1\hat{X}^{(T)}(\Omega)\hat{\mathbf{j}}'(k_1a)\mathbf{b},\end{aligned}\quad (3.17)$$

where the primes denote matrices that contain the derivatives of the spherical Bessel functions. Equations (3.17) now simplify to

$$\begin{aligned}\hat{\mathbf{j}}(k_1a)\mathbf{b} &= [\hat{\mathbf{j}}(ka)\mathbf{e} + \hat{\mathbf{h}}(ka)\mathbf{a}], \\ k_r\hat{\mathbf{j}}'(k_1a)\mathbf{b} &= [\hat{\mathbf{j}}'(ka)\mathbf{e} + \hat{\mathbf{h}}'(ka)\mathbf{a}],\end{aligned}\quad (3.18)$$

where $k_r = k_1/k$. By inverting these expressions we obtain

$$\begin{aligned}\mathbf{a} &= [\hat{\mathbf{j}}(k_1a)\hat{\mathbf{h}}'(ka) - k_r\hat{\mathbf{j}}'(ka)\hat{\mathbf{h}}(ka)]^{-1} [k_r\hat{\mathbf{j}}'(k_1a)\hat{\mathbf{j}}(ka) - \hat{\mathbf{j}}(k_1a)\hat{\mathbf{j}}'(ka)]\mathbf{e}, \\ \mathbf{b} &= [\hat{\mathbf{j}}(k_1a)\hat{\mathbf{h}}'(ka) - k_r\hat{\mathbf{j}}'(ka)\hat{\mathbf{h}}(ka)]^{-1} [\hat{\mathbf{h}}'(k_1a)\hat{\mathbf{j}}(ka) - \hat{\mathbf{h}}(k_1a)\hat{\mathbf{j}}'(ka)]\mathbf{e}.\end{aligned}\quad (3.19)$$

The equation above allows us to define the T-matrix

$$\mathbf{a} = \hat{\mathbf{T}}\mathbf{e},\quad (3.20)$$

which means that the full external field can now be written as

$$\mathbf{E}_{ext} = \hat{X}^{(T)}(\Omega)\hat{\mathbf{j}}(kr)\mathbf{e} + \hat{X}^{(T)}(\Omega)\hat{\mathbf{h}}(kr)\hat{\mathbf{T}}\mathbf{e}.\quad (3.21)$$

Having completed our brief analysis of the one-sphere T-matrix, we are now able to examine the T-matrix for two-spheres in the next section.

3.2.2 The T matrix for two spheres

In this section we take a step closer to the study of the two-body problem with a view to include the results in existing EMT. While we consider the two-body effects in later Chapters from a slightly different perspective, eg, we consider multi-dimensional inclusions and not just spheres, we can appreciate the results by remaining faithful to the T-matrix method for 2-spheres. Observing eqn (3.21) more closely we see that it contains terms from both spheres:

$$\mathbf{E}_{ext} = \hat{X}^{(T)}(\Omega)\hat{\mathbf{j}}(kr_0)\mathbf{e} + \hat{X}^{(T)}(\Omega_1)\hat{\mathbf{h}}(kr_1)\mathbf{a}_1 + \hat{X}^{(T)}(\Omega_2)\hat{\mathbf{h}}(kr_2)\mathbf{a}_2,\quad (3.22)$$

where the first term is the usual incident field and the next two terms are the scattered fields from the two spheres, written in their self-coordinates, respectively. The fact that we are dealing with two-spheres means that we require translation formulae for shifting coordinates from one sphere to the other ⁴ (Danos and Maximon 1965). The required shift formulae take the form

$$\begin{aligned}\hat{\mathbf{X}}^{(T)}(\Omega_i)\hat{\mathbf{h}}(kr_i)\mathbf{a}_i &= \hat{\mathbf{X}}^{(T)}(\Omega_j)\hat{\mathbf{j}}(kr_j)\hat{\alpha}_{ji}\mathbf{a}_i, \\ \hat{\mathbf{X}}^{(T)}(\Omega_i)\hat{\mathbf{j}}(kr_i)\mathbf{a}_i &= \hat{\mathbf{X}}^{(T)}(\Omega_j)\hat{\mathbf{j}}(kr_j)\hat{\beta}_{ji}\mathbf{a}_i.\end{aligned}\quad (3.23)$$

Using these shift formulae, we can rewrite eqn (3.22) as

$$\mathbf{E}_{ext} = \hat{\mathbf{X}}^{(T)}(\Omega)\hat{\mathbf{j}}(kr_1)\hat{\beta}_{10}\mathbf{e} + \hat{\mathbf{X}}^{(T)}(\Omega_1)\hat{\mathbf{h}}(kr_1)\mathbf{a}_1 + \hat{\mathbf{X}}^{(T)}(\Omega_2)\hat{\mathbf{j}}(kr_1)\hat{\alpha}_{12}\mathbf{a}_2. \quad (3.24)$$

The first and last terms of eqn (3.24) can be combined to act as an incident field on the first sphere. Thus we can write the T-matrix in the form of a one-sphere solution as follows:

$$\mathbf{a}_1 = \hat{\mathbf{T}}_{1,(1)} [\hat{\beta}_{10}\mathbf{e} + \hat{\alpha}_{12}\mathbf{a}_2]. \quad (3.25)$$

We can derive a similar formula for the second sphere, which by symmetry (for equal spheres) is easily shown to be

$$\mathbf{a}_2 = \hat{\mathbf{T}}_{2,(1)} [\hat{\beta}_{20}\mathbf{e} + \hat{\alpha}_{21}\mathbf{a}_1], \quad (3.26)$$

where we have used a notation in which $\hat{\mathbf{T}}_{i,(1)}$ is the one-sphere T matrix for the i th sphere. Now eqns (3.25) and (3.26) can be inverted to give the two-sphere T matrices as

$$\mathbf{a}_1 = \hat{\mathbf{T}}_{1,(2)} [\hat{\beta}_{10}\mathbf{e}], \quad (3.27)$$

and

$$\mathbf{a}_2 = \hat{\mathbf{T}}_{2,(2)} [\hat{\beta}_{20}\mathbf{e}], \quad (3.28)$$

where these two-sphere T matrices are formally given by

$$\begin{aligned}\hat{\mathbf{T}}_{1,(2)}\hat{\beta}_{10}\mathbf{e} &= [\mathbf{I} - \hat{\mathbf{T}}_{1,(1)}\hat{\alpha}_{12}\hat{\mathbf{T}}_{2,(1)}\hat{\alpha}_{21}]^{-1} \hat{\mathbf{T}}_{1,(1)} [\hat{\beta}_{10} + \hat{\alpha}_{12}\hat{\mathbf{T}}_{2,(1)}\hat{\beta}_{20}] \mathbf{e}, \\ \hat{\mathbf{T}}_{2,(2)}\hat{\beta}_{20}\mathbf{e} &= [\mathbf{I} - \hat{\mathbf{T}}_{2,(1)}\hat{\alpha}_{21}\hat{\mathbf{T}}_{1,(1)}\hat{\alpha}_{12}]^{-1} \hat{\mathbf{T}}_{2,(1)} [\hat{\beta}_{20} + \hat{\alpha}_{21}\hat{\mathbf{T}}_{1,(1)}\hat{\beta}_{10}] \mathbf{e},\end{aligned}\quad (3.29)$$

⁴In later Chapters when we solve for the two body problem, we will derive such a shifting formula within a d dimensional framework.

and where the factor $\hat{\beta}_{i0}$ ensures that the incident field is in the coordinates of the i th sphere. As we have discussed in previous sections, the beauty of the T-matrix method is that we have used the one-sphere T-matrix results to obtain the two-sphere T-matrix. While the two-sphere problem will suffice for our needs here, for the sake of completeness a generalisation to the n -sphere T-matrix will be outlined in the next section.

3.2.3 The T matrix for n spheres

The two-sphere solutions were obtained by using the one-sphere results and it stands to reason that we can extend the process to n -spheres such that the field is given as (Choy (1999)):

$$\mathbf{E}_{ext} = \hat{\mathbf{X}}^{(T)}(\Omega)\hat{\mathbf{j}}(kr_0)\mathbf{e} + \sum_{i=1}^n \hat{\mathbf{X}}^{(T)}(\Omega_i)\hat{\mathbf{h}}(kr_i)\hat{\mathbf{T}}_{i,(n)}\hat{\beta}_{i0}\mathbf{e}. \quad (3.30)$$

The scattered field has been expressed in the self-coordinates of each sphere in terms of the incident field via the n -sphere T-matrix, $\hat{\mathbf{T}}_{i,(n)}$. The T-matrix for the $(n+1)$ -sphere can be obtained from that of the n th-sphere

$$\begin{aligned} \mathbf{E}_{ext} = & \hat{\mathbf{X}}^{(T)}(\Omega)\hat{\mathbf{j}}(kr_0)\mathbf{e} + \sum_{i=1}^n \hat{\mathbf{X}}^{(T)}(\Omega_i)\hat{\mathbf{h}}(kr_i)\hat{\mathbf{T}}_{i,(n+1)}\hat{\beta}_{i0}\mathbf{e} \\ & + \hat{\mathbf{X}}^{(T)}(\Omega_{n+1})\hat{\mathbf{h}}(kr_{n+1})\hat{\mathbf{T}}_{n+1,(n+1)}\hat{\beta}_{n+1,0}\mathbf{e}, \end{aligned} \quad (3.31)$$

where we have separated out the $(n+1)$ th term which, together with the first term, can be viewed as an incident field interacting with each of the $i = 1, 2, \dots, n$ spheres. By the use of eqn (3.27) and eqn (3.28) we now have

$$\hat{\mathbf{T}}_{i,(n+1)}\hat{\beta}_{i0}\mathbf{e} = \hat{\mathbf{T}}_{i,(n)} \left[\hat{\beta}_{i0}\mathbf{e} + \hat{\alpha}_{i,n+1}\hat{\mathbf{T}}_{n+1,(n+1)}\hat{\beta}_{n+1,0}\mathbf{e} \right], \quad (3.32)$$

where the i th sphere coordinates have been expressed by the shift formula given by eqn (3.23). The recursive procedure gives the final form for the T-matrix for n -spheres.

$$\begin{aligned} \hat{\mathbf{T}}_{n+1,(n+1)}\hat{\beta}_{n+1,0}\mathbf{e} = & \left[\mathbf{I} - \hat{\mathbf{T}}_{n+1,(1)} \sum_{i=1}^n \hat{\alpha}_{n+1,i} \hat{\mathbf{T}}_{i,(n)} \hat{\alpha}_{i,n+1} \right]^{-1} \\ & \times \hat{\mathbf{T}}_{n+1,(1)} \left[\hat{\beta}_{n+1,0} + \sum_{i=1}^n \hat{\alpha}_{n+1,i} \hat{\mathbf{T}}_{i,(n)} \hat{\beta}_{i,0} \right] \mathbf{e} \end{aligned} \quad (3.33)$$

Equations (3.32) and (3.33) now furnish a recursion algorithm, whereby $\hat{\mathbf{T}}_{i,(n+1)}$ for $i = 1, 2, \dots, n+1$, can all be calculated in terms of the previously known values

$\hat{\mathbf{T}}_{i,(n)}$ for $i = 1, 2, \dots, n$ (Chew *et al.* 1990, Mackowski 1991). It should be noted that this procedure requires $O(n^2 m^3)$ floating point operations, compared to other algorithms which are $O(n^3 m^3)$ (Peterson and Strom, 1973). Furthermore the results we obtain in later Chapters for not just spheres but hyperspheres can be compared to the technique studied in this Chapter in the long-wavelength limit, by replacing terms as follows (Chew *et al.* (1990)):

$$j_l(kr) \rightarrow r^l, \quad (3.34)$$

$$h_l(kr) \rightarrow r^{-(l+1)},$$

$$kj'_l(kr) \rightarrow lr^{l-1},$$

$$kh'_l(kr) \rightarrow -(l+1)r^{-(l+2)}. \quad (3.35)$$

The \mathbf{a} and \mathbf{b} column vectors have the elements which are now the familiar one-sphere values:

$$\begin{aligned} a_{lm} &= - \left[\frac{\epsilon_r - 1}{(l+1) + \epsilon_r l} \right] l a^{2l+1} e_{lm}, \\ b_{lm} &= \left[\frac{2l+1}{(l+1) + \epsilon_r l} \right] e_{lm}. \end{aligned} \quad (3.36)$$

The potential of one sphere is given by

$$\phi_{ext} = \mathbf{Y}^{(T)}(\Omega) \bar{\mathbf{r}} \mathbf{e} + \mathbf{Y}^{(T)}(\Omega) (\bar{\mathbf{r}} \mathbf{r})^{-1} \mathbf{T} \mathbf{e}, \quad (3.37)$$

where \mathbf{Y} is now the column vector containing the scalar spherical harmonics, $\bar{\mathbf{r}}$ is the vector containing the elements r^l , and \mathbf{T} is diagonal here, with elements,

$$T_{lm,l'm'} = - \left[\frac{\epsilon_r - 1}{(l+1) + \epsilon_r l} \right] l a^{2l+1} \delta_{lm,l'm'}. \quad (3.38)$$

For both the static case (Chew *et al.* 1990) and the dynamic case (Rouleau 1996) up to 30 spheres have been computed at the present time using modest computer systems. A deeper understanding of the dynamical case requires the use of Feynman diagrams which may prove useful in exploring extensions to EMT (see Choy (1999)). Either way, whatever method is used, the power of the T-matrix (or transition matrix) has proven so successful that it has been used extensively in various other

fields. For instance it is well known in the quantum theory of scattering where the T-matrix is used with the Heisenberg S-matrix formulation via the expression

$$\hat{S} = 1 + 2\hat{T}, \quad (3.39)$$

see N'yuton (1969). As previously discussed, the T-matrix connects the coefficients of the expansions of the scattered and incident fields in terms of a complete system of the vector basis functions, as compared to other techniques such as the coordinate representation in the integral equation method, where the scattered and incident fields are connected by the Green's function. In contrast to the latter, the T-matrix is easily extended to the many-body problem, thus it is of no surprise that it has become so popular starting with its application in the theory of EM scattering first pioneered by Waterman (1965,1969,1971,1979). Waterman's initial treatment used the Huygen principle for perfectly conducting (see Waterman (1965)) and dielectric (see Waterman (1969)) inclusions, which he later generalised and considered different ways of formulation of the equations without resorting to the Huygen's principle, Waterman (1979). Waterman's exhaustive treatment of the T-matrix approach also found favour within the area of optics especially after the noticeable paper by Barber and Yeh (1975) in which they formulated the method of Waterman based on the Shelkunov equivalence theorems in what has come to be known as the extended boundary condition method (EBCM). The EBCM and the T-matrix have now become synonymous. Work on generalising the T-matrix method for multi-particle systems has been undertaken by Kristensson and Stroem (1982), Stroem (1974) and Peterson and Stroem (1973), while Kristensson and Stroem (1982), Peterson and Stroem (1974) and Wang and Barber (1979) have studied multi-layered scatterers. Chiral particles of non-spherical shape are studied in the works of Lakhtakia (1991) and Lakhtakia *et al.* (1985). The convergence of the T-matrix method is rather inaccurate for non-spherical weakly absorbing particles, thus an iterative modification of the method has been put forward by Iskander *et al.* (1982) whose work has been developed further and applied to various systems, see Iskander and Lakhtakia (1984), Iskander *et al.* (1983) and Iskander *et al.* (1986). From a computational perspective, the convergence problem associated with non-spherical particles of large

size are due to the errors occurring in the calculations of the integrals defining the T-matrix, therefore it appears that a way out of this situation is to compute all numbers with very high precision, Mishchenko and Travis (1994), Mishchenko *et al.* (1994). The various advantages of the T-matrix technique in the analysis of multi-scattering wave theory can be found in the papers of Ma *et al.* (1988), Tsang (1984), Tsang and Kong (1982), Zardecki and Gerstl (1987), Tsang and Kong (1983), Varadan *et al.* (1979), Varadan *et al.* (1983), Varadan *et al.* (1984) and Varadan *et al.* (1987). Use of the T-matrix method in scattering by clusters of particles are dealt with in the papers by Cruz *et al.* (1989), Mishchenko and Mackowski (1996), Mishchenko and Mackowski (1994) and Mishchenko *et al.* (1995). For particles of irregular shape see the paper by Cooper *et al.* (1983). Finally, it is interesting to point out that our analysis in this section can be used to rederive the Bruggeman and Maxwell-Garnett approximations using the T matrix formulation.

3.3 Beyond the 1-body EMT: Other methods

Our search for a way to improve aspects of EMT has lead us to the study of scattering of multiple inclusions using the T-matrix method. No doubt there are other alternatives to this procedure that can prove useful as a way forward. One such alternative that is worth mentioning is that of competing interactions, or the coherent potential approximation (CPA). The coherent potential approximation is a very versatile technique that is used in many areas, eg, it is one of the best known of all the effective medium theories in elasticity (Hill (1965), Budiansky (1965)). Since throughout we have favoured spherical inclusions, it is interesting to add that these results are equivalent to those obtained by Korringa *et al.* (1979) and Berryman (1982) based on the CPA from the theory of alloys, see Gubernatis and Krumhansl (1975). However, these results can be misleading if the inclusions are not spherical in nature. Comparison of CPA and the self-consistent theory as used in elasticity for example, shows that the former is accurate in providing estimates that always lie between known rigorous bounds (Berryman (1982), Milton (1985)), such as the familiar Hashin-Shtrikman bounds (Hashin and Shtrikman (1961)). The latter, ie,

the self-consistent formulation is known to sometimes violate these bounds except in the case of spherical inclusions. The CPA has also been generalised for use in higher frequencies, see Kaelin and Johnson (1998a) and (1998b). At the same time dynamical effects can be represented in terms of magnetic and electric competing interactions respectively. For a time averaged energy \bar{U} , frequency ω and wavelength λ we can obtain competing interaction terms of magnetic type (Landau *et al.* (1984), see also Choy (1999)) as

$$\bar{U} = \frac{1}{16\pi} \int \left[\frac{\lambda^2}{\epsilon} |\text{curl}\mathbf{H}|^2 + \mu |\mathbf{H}|^2 \right] dV, \quad (3.40)$$

while competing interactions of the electric type can be represented by

$$\bar{U} = \frac{1}{16\pi} \int \left[\epsilon |\mathbf{E}|^2 + \frac{\lambda^2}{\mu} |\text{curl}\mathbf{E}|^2 \right] dV. \quad (3.41)$$

Choy (1999) does not make it clear as to what is competing with what in his formulation of the problem. It appears that the *curl* terms present in the above equations can be thought of as being a form of competing interactions. In order to understand why, we may look at such competing interactions in the context of spin glasses. Spin glasses form an important part of materials whose low-temperature state is a frozen disordered one. This type of state can occur if there is randomness and frustration among the different interactions between the spins (or magnetic moments). What is meant by frustration here is that no particular spin configuration is chosen by all the interactions. Magnetic impurity moments create such competing interactions. At a certain site you have a competing ferro-magnetic and anti-ferromagnetic interaction at the same time so that a particle will not know where to point. Analyzing the *curl* and non-*curl* terms at this site may point to the fact that these are competing interactions, ie, via the *curl* terms. The ferro-magnetic and anti-ferromagnetic forces present may destroy the simple order of each phase via the competition between these forces. As a consequence, that is when frustration sets in because the system cannot simultaneously satisfy all the interactions. It is worth pointing out that in the dynamical case, the system evolves slowly through different metastable states, and two time quantities, like spin-spin autocorrelations and responses to external fields, show a deterioration effect-see the fluctuation dissipation theorem (FDT) dealing

with this in the paper by Stariolo and Cannas (1999). Returning to the static case, we can similarly cater for this if we consider the external potential

$$\phi_{ext} = \mathbf{Y}^{(T)}(\Omega)\bar{\mathbf{r}}\mathbf{e} + \sum_{i=1}^n \mathbf{Y}^{(T)}(\Omega_i)\bar{\mathbf{r}}_i\beta_{i,0}\mathbf{T}_{i,(n)}\mathbf{e}. \quad (3.42)$$

For this static case the energy that the fields possess is given by

$$U_{ext} = \int \epsilon(\mathbf{r}) \left[\sum_{i=1}^n \Lambda_i \mathbf{T}_{i,(n)} + \sum_{i,j=1}^n \Xi_{ij} \mathbf{T}_{i,(n)} \mathbf{T}_{j,(n)} \right] dV, \quad (3.43)$$

where Λ_i and Ξ_{ij} are appropriate interaction matrices. The second term of (3.43) is that which represents the competing interactions. Befatto and Gallavotti (1995) show that (3.43) is particularly important for a system near the critical point where methods based on the *RG* theory have numerous applications. Thus, the issue of criticality is a major problem for which current EMT fails to satisfy, but if (3.43) is combined with Monte-Carlo *RG* techniques, it may yield a better result for conductivity or the dielectric constant (Ma (1976), Burkhart and van Leeuwen (1982)).

The problem associated with 1-body EMT may be resolved if we attempt to use the methods examined so far for the solution of the 2-body problem. Unfortunately even the 2-sphere problem is not as transparent as we would like when we try to incorporate the method to extend the Maxwell-Garnett theory or ATA approximation. From the results of Chapter 2 we can attempt to express the Maxwell-Garnett equation in terms of *n*-spherical inclusions in a medium as

$$\frac{\epsilon - \epsilon_0}{\epsilon + 2\epsilon_0} = \langle \mathbf{T}_{i,n} \rangle. \quad (3.44)$$

In fact for the 2-body result we can express this more concisely as

$$\frac{\epsilon - \epsilon_0}{\epsilon + 2\epsilon_0} = \eta_1 \frac{\epsilon_1 - \epsilon_0}{\epsilon_1 + 2\epsilon_0} (1 + \langle \mathbf{S}_{i,2} \rangle). \quad (3.45)$$

However, matters are not so simple since the term $\langle \mathbf{S}_{i,2} \rangle$ is not a straightforward calculation because the distribution of all the two-body inclusions in the medium must be known. Our basic desire is to try and improve the results in the low-density limit. Thus, in general, excluding the perfect-conducting limit, we can use the approximation

$$\langle \mathbf{S}_{i,2} \rangle = 2\eta_1 \sum_{s=0}^{\infty} \left(\frac{1}{2}\right)^{2s+3} \binom{s+2}{s} \left[\frac{\frac{\epsilon_1}{\epsilon_0} + 2}{\frac{\epsilon_1}{\epsilon_0}(s+1) + s + 2} \right], \quad (3.46)$$

which can be compared to the results presented later where our approach is via the use of a virial expansion for the dielectric function with the appropriate coefficients determined in d -dimensions. We can compare those results with the expansion for the dielectric function as obtained by the use of (3.46) in the low-density limit,

$$\varepsilon = \varepsilon_0 \left(1 + 3\eta_1 \frac{\varepsilon_1 - \varepsilon_0}{\varepsilon_1 + 2\varepsilon_0} \eta_1 + \kappa \eta_1^2 + \dots \right), \quad (3.47)$$

which might also help illuminate the problems associated with criticality. While different approaches have been undertaken to resolve these issues, some have not yielded the right outcome as in the case of the CPA theory of alloys mentioned in the previous sections (Elliot *et al.* (1974)). The failure to preserve the Herglotz property of the Green's functions has been identified as the major problem facing CPA theory in this area (Nickel and Butier (1973)). Mills and Ratanavararaksa (1978) have only succeeded in using this method for one dimensional linear arrays (Kaplan *et al.* (1980)). In the case of Bruggeman's theory, it appears that even the 2-body solutions are quite difficult to obtain, even though the requirement is rather simple. By using the T-matrix approach we require a self-consistent equation that includes n -body terms using the T-matrix, where the effective medium in question defines all the T-matrix components. Alternatively, still in the context of scattering, such an extension is possible by using the theory of strong permittivity fluctuations (SPF), see Kong (1986). The basic idea is to use (SPF) and incorporate the effects of scattering into an effective permittivity description of a binary composite mixture of spherical inclusions in a host medium. This is done by utilizing the low-density limit of the SPF theory in an iterative formulation that is analogous to that used to derive the asymmetric Bruggeman effective medium theory (McLachlan *et al.* (1992), Böttcher and Bordewijk (1978)). In the end, the method that one can use to address issues of criticality or the low-density limit correctly is reflected by the problems inherent in each theory. Questions arise as to the correctness of solutions and their feasibility because of analytical difficulties as is the case with CPA or convergence as in the case of the T-matrix approach after terms have been truncated. All this indicates that there is still a need to keep investigating other possibilities that might prove more useful, eg, variational bounds (Torquato (1985)) or Green's functions and

many others that we will not attempt to go into here. Exact results for the two-body T-matrix are now known (Choy *et al.* (1998a), and (1998b)), but further studies must be made so that existing EMT theories can improve with the addition of higher order interactions, giving more precise results than ever before. The ideas that have been expressed here on the basis of a mean-field approach where inhomogeneous inclusions are treated in essence as homogeneous ones embedded in a uniform field, have been extended by Huang *et al.* (2004) to the study of biological cells and colloidal particles. Huang *et al.* have presented a study of the electrokinetic behaviour of two touching inhomogeneous particles in suspension. By using the Tartar formula, see Milton (2002), the effective complex dielectric constant can be calculated exactly which can then be used in order to calculate the relevant dipole moment. Siu *et al.* (2001) have used the point-dipole approximation to compute the interparticle force for a polydisperse electrorheological fluid in terms of a pair of spheres of different dielectric constants and have as a consequence determined the force as a function of separation. However, the point dipole approximation they use does not consider many-body and multipolar interactions and it is for this reason that their results are erroneous in this limit. Siu *et al.* later show that the results can be improved considerably by the use of a multipole induced dipole model to calculate the force between the two spheres and compare the results to the empirical force expression of Klingenberg *et al.* (1990) with good agreement. Lo *et al.* (2001) have used a tetragonal lattice of point dipoles to examine the effects of geometric anisotropy on the local field distribution. Their results show that this geometric anisotropy greatly influences the local field distribution which results in the formulation of a more generalised Clausius-Mossotti equation. Further use of the image method has been made for a pair of dielectric spheres by Huang *et al.* (2002) who have studied the interaction of the two spheres while approaching each other in the presence of a rotating electric field. Non-linear effects have also been investigated, especially in the context of electrorheological fluids using a self-consistent mean field approach and the multipole method-see Gao *et al.* (2000). The latter takes into account the non-linearity of the host medium and the interparticle force is studied showing a

non-monotonic increase with higher electric fields. Investigations have also taken place on non-linear effects in electrorheological fluids by using an *ac* applied field by Wan *et al.* (2001a) and Wan *et al.* (2001b).

CHAPTER 4

Multipole Expansion Method

4.1 Introduction

There has been an enormous interest in the study of the properties of random mixtures or suspensions containing a low-volume fraction of inclusions since the time of Maxwell (1873). The problems concerned are applicable to the study of electrical conduction, thermal conduction, electric permittivity, magnetic permeability and others, by virtue of the universality of Laplace's equation. From now on we will specifically concentrate on the case of dielectric inclusions and solve for a binary system. In fact Maxwell (1873) provided the exact first-order coefficient to $O(c)$ for a system of spherical inclusions. It is worth mentioning here that other problems to $O(c)$ have attracted much interest as well, for example the $O(c)$ coefficient for the viscosity of a suspension containing a system of hard spheres was found by Einstein (1906). More recent exact results for the $O(c)$ coefficient of electrical conductivity for inclusions of other shapes in two dimensions were obtained by Thorpe (1992), using conformal mapping—a technique favoured by Maxwell himself. Most recently the dielectric behaviour of non-spherical inclusions has been made which might explicate some of the pitfalls of previous methods, Lei *et al.* (2001). The second-order coefficient $O(c^2)$ had been left on the sideline for nearly 100 years before any serious quantitative studies were made, original work being done by Batchelor (1972) and Batchelor and Green (1972). They studied the problem of suspensions in a fluid, a more complicated problem than the electrostatic one. In fact to this day very few exact results are known (Batchelor 1974, 1977). It is worth noting here that the second-order coefficient in which we are interested is related to the so-called Huggins coefficient κ_H for fluid suspensions, ie, the expansion of the viscosity is given by $\eta = \eta_0 (1 + [\eta]c + \kappa_H ([\eta]c)^2 + \dots)$, where $[\eta]$ is the first-order coefficient.

Unfortunately, no established name is given to the corresponding coefficient for the dielectric systems in the literature. We will define it to be κ , the quantity of central focus from now on, given by the low-volume fraction expansion as

$$\epsilon = \epsilon_0 (1 + [\epsilon]c + \kappa c^2 + \dots). \quad (4.1)$$

Here $[\epsilon]$ the first-order coefficient, as given by Maxwell (1873) can be written in a d -dimensional form as:

$$[\epsilon] = d\beta \equiv d \left(\frac{\epsilon_1 - \epsilon_0}{\epsilon_1 + (d-1)\epsilon_0} \right), \quad (4.2)$$

where β , the expression in brackets, is proportional to the polarizability associated with an isolated spherical inclusion with dielectric constant ϵ_1 in a host medium with dielectric constant ϵ_0 . Of particular interest to us here is the work of Jeffrey (1973), who essentially transferred the Batchelor-Green multipole expansion formalism to the more tractable problem of dielectric inclusions, by all accounts a classic work even to this day. Binns and Lawrenson (1973) and more recently Djordjević *et al.* (1996) have also studied this problem, but in two dimensions, where the method of images simplifies, leading to an infinite series with much better convergence properties than the multipole expansion method. Such a closed-form solution does not exist for higher dimensions as we will see later. Nonetheless, the image method is still very useful and it seems that a direct link between the method of images and the multipole expansions would provide additional insight, as well as a means to probe the poor convergence properties of the latter. The equivalence of the two methods will be demonstrated in the next Chapter.

The history of this problem seems to be plagued by a misunderstood conditionally convergent integral in the final expression for the dielectric function; a difficulty first encountered by Lord Rayleigh (1892) in his famous regular array of spheres problem. Batchelor (1972) and Jeffrey (1973) appear to favour a renormalization procedure to treat this problematic integral, while Felderhof *et al.* (1982) rederive their result, bypassing this difficulty via a virial series expansion analogous to those done in statistical mechanics. In this Chapter we will show that this apparent difficulty can be avoided following the earlier method of first integrating over orientations

(Djordjević *et al.* 1996). The troublesome divergent dipole integral term is removed naturally in this approach, and as part of the motivation for this work we will rederive and show complete agreement with Jeffrey (1973) for $d = 3$ and Djordjević *et al.* (1996) for $d = 2$. Furthermore we will generalize Jeffrey's solution to arbitrary dimensions d using some known and some newly derived properties of d -dimensional spherical harmonics. In this way we will see how all previous results for $d = 1, 2, 3$, can be developed on the basis of a general d -dimensional framework. In the next Chapter we will also derive results via a different method, ie, the method of images; albeit through a considerably more complex procedure than in the two-dimensional case of Djordjević *et al.* (1996). This method has the advantage of more rapid convergence than that of Jeffrey (1973) and can be shown to be equivalent to the latter via an order-by-order expansion for the polarization as a function of $\xi = \frac{a}{R}$, where a is the sphere radius and R the separation between the two spheres. It is as we shall see, computationally much more involved and less direct for $d > 2$.

One other reason why this work has been carried out is to derive and collect the results for arbitrary d for future studies of effective medium theories that seek to improve the poor value of κ , especially in the perfect-conducting limit. To this end, in what follows we will derive the general multipole expansion for arbitrary d and show how Jeffrey's (1973) solution can be generalized. Various mathematical results and theorems regarding d -dimensional spherical harmonics will be obtained along the way, which have been included in more detail in the appendices section. We then show results for the dimensions $d = 1, 2, 3$, and we discuss the results obtained for higher dimensions as well as study the trend of κ versus dimensionality.

4.2 Extending Jeffrey's solution to d -dimensions

The classical problem of two spheres of radii $a_{1,2}$ at a distance apart of R in a uniform electric field \mathbf{E} has been studied by a variety of methods in the past. Among these are: the method of bispherical coordinates (Jeffrey 1912; Moons and Spencer 1988; Morse and Feshbach 1953), the method of images (Binns and Lawrenson 1973; Landau *et al.* 1984) and the twin spherical harmonics expansion (Ross 1968,

Jeffrey 1973). Although Laplace's equation is separable in bispherical coordinates, this method turns out to be less well suited to the problem of two spheres, as the boundary conditions lead to a set of four simultaneous difference equations for which there are no known solution (Davis 1964). In fact the twin spherical harmonics expansion (Ross 1968) turns out to be the most appropriate method as long as a method for transferring spherical harmonics, as obtained by Hobson (1931) for $d = 3$ is generalizable. A major step is therefore to generalize Hobson's theorem to arbitrary d -dimensions, see Appendix A. Before proceeding any further a word about the method of images. The work of Djordjević *et al.* (1996) seems to show that this is a promising approach. Unfortunately as we shall see in the next Chapter, the general d -dimensional image method is not as mathematically and computationally convenient as the multipole series, except in appropriate limits; in particular when the inclusions are perfect-conductors or holes. However even in the case of the perfect-conducting limit, higher order calculations that are needed in order to achieve the required convergence to known values have proven to be complicated, due to the difficulty in mapping an infinite series of point charges and dipoles between the inclusions (Choy *et al.* 1998b). Recently this problem has been overcome and it is now possible to go to any order subject to computational power (Alexopoulos 2004). Lastly we mention that the image approach is also very useful in the weak scattering limit but more on all this in the next Chapter.

4.2.1 Parallel field case

We choose a coordinate system similar to the one of Jeffrey (1973), but instead we consider two *hyperspheres* embedded in a d -dimensional space, see Fig 4.1. Next we look at the case where the electric field \mathbf{E}_0 is parallel to \mathbf{R} , the vector joining the centres of the two spheres, which we take as the z -axis. The twin spherical harmonic expansion for the potential inside each sphere is given by

$$\Phi^{(i)} = E_0 z + \sum_{n=0}^{\infty} E_0 d_n^{(i)} \left(\frac{r_i}{a_i} \right)^n C_n^{p/2}(\cos \theta_i), \quad (4.3)$$

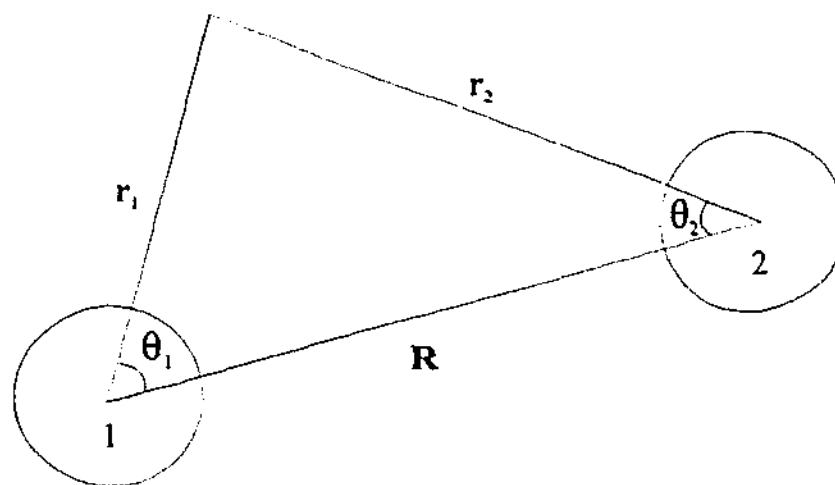


Figure 4.1: Twin spherical coordinates. We note that in d -dimensions there is a common azimuthal angle ϕ , around the line joining the two centres, and $p = d - 2$ polar angles. The two polar angles shown, θ_1 and θ_2 , have a special significance by virtue of the axial symmetry.

where $i = 1, 2$ labels the spheres, and the electric field is taken to be in the direction of the centres, 1 to 2, along the vector \mathbf{R} . For the potential outside the spheres,

$$\Phi = E_0 z + \sum_{n=0}^{\infty} E_0 \left[g_n^{(1)} \left(\frac{a_1}{r_1} \right)^n C_n^{p/2}(\cos \theta_1) + g_n^{(2)} \left(\frac{a_2}{r_2} \right)^n C_n^{p/2}(\cos \theta_2) \right]. \quad (4.4)$$

In the above equations, the $C_n^{p/2}(\cos \vartheta)$ are the Gegenbauer polynomials in the standard notation of Erdélyi (1953), but we will also refer to them as the generalized p -Legendre polynomial of order n (see Hochstadt 1971) and use the notation $P_n(\cos \vartheta)$ for similarity and simplicity. The coefficients $d_n^{(i)}$ and $g_n^{(i)}$ are to be found by the boundary conditions on the surface of each sphere, which require the continuity of the potential and its derivative normal to the surface, weighted with the appropriate dielectric constant. In order to achieve this goal, a key formula for the shifting of the spherical harmonics from one centre to the other has to be obtained. The proof of this formula is somewhat involved and the details are given in Appendix A. Suffice to say that it is a generalization of a theorem by Hobson (1931) and here we state the result:

$$\left(\frac{a_i}{r_i} \right)^{n+p} P_n(\cos \theta_i) = \left(\frac{a_i}{R} \right)^{n+p} \sum_{s=0}^{\infty} \binom{p+s+n-1}{p+s-1} \frac{r_{3-i}^s}{R} P_s(\cos \theta_{3-i}). \quad (4.5)$$

Using the formula in the boundary conditions and letting $\alpha_i = \frac{a_i}{a_0}$, we have the two equations,

$$d_n^{(i)} = g_n^{(i)} + \sum_{s=0}^{\infty} \binom{p+s+n-1}{p+s-1} \left(\frac{a_{3-i}}{R}\right)^{s+p} \left(\frac{a_i}{R}\right)^n g_s^{(3-i)}, \quad (4.6)$$

and

$$\alpha_i d_n^{(i)} + (1+pn)g_n^{(i)} - \sum_{s=0}^{\infty} \binom{p+s+n-1}{p+s-1} \left(\frac{a_{3-i}}{R}\right)^{s+p} \left(\frac{a_i}{R}\right)^n g_s^{(3-i)} = (-1)^i (\alpha_i - 1) \alpha_i \delta_{1,n} \left(\frac{1}{p}\right), \quad (4.7)$$

where we have used the property of the p -Legendre polynomial: $P_1(x) = px$ in deriving the latter formula. The solution for the coefficients $d_n^{(i)}$ and $g_n^{(i)}$ in eqn (4.6) and eqn (4.7) determine the potentials eqn (4.3) and eqn (4.4) uniquely. We can now consider the perpendicular field case.

4.2.2 Perpendicular field case

In defining the z -axis as the axis along the centre of the two spheres, the case of the electric field perpendicular to the axis admits $d - 1$ possible directions. It is clear that the $d - 1$ cases are degenerate because of the axial symmetry. Let us first set up the notation for the generalized associated p -Legendre polynomials as follows:

$$P_n^m(\cos \theta) = (-1)^m \sin^m(\theta) \left(\frac{d^m}{d(\cos \theta)^m}\right) P_n(\cos \theta). \quad (4.8)$$

Now the spherical harmonic expansion for the perpendicular case is dictated by the direction of the field in the following way. Recall that the polar coordinates in $d = p + 2$ dimensional space are related to the Cartesian coordinates by

$$\begin{aligned} x_{(0)} &= r \cos \theta_{(1)} \\ x_{(1)} &= r \sin \theta_{(1)} \cos \theta_{(2)} \\ x_{(2)} &= r \sin \theta_{(1)} \sin \theta_{(2)} \cos \theta_{(3)} \\ &\dots \end{aligned} \quad (4.9)$$

Then the multipole expansion we seek is

$$\Phi^{(i)} = E_0 x_{(j)} + \sum_{n=1}^{\infty} E_0 d_n^{(i)} \left(\frac{r_i}{a_i}\right)^n P_n^1(\cos \theta_{i,(j)}) \left[\frac{x_{(j)}}{r \sin \theta_{(1)}}\right]. \quad (4.10)$$

Without loss of generality we consider the most convenient choice with the perpendicular field along the first orthogonal axis $x_{(1)}$ (counting the zero), where $x_{(0)} = z$. Thus eqn (4.10) becomes

$$\Phi^{(i)} = E_0 x_{(1)} + \sum_{n=1}^{\infty} E_0 d_n^{(i)} \left(\frac{r_i}{a_i} \right)^n P_n^1(\cos \theta_{i,(2)}) \cos \theta_{i,(2)}. \quad (4.11)$$

This choice of axes is identical to that of Jeffrey (1973). The other choices can be treated in a similar way since the additional angles are superfluous when we come to match the boundary conditions, as they only require the continuity of the potential and its derivative along the radial \hat{r}_i directions. However, the calculation of the flux integrals for these cases is non-trivial. They need careful consideration in order to verify the flux formula for the perpendicular case in general. We can now write the potential outside the spheres as follows:

$$\Phi = E_0 x_{(1)} + \sum_{n=1}^{\infty} E_0 \left[g_n^{(1)} \left(\frac{a_1}{r_1} \right)^n P_n^1(\cos \theta_{1,(1)}) \cos \theta_{1,(2)} + g_n^{(2)} \left(\frac{a_2}{r_2} \right)^n P_n^1(\cos \theta_{2,(1)}) \cos \theta_{2,(2)} \right]. \quad (4.12)$$

The fundamental shift formula for this case is cumbersome to prove (see Appendix B). The result is given by the formula

$$\left(\frac{a_i}{r_i} \right)^{n+p} P_n^1(\cos \theta_i) = \left(\frac{a_i}{R} \right)^{n+p} \sum_{s=0}^{\infty} \binom{p+s+n-1}{p+s} \frac{r_{3-i}^s}{R^s} P_s^1(\cos \theta_{3-i}). \quad (4.13)$$

Using this result we can again match boundary conditions to obtain the analogous equations to eqn (4.6) and eqn (4.7) as

$$d_n^{(i)} = g_n^{(i)} + \sum_{s=1}^{\infty} \binom{p+s+n-1}{p+n} \left(\frac{a_{3-i}}{R} \right)^{s+p} \left(\frac{a_i}{R} \right)^n g_s^{(3-i)}, \quad (4.14)$$

and

$$\alpha_i d_n^{(i)} + (1+pn)g_n^{(i)} - \sum_{s=1}^{\infty} \binom{p+s+n-1}{p+n} \left(\frac{a_{3-i}}{R} \right)^{s+p} \left(\frac{a_i}{R} \right)^n g_s^{(3-i)} = (\alpha_i - 1) \alpha_i \delta_{1,n} \left(\frac{1}{p} \right). \quad (4.15)$$

In deriving the latter result, we have used the property of the associated p -Legendre polynomial: $P_1^1(\cos \theta) = -p \sin \theta$. Note that by virtue of the degeneracy mentioned above, all $d_n^{(i)}$ and $g_n^{(i)}$ are identical for any perpendicular direction of the

field. To complete the solution we now have to evaluate the flux integral for each sphere given by

$$\mathbf{S}_{\parallel}^{(i)} = \varepsilon_0(\alpha_i - 1) \int \nabla \Phi^{(i)} dV \quad (4.16)$$

where the integral is over the volume of the sphere (Jeffrey 1973). We now recall that the d -dimensional gradient operator is given by (Erdélyi *et al.* 1953)

$$\begin{aligned} \nabla = \hat{r} \frac{\partial}{\partial r} + \hat{\theta}_{(1)} \frac{1}{r} \frac{\partial}{\partial \theta_{(1)}} + \hat{\theta}_{(2)} \frac{1}{r \sin \theta_{(1)}} \frac{\partial}{\partial \theta_{(2)}} + \hat{\theta}_{(3)} \frac{1}{r \sin \theta_{(1)} \sin \theta_{(2)}} \frac{\partial}{\partial \theta_{(3)}} \\ + \dots + \hat{\theta}_{(p)} \frac{1}{r \sin \theta_{(1)} \sin \theta_{(2)} \dots \sin \theta_{(p-1)}} \frac{\partial}{\partial \theta_{(p)}}. \end{aligned} \quad (4.17)$$

4.2.3 Parallel flux integral

It is necessary to consider the parallel and perpendicular cases separately. The parallel case is the simpler case as here the potential depends only on r and θ . We thus have

$$\begin{aligned} \int \nabla \Phi^{(i)} dV = \frac{\omega_p a_i^d}{d} E_0 \hat{z} + \int \sum_{n=1}^{\infty} E_0 d_n^{(i)} \left(\frac{nr_i^{n-1}}{a_i^n} \right) P_n(\cos \theta_i) dV \hat{r} \\ + \int \sum_{n=1}^{\infty} E_0 d_n^{(i)} \left(\frac{r_i^{n-1}}{a_i^n} \right) P_n^1(\cos \theta_i) dV \hat{\theta}_i, \end{aligned} \quad (4.18)$$

where $\omega_p = 2\pi^{1+p/2}/\Gamma(1 + \frac{1}{2}p)$ is the p -solid angle. Using the d -dimensional volume element, we note that only the projections of all unit vectors onto the \hat{z} direction survive the angular integrations. Then we can obtain

$$\begin{aligned} \int \nabla \Phi^{(i)} dV = \frac{\omega_p a_i^d}{d} E_0 \hat{z} \\ + \omega_{p-1} \sum_{n=1}^{\infty} E_0 d_n^{(i)} \left(\frac{na_i^{p+1}}{n+p+1} \right) \int \sin^p \theta_i \cos \theta_i P_n(\cos \theta_i) d\theta_i \hat{z} \\ - \omega_{p-1} \sum_{n=1}^{\infty} E_0 d_n^{(i)} \left(\frac{na_i^{p+1}}{n+p+1} \right) \int \sin^p \theta_i \sin \theta_i P_n^1(\cos \theta_i) d\theta_i \hat{z}. \end{aligned} \quad (4.19)$$

Using the orthogonal properties of the p -Legendre polynomials, we see that only the $n = 1$ term survives, with the result

$$\begin{aligned} \int \nabla \Phi^{(i)} dV = \frac{\omega_p a_i^d}{d} E_0 + \omega_{p-1} E_0 d_1^{(i)} \left(\frac{a_i^{p+1}}{d} \right) \\ \times \left[\int \sin^p \theta_i p \cos^2 \theta_i d\theta_i + \int \sin^p \theta_i p \sin^2 \theta_i d\theta_i \right] \hat{z} \\ = \frac{\omega_p a_i^d}{d} E_0 \hat{z} \left[1 + \frac{d_1^{(i)}}{a_i} p \right]. \end{aligned} \quad (4.20)$$

From the parity of the polar angles in Fig 4.1, we obtain the final result for the parallel flux,

$$S_{\parallel}^{(i)} = v_i^d E_0 \epsilon_0 (\alpha_i - 1) \hat{z} \left[1 + (-1)^{3-i} \frac{d_1^{(i)}}{a_i} p \right], \quad (4.21)$$

where the volume of the sphere i is denoted by $v_i^d = \omega_p a_i^d / d$.

4.2.4 Perpendicular flux integral

The flux integ: ' for the perpendicular case is quite troublesome to explain. By using the results obtained for the case where the field is along $x_{(1)}$, all other cases follow by symmetry arguments. That is to say, that all perpendicular directions are equivalent. Let us first consider sphere 1. From eqn (4.11), the gradient of $\Phi^{(1)}$, say, is given by

$$\begin{aligned} \nabla \Phi^{(1)} = & E_0 \hat{x}_{(1)} + \sum_{n=1}^{\infty} E_0 d_n \left(\frac{n r_1^{n-1}}{a_1^n} \right) P_n^1(\cos \theta_{(1)}) \cos \theta_{(2)} \hat{r} \\ & + \sum_{n=1}^{\infty} E_0 d_n \left(\frac{r_1^{n-1}}{a_1^n} \right) \frac{\partial P_n^1(\cos \theta_{(1)})}{\partial \theta_{(1)}} \cos \theta_{(2)} \hat{\theta}_{(1)} \\ & - \sum_{n=1}^{\infty} E_0 d_n \left(\frac{r_1^{n-1}}{a_1^n} \right) P_n^1(\cos \theta_{(1)}) \frac{\sin \theta_{(2)}}{\sin \theta_{(1)}} \hat{\theta}_{(2)}, \end{aligned} \quad (4.22)$$

where all quantities are understood to refer to sphere 1. Here again the integral $\int dV$ projects out only the $x_{(1)}$ terms due to the orthogonality of integrals of the type $\int \sin^p \theta \cos \theta d\theta = 0$. This can be seen easily by writing down the unit vectors $\hat{r}, \hat{\theta}_{(1)}, \hat{\theta}_{(2)}, \dots$ etc., in the original Cartesian basis. The result with $i = 1$ or 2, looks somewhat like eqn (4.18):

$$\begin{aligned} \int \nabla \Phi^{(1)} dV = & \frac{\omega_p a_i^d}{d} E_0 \hat{x}_{(1)} \\ & + \int \sum_{n=1}^{\infty} E_0 d_n^{(i)} \left(\frac{n r_i^{n-1}}{a_i^n} \right) P_n^1(\cos \theta_i) \sin \theta_{i,(1)} \cos^2 \theta_{i,(2)} dV \hat{x}_{(1)} \\ & + \int \sum_{n=1}^{\infty} E_0 d_n^{(i)} \left(\frac{r_i^{n-1}}{a_i^n} \right) \frac{\partial P_n^1(\cos \theta_i)}{\partial \theta_{i,(1)}} \cos \theta_{i,(1)} \cos^2 \theta_{i,(2)} dV \hat{x}_{(1)} \\ & + \int \sum_{n=1}^{\infty} E_0 d_n^{(i)} \left(\frac{r_i^{n-1}}{a_i^n} \right) \frac{P_n^1(\cos \theta_i)}{\sin \theta_{i,(1)}} \sin^2 \theta_{i,(2)} dV \hat{x}_{(1)}, \end{aligned} \quad (4.23)$$

but there are enough differences to need more work. We first perform the $\theta_{(2)}$ integration and using the results

$$\int \sin^{p-1} \theta_{(2)} \cos^2 \theta_{(2)} d\theta_{(2)} = \frac{1}{p+1} \int \sin^{p-1} \theta_{(2)} d\theta_{(2)}, \quad (4.24)$$

and

$$\int \sin^{p+1} \theta_{(2)} d\theta_{(2)} = \frac{p}{p+1} \int \sin^{p-1} \theta_{(2)} d\theta_{(2)}, \quad (4.25)$$

the factors $\int \sin^{p-1} \theta_{(2)} d\theta_{(2)}$ can now be reabsorbed back into the volume integral, so that eqn (4.23) becomes

$$\begin{aligned} \int \nabla \Phi^{(1)} dV = v^d E_0 \hat{x}_{(1)} + \frac{1}{p+1} \int \sum_{n=1}^{\infty} E_0 d_n^{(i)} \left(\frac{nr_i^{n-1}}{a_i^n} \right) P_n^1(\cos \theta_i) \sin \theta_{i,(1)} dV \hat{x}_{(1)} \\ + \frac{1}{p+1} \int \sum_{n=1}^{\infty} E_0 d_n^{(i)} \left(\frac{r_i^{n-1}}{a_i^n} \right) \frac{\partial P_n^1(\cos \theta_i)}{\partial \theta_{i,(1)}} \cos \theta_{i,(1)} dV \hat{x}_{(1)} \\ + \frac{p}{p+1} \int \sum_{n=1}^{\infty} E_0 d_n^{(i)} \left(\frac{r_i^{n-1}}{a_i^n} \right) \frac{P_n^1(\cos \theta_i)}{\sin \theta_{i,(1)}} dV \hat{x}_{(1)} \end{aligned} \quad (4.26)$$

Upon grouping the terms, we find that the integrand is an expression containing the p -Legendre polynomials of the form

$$n \sin \theta_{(1)} P_n^1 + \cos \theta_{(1)} \frac{\partial P_n^1}{\partial \theta_{(1)}} + \frac{p}{\sin \theta_{(1)}} P_n^1 \quad (4.27)$$

$$= \left(n \sin \theta_{(1)} + \frac{p}{\sin \theta_{(1)}} \right) \frac{\partial P_n^1}{\partial \theta_{(1)}} + \cos^2 \theta_{(1)} \frac{\partial^2 P_n^1}{\partial \theta_{(1)}^2}, \quad (4.28)$$

where we have suppressed the arguments of the p -Legendre polynomials for convenience. Further progress requires the use of the p -Legendre differential equation which is given by

$$\frac{1}{\sin^p \theta} \frac{d}{d\theta} \left(\sin^p \theta \frac{dP_n^1}{d\theta} \right) + n(n+p)P_n^1 = 0 \quad (4.29)$$

(see Appendix A). Using this expression eqn (4.28) can be integrated, again employing the orthogonality properties of the p -Legendre functions, we obtain

$$(n+p) \int \sin^p \theta_{(1)} \left(\sin \theta_{(1)} \frac{dP_n^1}{d\theta_{(1)}} - n \cos \theta_{(1)} P_n^1 \right) d\theta_{(1)} = -p(1+p) \int \sin^p \theta_{(1)} d\theta_{(1)}. \quad (4.30)$$

The latter, we see again, can be reabsorbed back into the volume integral. Similar considerations apply to sphere 2, which has no parity difference in this case. Thus for the perpendicular flux in the direction $\hat{x}_{(1)}$, we have

$$S_{\perp}^{(i)} = v_i^d E_0 \epsilon_0 (\alpha_i - 1) \hat{x}_{(1)} \left[1 - \frac{d_1^{(i)}}{a_i} p \right]. \quad (4.31)$$

This result is primary to all subsequent derivations of the flux integrals in *arbitrary* perpendicular directions, which also reduce in this case, as expected from symmetry considerations (see Appendices section). Hence for the field in an arbitrary perpendicular axis $\hat{x}_{(j)}$, where $j = 1, 2, 3, \dots, (p+1)$, the flux integral takes the form

$$\mathbf{S}_{\perp}^{(i)} = v_i^d E_0 \epsilon_0 (\alpha_i - 1) \hat{x}_{(j)} \left[1 - \frac{d_1^{(i)}}{a_i} p \right]. \quad (4.32)$$

Using all the results that we have so far, we are in a good position to move closer to the derivation of the dielectric function κ to $O(c^2)$. We shall do this in the next section.

4.3 Symmetrical bihyperspheres

The results in the previous sections generalize the Jeffrey solution to d -dimensions. For the remainder of this thesis we will concentrate on the symmetrical case, ie, where $a_1 = a_2 = a$ and $\epsilon_1 = \epsilon_2$ so that $\alpha_i = \alpha = \epsilon_1/\epsilon_0$. In this case we can easily eliminate $d_{m,n}$ from eqn (4.6), eqn (4.7), eqn (4.14) and eqn (4.15), and by symmetry, we can replace

$$g_{m,n}^{(1)} = (-1)^{(m-1)} g_{m,n}^{(2)} = a g_{m,n}, \quad (4.33)$$

where following Jeffrey (1973), we have used the notation $g_{m,n}$, with $m = 0, 1$ for the parallel-field and perpendicular-field case respectively. Since $g_{m,0} = 0$, as there are no point charges within the spheres, we obtain by straightforward manipulations the overall expression

$$(-1)^{(m-1)} p g_{m,n} + \beta_n \sum_{s=1}^{\infty} \binom{n+p+s-1}{n+p+m-1} p g_{m,s} \left(\frac{a}{R} \right)^{n+p+s} = \beta_n \delta_{1,n}. \quad (4.34)$$

In eqn (4.34), the β_n is a generalized polarizability that is given by

$$\beta_n = \frac{n(\alpha - 1)}{n\alpha + n + p}. \quad (4.35)$$

Using the expression for $d_{m,n}$ obtained above, we can show that the formula for the flux integrals eqn (4.21) and eqn (4.32) is

$$\mathbf{S}_m = v^d \mathbf{E}_m \epsilon_0 (p+2) (-1)^{m-1} p g_{m,1}, \quad (4.36)$$

where $m = 0, 1$ for the parallel and perpendicular cases as before. Notice that the quantity $pg_{m,1}$ is very important, but to obtain the latter we need to solve the system of eqn's (4.34). This has to be achieved by expanding the $g_{m,n}$ as a power series in $\xi = a/R$. The result of this expansion can be written in the form

$$\mathbf{S}(\mathbf{R}) = v^d \left[d\beta_1 \epsilon_0 \mathbf{E} - d\beta_1 \epsilon_0 \sum_{s=d}^{\infty} \left(\frac{a}{R} \right)^s \left(A_s \mathbf{E} - B_s \frac{\mathbf{E} \cdot \mathbf{R}}{R^2} \mathbf{R} \right) \right] \quad (4.37)$$

(Batchelor 1972; Jeffrey 1973), where $\beta_1 = \beta$ and we have here explicitly emphasized the \mathbf{R} dependence in \mathbf{S} . The first few coefficients in the above expansion are readily obtained:

$$\begin{aligned} A_d &= \beta_1, & A_{d+1} &= A_{d+2} = \dots = A_{2d-1} = 0, \\ A_{2d} &= -\beta_1^2, & A_{2d+1} &= 0, & A_{2d+2} &= -d\beta_1\beta_2\dots, \\ B_d &= d\beta_1, & B_{d+1} &= B_{d+2} = \dots = B_{2d-1} = 0, \\ B_{2d} &= dp\beta_1^2, & B_{2d+1} &= 0, & B_{2d+2} &= \frac{1}{2}d(d+1)p\beta_1\beta_2\dots, \end{aligned} \quad (4.38)$$

and so on. The structure of eqn (4.37) deserves some further attention. It has the form of a dipole flux field, the first term being the trivial single hypersphere polarizability eqn (4.2) and the rest are due to the two-hypersphere interactions. The first term of the latter is the bare dipole field from the second hypersphere and it corresponds to the first image correction in image theory (see next Chapter). All subsequent terms can be viewed as corrections due to multiple images. This is particularly obvious in two dimensions where all the B 's vanish for $s > 2$. The resultant series can be put into one-to-one correspondence with the continued fraction expansion results of Djordjević *et al.* (1996). The relation to image theory for $d > 2$ is more complicated and will be discussed in the next Chapter.

We proceed by performing the angular averages first, by necessity the first action we must take, as the leading first-image dipole term diverges. The justification for this is that it reproduces the results of Batchelor (1972) and Jeffrey (1973) and should thus be equivalent to their more complicated renormalization procedure. Alternatively, one can use the approach of Lord Rayleigh (1892) by considering a finite sample L which is taken to ∞ at the end of the calculation. In performing

the angular average, we observe that the field \mathbf{E} and the vector \mathbf{R} together define a hypersurface in d -space. In view of the degeneracy of this surface, we can for convenience choose the simplest case for the perpendicular field; the other cases correspond to a rotation about the symmetry axis. Thus the average flux is given by

$$\bar{S} = n \int_{2a}^{\infty} R^{d-1} dR \int d\Omega_p (\cos^2 \theta \mathbf{S}_{\parallel} + \sin^2 \theta \mathbf{S}_{\perp}), \quad (4.39)$$

where n is the number of hyperspheres per unit volume; θ is understood to be the first polar angle $\theta_{(1)}$ and $d\Omega_p$ is an element of solid angle.

We make the remark here that this averaging procedure corresponds to a well-stirred suspension in which the second hypersphere is allowed to occupy all positions with equal probability, subject only to a *hard-sphere* constraint. This is the same as saying that the usual pair correlation function is unity, unless the centres of the hyperspheres are closer than the sum of the two radii, in which case the pair correlation function is zero. Without additional input from the process of manufacture or microstructural information on the sample, this seems to be a reasonable assumption and is used widely. After performing the angular integrals, the divergent term is eliminated and we have the net result

$$\bar{S} = v^d d\beta \varepsilon_0 c \sum_{s=2d} \frac{B_s - dA_s}{(s-d)2^{s-d}}. \quad (4.40)$$

This expression corresponds to the averaged dipole moment $\bar{\mathbf{P}}'$ of Djordjević *et al.* (1996). Following similar arguments using a Clausius-Mossotti-type formula, we now have the d -dimensional dielectric function to $O(c^2)$:

$$\varepsilon = \varepsilon_0 \left[1 + d \left(\frac{\varepsilon_1 - \varepsilon_0}{\varepsilon_1 + (d-1)\varepsilon_0} \right) c + d\beta \left(\beta + \sum_{s=2d} \frac{B_s - dA_s}{(s-d)2^{s-d}} \right) c^2 + \dots \right], \quad (4.41)$$

where κ from eqn (4.41) is defined to be

$$\kappa = d\beta \left(\beta + \sum_{s=2d} \frac{B_s - dA_s}{(s-d)2^{s-d}} \right). \quad (4.42)$$

In two dimensions, all β_n collapse to β and as we shall see later on as part of our results, the sum given by eqn (4.42) above, corresponds with Djordjević *et al.* (1996), up to 100 terms and more. In three dimensions we succeed in reproducing

the results of Jeffrey (1973) and in one dimension, $\kappa = \beta^2$, which is an exact result. The conductances, which are equivalent to the dielectric constants add in parallel to give $c/c_0 = (1 - c\beta)^{-1}$, and all β_n reduce to $1 - (1/\alpha)$ and only the parallel case with $g_1 = \beta$ survives the limit. In later Chapters we will thus show that the results derived here are verified against all known limits. Furthermore we will look at limits of particular interest such as that for the perfect-conductor, where $\alpha \rightarrow \infty$ and thus $\beta \rightarrow 1$. Another interesting limit is that for *holes*, where $\alpha \rightarrow 0$. The two-dimensional case is unique here, as all $\beta_n \rightarrow -1$, and there is a duality relation: $\kappa - 2$ for holes and $2 - \kappa$ for perfect-conducting inclusions (see eqn (4.42)). Hence, the sum of the κ for holes and perfect-conducting inclusions is 4 in two dimensions. This duality however, does not hold in other dimensions. Before proceeding any further, we will discuss higher dimensions in the next section.

4.4 Higher dimensions

Results have been calculated for $d = 4$ and as we shall see later, convergence is better at the *holes* limit and poorer at the perfect-conducting limit. In fact for the latter, we see that the convergence for $d = 4$ is even slower than for the $d = 3$ case. This all brings us to the question of the large d -limit. The eqn's (4.34) are somewhat difficult to study in the limit $d \rightarrow \infty$. One may think that the interaction between the hyperspheres will vanish, and this is essentially what happens. Here and in later Chapters we will define the function $F_d(\beta)$ via

$$\kappa = d\beta^2 + \beta^3 F_d(\beta), \quad (4.43)$$

so that from eqn (4.42) we have

$$F_d(\beta) = \frac{d}{\beta^2} \sum_{s=2d} \frac{B_s - dA_s}{(s-d)2^{s-d}}. \quad (4.44)$$

The method we use for computing the coefficients becomes increasingly inefficient as d increases, and thus it is difficult to answer that question concerning the behaviour of $F_d(\beta)$ as d increases, but we show in the next Chapter that the simple law of mixtures is recovered as $d \rightarrow \infty$. This is equivalent to saying that $\kappa \rightarrow 0$ as $d \rightarrow \infty$,

which will become clear for $\alpha < 1$. For $\alpha > 1$, the rise in κ moves out to higher and higher α as the dimension d increases. Hence $\kappa \rightarrow 0$ for all d as $d \rightarrow \infty$.

In conclusion, we have studied the dielectric function for the bi-hyperspherical system in arbitrary integer dimensions d . We have shown that Jeffrey's (1973) solution can be generalized once the required mathematical results regarding d -dimensional spherical harmonics are obtained as given in the appendices. We will see explicitly that our results are in agreement with the previous work of Jeffrey (1973) for $d = 3$, and Djordjević *et al.* (1996) for $d = 2$. We have shown that the limiting behaviour is simple as both $d \rightarrow 1$ and $d \rightarrow \infty$. Our approach allows results to be obtained for general d ; albeit as an infinite series that converges somewhat slowly. Nevertheless, the d dependence is shown explicitly as d appears as a parameter throughout this body of work. Finally, the multipole approach used in this Chapter will be compared with the image method in the next.

CHAPTER 5

Method of Images

5.1 Introduction

The method of images is a well-known technique for the solution of problems in classical electrostatics (Jackson 1975; Landau *et al.* 1984) and the electromagnetic theory, with applications in various areas including scanning tunnelling microscopy STM (Kalotas *et al.* 1996), antennae (Slater 1942) and so on. The latter, as an application of images in dynamical cases, is particularly interesting and offers useful insight for the analysis of fundamental forces, like the Van der Waals attraction of atoms and molecules near surfaces (den Hertog and Choy 1995). The theory of images was initiated by Lord Kelvin (Thomson) (1848), who must have been the first to observe that the potential due to a charge Q outside a perfect conducting sphere in three dimensions is mathematically equivalent to that due to two point charges. One of these is at the image point $d_K = a^2/R$ with charge $Q_K = -aQ/R$, where a is the radius of the sphere and R is the distance of the charge from the centre. The other point charge equal to $-Q_K$, assuming the sphere is uncharged, is located at the centre of the sphere. This result is in fact valid for any dimension d , as is evident by examining the proofs in standard texts (Jackson 1975; Landau *et al.* 1984, see also the work presented in this Chapter). Point charges solve the case of a point charge outside a dielectric disc in two dimensions *only* (Binns and Lawrenson 1973).

Less known is the case of a dielectric sphere and the first results for three dimensions are hidden in an old classic text of Carl Neumann (1883). Generalization of Kelvin images for a dielectric sphere is rather non-trivial. A modern discussion of this subject, relevant to our study of the bi-spherical system, can be found in Lindell (1993) and Bussemer (1994), whose results are crucial to the work presented here.

Suffice to say that the image of a point charge outside a dielectric sphere is a point charge at the image point d_K , plus a line charge $\rho(z)$ from d_K to the centre O , with a power law following Lindell (1993). Thus in general the image of dipoles outside a dielectric sphere will lead to line charges and line dipoles, a highly complicated affair. From this viewpoint, in the unique case of two dimensions, Neumann's theory reduces to Kelvin's theory. Especially intriguing is the fact that when only the parallel dipole configurations are considered, the $d = 2$ case is really quite simple by comparison to $d > 2$, even for the perfect-conductor.

In this Chapter we will continue the study of the previous Chapter by exploiting some of these image results and their non-trivial extensions to the bi-spherical system in an arbitrary d -dimensional space. We will demonstrate that the method of images furnishes a complementary approach to the multipole moment expansion solution derived earlier and that it simultaneously offers a better convergence and some new physical insight, albeit at the expense of greater mathematical complexity. Moreover, this theory, the author believes, will serve as the basis in some future work for the study of the resummation of the slowly convergent series for κ in the previous Chapter. The results that will be presented in subsequent sections, were initially motivated by the work of Djordjević *et al.* (1996), who applied an image theory of dipoles (Binns and Lawrenson 1973) to study the bi-spherical system in two dimensions. That the method of Djordjević *et al.* (1996) cannot be extended readily to arbitrary integer dimensions follows from our previous remarks about the complexity of line dipole images in general for $d > 2$.

In what is to follow we explore the image of dipoles outside a d -dimensional sphere. We discuss higher-order dipole images for any dimension d and dielectric constant ϵ up to the third reflection image \mathbf{p}_3 . We will formulate, but not solve, both the perpendicular and parallel configurations in general. Unfortunately, this formulation, though elegant, does not seem to be amenable to an iterative solution beyond \mathbf{p}_4 , except in the perfect-conductor limit. We will then show, in the case of the latter limit, the method that allows us to calculate all images up to the 23^{rd} reflection image \mathbf{p}_{23} , the results will in the end be shown to agree with those of the

previous Chapter. At the same time we will derive mathematical expressions that will allow higher-order calculations to be carried out (Alexopoulos 2004) subject to available computing power, while the general dielectric case appears intractable. We will then consider a *weak – scattering* approximation, which is good everywhere and particularly so in the *holes* limit. We furthermore simplify the integral that appears in the weak scattering limit, to obtain a very simple algebraic approximation for κ that is useful for all d and for all ratios $\alpha = \epsilon_1/\epsilon_0$, where ϵ_1 is the dielectric constant of the inclusion, and ϵ_0 is the dielectric constant of the host medium. We are reminded that we will be treating the symmetrical case of bi-hyperspheres, as we have done for the multipole expansion method earlier and eventually the results of the two methods will be compared. We will conclude this Chapter with some discussion of higher-dimensional images, other limits and a few interesting questions that arise from this work.

5.2 Image theory in d -dimensions

In this section we discuss the extension of the Neumann image theory due to point charges in d dimensions. Subsequently, we use this theory to derive images for dipoles, which is of major interest to us here.

5.2.1 Neumann images of a point charge

We will begin any discussions here by summarizing the results (see Appendix D) for the d -dimensional extensions of the Neumann image theory. This is an important first step, as the line charge image theory of Neumann was originally derived only in *three* dimensions. *A priori*, there are no reasons to expect that in higher dimensions these line charges *do not* transform into hypersurfaces of higher dimension than one. If this were not the case, the mathematical complexity of the present work would have been unmanageable. Fortunately, as we can see from Appendix D, for a point charge Q outside a d -dimensional dielectric sphere (see Fig 5.1) whose permittivity is ϵ_1 , there exists an image point charge at the image point d_K given by

$$Q_K = -Q \left(\frac{\alpha - 1}{\alpha + 1} \right) \left(\frac{a}{R} \right)^{d-2}, \quad (5.1)$$

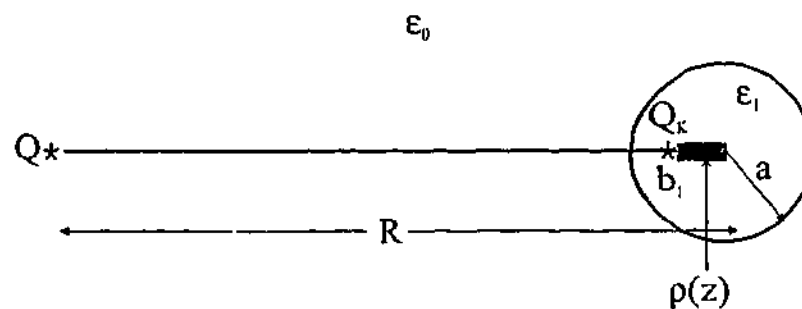


Figure 5.1: The Neumann image for a point charge Q outside a d -dimensional sphere. The origin is at the centre of the hypersphere, and the point image Q_K and the line image $\rho(z)$ are shown.

where $\alpha = \epsilon_1/\epsilon_0$ is the relative permittivity between the hypersphere and the medium. In addition, there exists a *line* image from the centre O to the image point d_K , which we rename here as $b_1 = d_K = a^2/R$, given by the charge density

$$\rho(z) = \left(\frac{Q}{a}\right) \left(\frac{a}{R}\right)^{d-3} (d-2) \frac{\alpha-1}{(\alpha+1)^2} \left(\frac{z}{b_1}\right)^{(d-3-\alpha)/(\alpha+1)} \quad (5.2)$$

These results are very elegant, because they appear as minor modifications to the three-dimensional Neumann image theory. Furthermore the following points should be noted:

1. The image charge Q_K diminishes with dimensionality d since $a < R$ for non-overlapping hyperspheres.
2. The image line charge $\rho(z)$ is a *one*-dimensional line density only, that reduces to a point charge $-Q_K$ at the origin for $d = 2$, and the result becomes that of Binns and Lawrenson (1973).
3. The image charge has a power-law density distribution which depends *both* on d and on α while the polarizability factor, $(\alpha-1)/(\alpha+1)$ is that of the *two*-dimensional sphere.
4. In the perfect-conducting limit $\alpha \rightarrow \infty$, the line charge density $\rho(z)$ vanishes for all d except for the survival of a point charge at the origin, whose strength is $-Q_K$, as required by charge neutrality. In other words, the line charge reduces to a delta function $\rho(z) = -Q_K\delta(z)$, in accordance with the Kelvin image theory.
5. For $d = 3$, the line charge density $\rho(z)$ is a constant for *holes*, when $\alpha \rightarrow 0$.
6. For all d , the line charge density $\rho(z)$ is also a constant at the single value

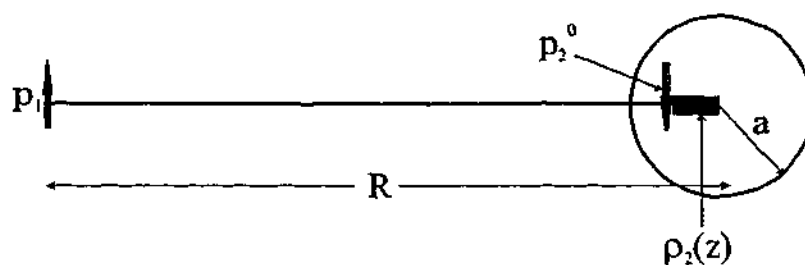


Figure 5.2: First image dipole $\mathbf{p}_2^{\perp 0}$ and line dipole $\vec{\rho}_2^{\perp}(z)$ as derived from the Neumann theory for the perpendicular configuration. The origin is at the centre of the hypersphere.

$$\alpha = d - 3.$$

These observations and their implications need to be pondered over in more detail. Here however, we are primarily interested in using the d -dimensional generalization of the Neumann image theory to study dipole images as in Djordjević *et al.* (1996), which will be applied to the bispherical system in any dimension d .

5.2.2 First perpendicular dipole image

We will use the results discussed above to derive the image of a point dipole of strength \mathbf{p}_1 outside a d -dimensional sphere, as shown in Figs 5.2 and 5.3 respectively. As in the previous Chapter, we must consider separately the perpendicular field (Fig 5.2) and the parallel field (Fig 5.3) configurations.

The complementary character of this work to that in the previous Chapter will manifest itself when we show that here it is the perpendicular configuration that is mathematically the simpler, which is the converse of the results via the multipole expansion method. Again, postponing details to Appendix E, the image for a point dipole \mathbf{p}_1^{\perp} in d dimensions and perpendicular to the line between the spheres R (see Fig 5.3) is an image point dipole $\mathbf{p}_2^{\perp 0}$ at the image point b_1 given by

$$\mathbf{p}_2^{\perp 0} = -\mathbf{p}_1^{\perp} \left(\frac{\alpha - 1}{\alpha + 1} \right) \left(\frac{a}{R} \right)^d. \quad (5.3)$$

The point dipole also creates a *line* dipole image $\vec{\rho}_2^{\perp}(z)$ for $0 < z < b_1$, given by

$$\vec{\rho}_2^{\perp}(z) = \left(\frac{\mathbf{p}_1^{\perp}}{a} \right) \left(\frac{a}{R} \right)^{d-1} (d-2) \frac{\alpha - 1}{(\alpha + 1)^2} \left(\frac{z}{b_1} \right)^{(d-2)/(\alpha+1)}. \quad (5.4)$$

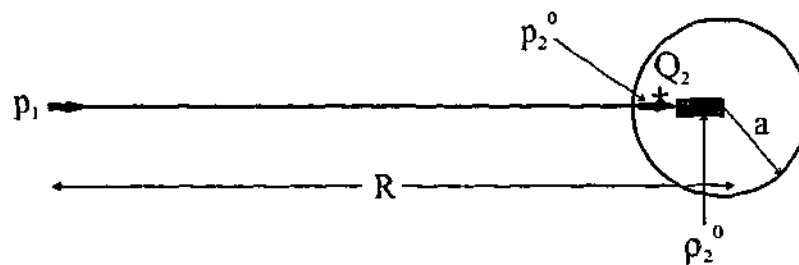


Figure 5.3: First image dipole $\mathbf{p}_2^{\perp 0}$ and line charge $\rho_2^{\perp 0}(z)$ and point charge Q_2 as derived from the Neumann theory for the parallel configuration. The origin is at the centre of the hypersphere.

These results constitute the first perpendicular set $(\mathbf{p}_2^{\perp 0}, \vec{\rho}_2^{\perp})$. Note that we write the image line charge as a vector $\vec{\rho}$ sometimes, where the direction of the vector is along the line itself. For $d = 2$ the line dipole distribution eqn (5.4) disappears completely (Binns and Lawrenson 1973). Integrating over this density and adding it to the image eqn (5.3) above, we get the *total* dipole moment for the first \mathbf{p}_2^{\perp} given by

$$\mathbf{p}_2^{\perp} = -\mathbf{p}_1^{\perp} \left(\frac{\alpha - 1}{\alpha + (d - 1)} \right) \left(\frac{a}{R} \right)^d. \quad (5.5)$$

Here we see the recovery of the d -dimensional polarizability factor β , missing in the theory so far. Note also that the orientation of the dipole $\mathbf{p}_2^{\perp 0}$ and the line dipole density $\vec{\rho}_2^{\perp}(z)$ are opposite in sign, which is a consequence of charge neutrality. We summarize the above results by writing the perpendicular image distribution as given by

$$\mathbf{p}_2^{\perp}(z) = \mathbf{p}_2^{\perp 0} \delta(z - b_1) + \vec{\rho}_2^{\perp}(z), \quad (5.6)$$

whose integral recovers eqn (5.5). We leave the study of higher-order images to the next section. Here we will mention that although the result for the total dipole moment eqn (5.5) appears to be simple, the detailed distribution eqn (5.6) is required explicitly for the next generation. In fact the straightforward guess following the work of Djordjević *et al.* (1996) for the total perpendicular dipole moment \mathbf{p}_3^{\perp} of the form

$$\mathbf{p}_3^{\perp} = -\mathbf{p}_2^{\perp} \left(\frac{\alpha - 1}{\alpha + (d - 1)} \right) \left(\frac{a}{R - b_1} \right)^d, \quad (5.7)$$

is not correct. Still eqn (5.7) is a useful formula to keep in mind when we study

approximations later. We will now consider in the next section the parallel configuration for the first image.

5.2.3 First parallel dipole image

The complexity of the bispherical problem first appears in this case. In Appendix F we have derived the following result using the generalized d -dimensional Neumann theory. The parallel dipole \mathbf{p}_1^{\parallel} first generates a point dipole at the image point b_1 given by

$$\mathbf{p}_2^{\parallel 0} = \mathbf{p}_1^{\parallel} \left(\frac{\alpha - 1}{\alpha + 1} \right) \left(\frac{a}{R} \right)^d, \quad (5.8)$$

similar to, but opposite in sign to, eqn (5.3). The dipole \mathbf{p}_1^{\parallel} here does not create a line dipole density as in the perpendicular case, but a line *charge* density from $0 < z < b_1$, of the form

$$\rho_2^{\parallel 0}(z) = \frac{p_1^{\parallel}}{a^2} \left(\frac{a}{R} \right)^{d-2} (d-2) \frac{\alpha(\alpha-1)}{(\alpha+1)^3} \left(\frac{z}{b_1} \right)^{(d-3-\alpha)/(\alpha+1)}. \quad (5.9)$$

In addition, we also have an image charge at the image point b_1 given by

$$Q_2 = -\frac{p_1^{\parallel} \alpha(\alpha-1)}{a(\alpha+1)^2} \left(\frac{a}{R} \right)^{d-1}. \quad (5.10)$$

We summarize these results by writing the first parallel image set as $(\mathbf{p}_2^{\parallel 0}, \rho_2^{\parallel})$ where the charge density is

$$\rho_2^{\parallel}(z) = \rho_2^{\parallel 0} + Q_2 \delta(z - b_1). \quad (5.11)$$

While deriving these results, charge neutrality furnishes a useful check, as is easily seen by integrating eqn (5.11). Calculating the net dipole moment \mathbf{p}_2^{\parallel} from the charge density eqn (5.11) via $(d-2) \int z \rho_2^{\parallel}(z) dV$ and then adding it to eqn (5.8), we have the total parallel dipole moment:

$$\mathbf{p}_2^{\parallel} = \mathbf{p}_1^{\parallel} (d-1) \left(\frac{\alpha-1}{\alpha+(d-1)} \right) \left(\frac{a}{R} \right)^d. \quad (5.12)$$

Before proceeding any further, we note that a useful check of this result is that the net angular averaged dipole moment $\bar{\mathbf{p}}_2$ should vanish (recall discussion in the previous Chapter). This is the notorious divergent term which must vanish for the theory to be meaningful. It is easy to show that this is indeed the case, for upon

performing the angular integrations *first* over the total dipole moments eqn (5.5) and eqn (5.12) and noting that $|\mathbf{p}_1^\perp| = |\mathbf{p}_1^\parallel| = p_1$,

$$\bar{\mathbf{p}}_2 = \mathbf{p}_2^\parallel + (d-1)\mathbf{p}_2^\perp = 0. \quad (5.13)$$

Although this total averaged dipole moment is zero, the image sets $(\mathbf{p}_2^{\perp 0}, \vec{\rho}_2^\perp)$ and $(\mathbf{p}_2^{\parallel 0}, \rho_2^\parallel)$ do not vanish from the scene completely. The theory depends on the totality of higher-order images generated from these sets, which we discuss in the following section.

5.3 Higher-order images

Having now secured the fundamentals, we can proceed to calculate the higher-order images. We are naturally thinking about the next image sets $(\mathbf{p}_3^{\perp 0}, \rho_3^\perp)$ and $(\mathbf{p}_3^{\parallel 0}, \rho_3^\parallel)$, and how they will transform. A moment's reflection will show that in the perpendicular case the mapping goes from point dipoles and line dipoles to point dipoles and line dipoles and so on. The parallel case is similar; the mapping goes from a point dipole with a line charge to another point dipole with line charge and so on. In all cases the density distributions develop ever-increasing complexities. In the parallel case, there is an additional step required for computing the total dipole moment from the resultant charge densities, thus increasing the work, but otherwise straightforward (provided that these densities are available).

5.3.1 Perpendicular higher-order images

A careful examination of the higher-order images shows that the total dipole moment of the n^{th} image is given by

$$\mathbf{p}_n^\perp = - \left(\frac{\alpha - 1}{\alpha + (d-1)} \right) \int_0^{b_{n-2}} \mathbf{p}_{n-1}^\perp(z) \left(\frac{a}{R-z} \right)^d dz, \quad (5.14)$$

where the key density here is the dipole density distribution which we write as

$$\mathbf{p}_n^\perp(z) = \mathbf{p}_n^{\perp 0} \delta(z - b_{n-1}) + \vec{\rho}_n^\perp(z). \quad (5.15)$$

Here the point dipoles $\mathbf{p}_n^{\perp 0}$ are given by the recursion relation

$$\mathbf{p}_{n+1}^{\perp 0} = -\mathbf{p}_n^{\perp 0} \left(\frac{\alpha - 1}{\alpha + 1} \right) \left(\frac{a}{R - b_{n-1}} \right)^d, \quad (5.16)$$

and b_n are the image positions, represented by the usual continued fraction (Djordjević *et al.* 1996)

$$b_n = \frac{a^2}{R - b_{n-1}}, \quad (5.17)$$

with the limits $b_0 = 0$ and $b_1 = a^2/R$. The dipole density $\bar{\rho}_n^\perp(z)$ is formally given by the following integral recursion relation:

$$\begin{aligned} \bar{\rho}_{n+1}^\perp(z) = & \frac{p_n^{\perp 0}}{a} \left(\frac{a}{R - b_{n-1}} \right)^{d-1} (d-2) \frac{\alpha-1}{(\alpha+1)^2} \left(\frac{z}{b_n} \right)^{(d-2)/(\alpha+1)} \\ & - \int_0^{b_{n-1}} \bar{\rho}_n^\perp(z') \left(\frac{\alpha-1}{\alpha+1} \right) \left(\frac{a}{R-z'} \right)^d \delta \left(\frac{a^2}{R-z'} - z \right) dz' \\ & - (d-2) \int_0^{b_{n-1}} \frac{\bar{\rho}_n^\perp(z')}{a} \frac{\alpha-1}{(\alpha+1)^2} \left(\frac{a}{R-z'} \right)^{d-1} \\ & \times \left(\frac{z(R-z')}{a^2} \right)^{(d-2)/(\alpha+1)} \theta \left(\frac{a^2}{R-z'} - z \right) dz'. \end{aligned} \quad (5.18)$$

Unfortunately, we know of no closed form solution of this system of difference integral equations, apart from resorting to direct step-by-step iteration. The starting point must of course be the expression eqn (5.6). By this procedure we have computed the image distribution $\bar{\rho}_3^\perp(z)$ whose details we will not exhibit further here, except to note that it is not a convenient expression. Here we briefly mention that eqn (5.18) has an algebraic kernel, though it is not of the difference type. It appears that the first few iterations are manageable, but the prospects diminish beyond $\bar{\rho}_4^\perp(z)$. The system of eqn's (5.18) deserve further study and could be useful for improving the convergence properties of the multipole expansion series in the previous Chapter. At this point we merely quote the result for the total perpendicular dipole moment p_3^\perp calculated by this method:

$$\begin{aligned} p_3^\perp = & p_1^\perp \left(\frac{a}{R} \right)^d \frac{(\alpha-1)^2}{(\alpha+1)(\alpha+d-1)} \\ & \times \left[\left(\frac{a}{R-b_1} \right)^d - \left(\frac{d-2}{\alpha+1} \right) \int_0^{b_1} \left(\frac{z}{b_1} \right)^{(d-2)/(\alpha+1)} \left(\frac{a}{R-z} \right)^d \frac{dz}{b_1} \right]. \end{aligned} \quad (5.19)$$

As the prefactor to the integral term vanishes in the limit $d \rightarrow 2$, eqn (5.19) clearly reproduces earlier results (Djordjević *et al.* 1996). Note that in the limit of the perfect conductor, this term also vanishes, leading to a considerable simplification. The

same cannot be said for *holes*, however, as the integral survives, but is nevertheless of a higher order in β . Later on we shall see that this justifies a *weak - scattering* approximation.

5.3.2 Parallel higher-order images

Again by careful examination of the results obtained previously, we now see that at the n^{th} generation, there exists a point dipole $p_n^{\parallel 0}$ at the image point b_{n-1} and a line charge $\rho_n^{\parallel}(z)$ from the centre O to that point. The point dipole at the next generation is easily written as:

$$P_{n+1}^{\perp 0} = P_n^{\parallel 0} \left(\frac{\alpha - 1}{\alpha + 1} \right) \left(\frac{a}{R - b_{n-1}} \right)^d. \quad (5.20)$$

The structure of the line charge at the next order $\rho_{n+1}^{\parallel}(z)$ is the sum of several parts. We will write down these contributions and explain their origins:

$$\rho_{n+1}^{\parallel}(z) = Q_{n+1} \delta(z - b_{n-1}) + \rho_{n+1}^{\parallel 0}(z) + \tilde{\rho}_{n+1}^{\parallel}(z) + \tilde{\tilde{\rho}}_{n+1}^{\parallel}(z). \quad (5.21)$$

Now the first two terms are given by the point charge

$$Q_{n+1} = -\frac{p_n^{\parallel 0}}{a} \frac{\alpha(\alpha - 1)}{(\alpha + 1)^2} \left(\frac{a}{R - b_{n-1}} \right)^{d-1}, \quad (5.22)$$

and by the charge density

$$\rho_{n+1}^{\parallel 0}(z) = \frac{p_n^{\parallel 0}}{a^2} \left(\frac{a}{R - b_{n-1}} \right)^{d-2} (d-2) \frac{\alpha(\alpha - 1)}{(\alpha + 1)^3} \left(\frac{z}{b_n} \right)^{(d-3-\alpha)/(\alpha+1)}. \quad (5.23)$$

Next the line charge of the n^{th} generation $\rho_n^{\parallel}(z)$ maps onto a sequence of point charges, which forms a line charge density given by

$$\tilde{\rho}_{n+1}^{\parallel}(z) = - \int_0^{b_{n-1}} \rho_n^{\parallel}(z') \left(\frac{\alpha - 1}{\alpha + 1} \right) \left(\frac{a}{R - z'} \right)^{d-2} \delta \left(\frac{a^2}{R - z'} - z \right) dz', \quad (5.24)$$

and another line charge due to eqn (5.2), namely

$$\tilde{\tilde{\rho}}_{n+1}^{\parallel}(z) = (d-2) \int_0^{b_{n-1}} \frac{\rho_n^{\parallel}(z')}{a} \frac{\alpha - 1}{(\alpha + 1)^2} \left(\frac{a}{R - z'} \right)^{d-3} \times \left(\frac{z(R - z')}{a^2} \right)^{(d-3-\alpha)/(\alpha+1)} \theta \left(\frac{a^2}{R - z'} - z \right) dz'. \quad (5.25)$$

Once again charge neutrality is an important check and this can be obtained by integrating eqn's (5.23)-(5.25). Note that in the integral recursion relations eqn (5.24) and eqn (5.25), it is the full density of the previous generation $\rho_n^{\parallel}(z')$ given by eqn (5.21) that must be known before the partial densities can be calculated for the next generation. Herein lies the complication of the parallel system. Furthermore, having somehow obtained these densities, we must also compute the dipole moment $(d-2) \int z \rho_{n+1}^{\parallel}(z) dV$ that is to be added to eqn (5.20) to find the total dipole moment p_{n+1}^{\parallel} . This increases the work but is otherwise straightforward. Just like eqn (5.18), the system of eqn's (5.21)-(5.25) does not seem to be amenable to a closed-form solution. Direct iteration is tedious but can be carried out by hand up to $\rho_3^{\parallel}(z)$, starting from eqn (5.11), with little prospects for going beyond $\rho_4^{\parallel}(z)$. Again we do not exhibit the details of $\rho_3^{\parallel}(z)$, which is even more messy than $\rho_3^{\perp}(z)$. Here, as before, we will merely quote the result for the total parallel dipole moment p_3^{\parallel} calculated via the above procedure:

$$\begin{aligned}
 p_3^{\parallel} = & p_1^{\parallel} \left(\frac{a}{R}\right)^d \left(\frac{a}{R-b_1}\right)^d \frac{(d-1)(\alpha-1)^2}{(\alpha+1)(\alpha+d-1)} \\
 & - p_1^{\parallel} (d-2)^2 \left(\frac{a}{R}\right)^{d-1} \frac{\alpha(\alpha-1)^2}{(\alpha+1)^3(\alpha+d-1)} \\
 & \quad \times \int_0^b \left(\frac{a}{R-z}\right)^{d-1} \left(\frac{z}{b_1}\right)^{(d-3-\alpha)/(\alpha+1)} \frac{dz}{b_1} \\
 & + p_1^{\parallel} \left(\frac{a}{R}\right)^{d-1} \left(\frac{a}{R-b_1}\right)^{d-1} \frac{\alpha(\alpha-1)^2}{(\alpha+1)^2} \left(\frac{d-2}{(\alpha+d-1)}\right). \quad (5.26)
 \end{aligned}$$

At this stage, we mention a few observations that might be useful for future work. Certainly, the key to further progress primarily lies in the solution of the pair of integral eqn's (5.18) and (5.25). The main hurdle appears not so much with the integrals, as in the *region* of integration; note the θ function in the integrands. As a result of this, closed-form expressions for the distributions $\rho_3^{\perp}(z)$ and $\rho_3^{\parallel}(z)$ already involve non-elementary functions. Hence at the next generation, it appears to involve indefinite integrals over these functions. Thus the prospect of going beyond this level diminishes. Apart from the usual perfect conductor and $d = 2$ limits which are familiar by now, another useful observation is that eqn (5.18) and eqn (5.25) can be expanded as a power series in $\xi = a/R$. Indeed, we will make

contact with the results of the previous Chapter in this way. By averaging over angles and using a Clausius-Mossotti-like formula, the coefficient κ up to the total averaged image \bar{p}_3 is now given by

$$\begin{aligned} \kappa = & d\beta^2 + d(d-1)\beta^2 \left(\frac{\alpha-1}{\alpha+1} \right) \\ & \times \left[\int_0^{1/2} s^{d-1} ds \left\{ \frac{2}{(1-s^2)^d} + (d-2) \left(\frac{\alpha-1}{\alpha+1} \right) \int_0^1 \frac{x^{(d-2)/(1+\alpha)}}{(1-s^2x)^d} dx \right\} \right]. \end{aligned} \quad (5.27)$$

This result admits a power-series expansion in s , under the integrals, as discussed above. Although it involves a double integral, we can rewrite eqn (5.27) as an infinite series by introducing the $F_d(\beta)$ function (see previous Chapter and Djordjević *et al.* (1996), whose $F(\beta) = \beta F_2(\beta)$ here). This is defined by

$$\kappa = d\beta^3 + \beta^3 F_d(\beta), \quad (5.28)$$

where the series

$$F_d(\beta) = d(d-1) \sum_{s=0}^{\infty} \left(\frac{1}{2} \right)^{d+2s} \binom{d+s-1}{s} \frac{\alpha+d-1}{\alpha(s+1)+d+s-1}, \quad (5.29)$$

and can be viewed as a partial resummation of

$$\bar{S} = v^d d\beta \epsilon_0 c \sum_{s=2d}^{\infty} \frac{B_s - dA_s}{(s-d)2^{s-d}}, \quad (5.30)$$

of the previous Chapter using the multipole expansion method to all terms in β^3 .

Leaving detailed results to later, we conclude this section by stating the leading-order values for small β : $F_1(0) = 0$, $F_2(0) = 2/3 = 0.666\dots$, $F_3(0) = (20-9\ln(3))/8 = 1.264\dots$ and $F_4(0) = 44/27 = 1.629\dots$. This is an exact result for $d = 1$ and in agreement with Djordjević *et al.* (1996) for $d = 2$. For $d = 3$, the result quoted by Jeffrey (1973), $F_3(0) = 87/80 = 1.087\dots$, only involved a part of the third-order dipole term, which can be obtained by taking the first two terms of the series eqn (5.29) in the limit $\alpha \rightarrow 1$. We must also remember that $\beta = \beta_1 = (\alpha-1)/(\alpha+d-1)$ has a dimensional dependence. Comparison of this series also shows agreement with eqn (5.30) up to the appropriate order in β .

5.4 Perfect conductor limit

In our study of the image method so far, we have seen that in order of difficulty, the $d = 2$ general dielectric stands out as the easiest, while the next simplest case is the perfect conductor for all d . Indeed, Kelvin's image theory is applicable *both* to a dielectric for $d = 2$ and for a perfect conductor in any d , a careful study also reveals that for $d > 2$ the perfect conductor is still complicated by the parallel case. This is because the point charges generated by the parallel configuration cannot be neglected, except for two dimensions. Nevertheless, the mapping of these point charges is still manageable and this is the case we will treat in this section. The perpendicular case is by now clear, as it leads only to point dipoles in each generation (see eqn (5.16)). Here we will use the opportunity to discuss the *point-dipoles-only approximation*.

5.4.1 Point dipoles only approximation

A close examination of all our previous work also shows that the result is contained in the point dipoles $\mathbf{p}_n^{\parallel 0}$ and $\mathbf{p}_n^{\perp 0}$, and we know that in two dimensions there are no other contributions. Therefore we start by keeping *only* all point dipoles; an approximation that is exact in two dimensions. The function $F_d(1)$ now takes the form (Djordjević *et al.* 1996)

$$\begin{aligned} F_d(1) &\approx \frac{2d(d-1)}{\omega_p E_0 a^{2d}} \int dR R^{d-1} \sum_{s=1}^{\infty} \bar{\mathbf{P}}_{2s+1} \\ &= \sum_{s=1}^{\infty} f_s, \end{aligned} \quad (5.31)$$

where f_s is given by the integral

$$f_s = 2d(d-1) \int_0^{1/2} \frac{x^{2sd-d-1}}{\left[1 + \sum_{k=1}^s (-1)^k \binom{2s-k}{k} x^{2k} \right]^d} dx. \quad (5.32)$$

This integral is rather interesting. For integer s and d , the integrand is a rational function of polynomials that can be integrated in closed form by reduction formulae (Gradshteyn and Ryzhik 1980). For example, for $d = 2$, we have

$$f_2 = \left[\frac{2}{5} + \frac{4}{5\sqrt{5}} \left\{ \ln(\sqrt{5} + 3) - \ln(\sqrt{5} - 3) + \ln(\sqrt{5} - \frac{5}{2}) - \ln(\sqrt{5} + \frac{5}{2}) \right\} \right]$$

$$= 0.0556728\dots, \quad (5.33)$$

in agreement with Djordjević *et al.* (1996). The latter, however, used a digamma function representation which does not seem to be generalizable to $d > 2$. These integrals can be reduced using computational code such as Mathematica and by summing eqn (5.31) to $s = 19$ terms; we obtain the value for $d = 2$ as $F_2(1) = 0.7449145\dots$, agreeing with the value $F_2(1) = 0.7449896\dots$ up to the fourth digit, as quoted by Djordjević *et al.* (1996), who summed the series eqn (5.31) to over 100 terms using digamma functions. We will see in more detail later, as part of our results, that $F_3(1) = 0.895007\dots$ in three dimensions. Suffice to say here that if this result was compared to that of Jeffrey (1973), namely $F_3(1) = 1.51\dots$, we see a great discrepancy that can be attributed to the fact that we are required to consider the *full* image series in order to improve the convergence.

5.4.2 Total dipole moments \mathbf{p}_4 and \mathbf{p}_5

At this point we will investigate the contributions from images beyond the point dipoles of the previous section for the perfect conductor. We are only concerned here with the parallel dipole moments, as the perpendicular case is just the point dipole sequence $\mathbf{p}_n^{\perp 0}$. From this point on we will suppress the superscript \parallel , and we will denote $\mathbf{p}_n^{\parallel} = \mathbf{p}_n$ for brevity. Here we need to keep track of the point charges in each generation, which are depicted in Fig 5.4. From them, together with \mathbf{p}_n^0 , we will calculate the total dipole moment at each generation.

The computation of the charges is straightforward but lengthy. We give the results for the preaveraged total dipole moment \mathbf{p}_n for $n = 2, 3, 4, 5$. We begin by rewriting \mathbf{p}_2 in eqn (5.12) as

$$\mathbf{p}_2 = \mathbf{p}_1 \omega_1^d (d - 1), \quad (5.34)$$

where $\omega_n = b_n/a$. The next generation gives us \mathbf{p}_3 as

$$\mathbf{p}_3 = \mathbf{p}_1 \omega_1^d \left[(d - 1) \omega_2^d + (d - 2) \omega_1^{-1} (\omega_2^{d-1} - \omega_1^{d-1}) \right], \quad (5.35)$$

and it appears that there might be a pattern emerging at \mathbf{p}_4 given by

$$\mathbf{p}_4 = \mathbf{p}_1 \omega_1^d \left[(d - 1) \omega_2^d \omega_3^d + (d - 2) \omega_1^{-2} \left\{ \omega_2^{d-1} \omega_3^{d-1} - 2 \omega_1^{d-1} \omega_2^{d-1} + \omega_1^{2(d-1)} \right\} \right]. \quad (5.36)$$

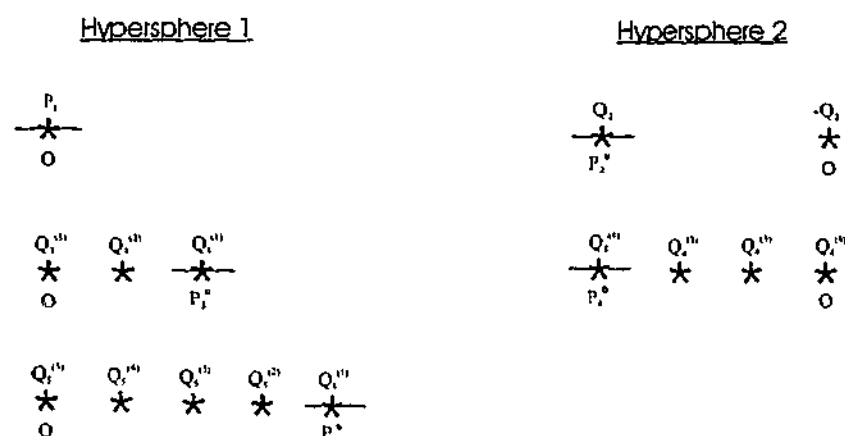


Figure 5.4: Sequence of point-charge images for each generation up to p_5^{\parallel} . The superscript j in Q_n^j refers to the image point h_{j-1} while n refers to the generation P_n .

Unfortunately, this does not prove to be the case, because when we carry out the calculations pertaining to higher-order dipole moments we find an increase in the complexity of the mappings between the two hyperspheres. Indeed this can be seen when we finally compute the expression for p_5

$$\begin{aligned}
 p_5 = & p_1 \omega_1^d (d-1) \omega_2^d \omega_3^d \omega_4^d \\
 & + p_1 \omega_1^d (d-2) \omega_1^{-3} \left\{ \omega_2^{d-1} \omega_3^{d-1} \omega_4^{d-1} (1 - \omega_1^2) - 2\omega_1^d \omega_2^{d-2} \omega_3^{d-1} - \omega_1^{d-1} \omega_2^{2(d-1)} \right\} \\
 & + p_1 \omega_1^d (d-2) \omega_1^{-3} \left\{ 2\omega_1^{2(d-1)} \omega_2^{d-1} + \omega_1^{2d-1} \omega_2^{d-2} - \omega_1^{3(d-1)} \right\}. \quad (5.37)
 \end{aligned}$$

It is therefore of interest to us here to generalize the method above so that we can carry out these higher order calculations, and in the next section we shall formulate this in such a way that the calculations can be carried out in analytical form to any order. Finally, we mention here that the results we obtain for $F_d(1)$ will be compared to the multipole expansion method later on and we will see that even though the convergence is relatively slow using the image method, it nevertheless proves to be much faster than the multipole expansion method of the previous Chapter.

5.5 Higher-order dipole moments for the perfect-conductor

In the previous section we showed the results for the perfect-conducting limit up to p_5 . We made the comment that going to higher orders is mathematically opaque, since the mapping of the dipoles and images increases in complexity as the order n

does, making it very difficult to use an iterative approach for instance. In this section we shall generalize the method so that we can produce calculations to any order (Alexopoulos 2004) for the total averaged dipole moments, subject to computational power. In doing so we will justify the results of the previous section by explaining in more detail the procedure (see Fig 5.4) that was used in order to get to p_5 .

5.5.1 Mapping of dipoles and charges

We consider the mapping of the parallel dipoles and charges for brevity reasons with the perpendicular field case being similar in nature. In Appendix F we see how we can define the first generation of the dipoles and charges (except here we take the limit $\alpha \rightarrow \infty$ for the perfect-conductor). Djordjević *et al.* (1996) have shown that these mappings consist of continued fractions but their solutions involve point-dipoles *only*, an exact result in two dimensions. Here we will need to also include contributions from the charges which in the limit $d = 2$ vanish and we recover the results of Djordjević *et al.* (1996). By looking at Fig 5.4, we see that the electric field in the parallel direction, induces a dipole p_1 on the left hypersphere at the origin O . On the second hypersphere we generate a dipole p_2 and charge Q_2 at a distance away from the origin defined by b_{j-1} . Charge conservation requires that we place another charge $-Q_2$ of equal but opposite magnitude at the origin. Now we can consider the 3rd generation on the original hypersphere with a dipole p_3 and additional charges. This mapping now proceeds backwards and forwards between the hyperspheres infinitely. The symmetry of the system, ie the hyperspheres have equal radii, means that these effects are doubled to account for the second hypersphere generating dipoles and charges onto the first.

By following the argument above we can obtain the second generation point dipole and charges from p_1 :

$$\begin{aligned} p_2 &= p_1 \left(\frac{a}{R}\right)^d \\ Q_2^{(2)} &= -(d-2) \left(\frac{p_1}{a}\right) \left(\frac{a}{R}\right)^{d-1} \\ Q_2^{(1)} &= (d-2) \left(\frac{p_1}{a}\right) \left(\frac{a}{R}\right)^{d-1}, \end{aligned} \tag{5.38}$$

where eqn's (5.38) above are the initial conditions of the system and thus the total dipole moment p_2^{tot} becomes

$$p_2^{tot} = p_2 - b_1 Q_2^{(2)} = p_1 (d-1) \left(\frac{a}{R}\right)^d. \quad (5.39)$$

On the third generation, we can use eqn (5.38) and derive p_3 and the charges as

$$\begin{aligned} p_3 &= p_1 \left(\frac{a}{R}\right)^d \left(\frac{a}{R-b_1}\right)^d \\ Q_3^{(3)} &= (d-2) \left(\frac{p_1}{a}\right) \left(\frac{a}{R}\right)^{d-2} \left(\frac{a}{R-b_1}\right)^{d-1} \\ Q_3^{(2)} &= -(d-2) \left(\frac{p_1}{a}\right) \left(\frac{a}{R}\right)^{d-2} \left(\frac{a}{R}\right)^{d-1} \\ Q_3^{(1)} &= (d-2) \left(\frac{p_1}{a}\right) \left(\frac{a}{R}\right)^{d-2} \left[\left(\frac{a}{R-b_1}\right)^{d-1} - \left(\frac{a}{R}\right)^{d-1} \right], \end{aligned} \quad (5.40)$$

with the total dipole moment $p_3^{tot} = p_3 + Q_3^{(3)}b_2 + Q_3^{(2)}b_1$ given as

$$p_3^{tot} = p_1 \left(\frac{a}{R}\right)^d \left\{ (d-1) \left(\frac{a}{R-b_1}\right)^d + (d-2) \left[\left(\frac{a}{R-b_1}\right)^{d-1} \left(\frac{R}{a}\right) - \left(\frac{a}{R}\right)^{d-2} \right] \right\}. \quad (5.41)$$

As can be seen by eqn (5.41), already there is evidence that higher orders will become extremely complex. By proceeding further we will encounter very large continued fractions, so it is necessary here to represent them in a recursive form. In particular the positions of the various charges can be written in the form

$$b_j = \frac{a^2}{R - b_{j-1}}, \quad (5.42)$$

and we can define the ratio ω_j as being

$$\omega_j = \frac{a}{R - b_{j-1}}, \quad (5.43)$$

where $b_j = a\omega_j$. At the same time we can derive the dipole in each successive generation by using

$$p_n = p_{n-1} \left(\frac{a}{R - b_{n-2}}\right)^d, \quad (5.44)$$

for $n \geq 2$. It is easy to show that we can rewrite eqn (5.44) in terms of the ω_j 's. In fact by using eqn's (5.42) and (5.43) we can rewrite eqn (5.41) in terms of ω and by doing so we obtain eqn (5.35) from the previous section. Indeed we note that eqn

(5.35) is written in terms of ω_1 and ω_2 , and when we consider higher orders we will have to deal with different continued fractions in ω . Fortunately, we can simplify then all down to $\omega_1 = \omega = a/R$. We can see this by expanding eqn (5.43) to $j = 4$ and after some simplification we obtain terms in ω

$$\omega_4 = \frac{\omega}{1 - \frac{\omega^2}{1 - \frac{\omega^2}{1 - \omega^2}}}. \quad (5.45)$$

All expressions for the dipoles and charges are written in the end in terms of ω , thus greatly simplifying any calculations.

At this time we can mention that by a similar routine we can calculate the expression for the perpendicular field case so that in the end the total averaged dipole moment to any order $\bar{p}_n = p_n^{\parallel tot} + (d-1)p_n^{\perp tot}$ for both the parallel and perpendicular contributions of the field can be written down as

$$\bar{p}_n = p_1 \left[1 + (d-1)(-1)^{n-1} \right] \prod_{i=1}^{n-1} \omega_i^d + (-1)^{n-1} (d-2) \sum_{j=2}^n Q_n^{(j)} b_{j-1}. \quad (5.46)$$

The non-trivial contributions of the line charges for each successive generation in eqn (5.46) are given as

$$Q_n^{(n)} = (-1)^{n-1} \left(\frac{p_1}{a} \right) \omega_{n-1}^{d-1} \prod_{i=1}^{n-2} \omega_i^{d-2}, \quad (5.47)$$

for $j = n$ while for the other charge contributions we have

$$Q_n^{(j)} = -Q_{n-1}^{(j-1)} \omega_{j-1}^{d-2}, \quad (5.48)$$

for $n > j > 1$. The line-charges that 'couple' with the dipoles are determined by

$$Q_n^{(1)} = -\sum_{j=2}^n Q_n^{(j)}, \quad (5.49)$$

where $n > 2$. We can now write down the dimensionally dependent coefficient κ in the series for the dielectric function $\epsilon/\epsilon_0 = (1 + c + \kappa c^2 + \dots)$, as

$$\kappa_n^{(d)} = d + \frac{d}{p_1 a^d} \int_{2a}^{\infty} R^{d-1} \left\{ p_1 \left[1 + (d-1)(-1)^{n-1} \right] \prod_{i=1}^{n-1} \omega_i^d + (-1)^{n-1} (d-2) \sum_{j=2}^n Q_n^{(j)} b_{j-1} \right\} dR. \quad (5.50)$$

Recalling that $\omega = a/R$, it is easy to substitute ω in eqn (5.50) so that the integral is performed over ω in the interval $[0, 1/2]$ (see results section). In the next section we shall discuss the potential between two hyperspheres.

5.6 Potential difference between two hyperspheres

The problem of finding the potential difference (or voltage) and therefore capacitance between two inclusions has been of great interest. In the case where the inclusions are spheres, considerable work has been undertaken to calculate special cases of the electrostatics of such spherical pairs. Moussiaux and Ronveaux (1979) have calculated the capacity of touching unequal metallic spheres. Jeffrey and Onishi (1980) have extended this method to non-touching spheres under a variety of conditions. In addition to capacitances and induced charges, O'Meara and Saville (1981) have calculated the electrostatic force between two spheres. Love (1975), has considered dielectric sphere pairs in uniform external fields using a Green's-function technique for difference equations. Batchelor and O'Brien (1977) have considered both separated conducting spheres and touching dielectric spheres, and have obtained the asymptotic behaviour of both these limiting configurations. The majority of the above work was done using field expansions in curvilinear coordinates, such as bispherical coordinates, which are discussed in detail by Lebedev *et al.* (1965).¹

In the case of a composite system, we are interested in such things as dielectric and conductive properties. These coefficients of the composite can be obtained from knowledge of the induced moments on the inclusions. Most methods lead to an infinite matrix equation, which must be truncated and inverted numerically to obtain the multipole moments. When the inclusions are close to touching, the number of multipole moments that need to be retained for an accurate solution makes numerical inversion impractical. A method for calculating the influence exerted between nearest-neighbour inclusions explicitly, that is without numerical inversion, and thus providing an estimate of the induced multipoles of all orders, would simplify the calculation of effective properties of close-packed composites. The method of images might be able to help us in this context, by allowing us to gain valuable insight into the problem. We will use the results that we have obtained in previous sections to calculate the d -dimensional voltage ΔV , between two inclusions. We will

¹An interesting extension of the work presented in this thesis would be to actually solve for the dielectric function using d -dimensional bispherical coordinates.

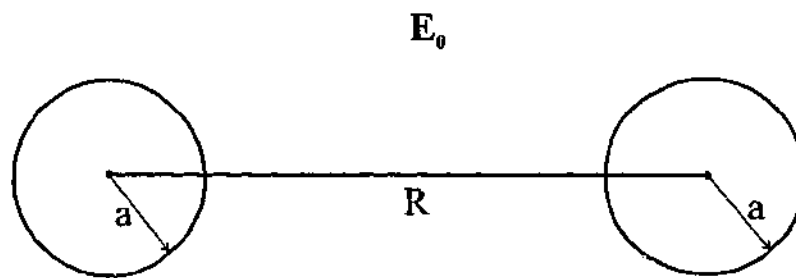


Figure 5.5: Hyperspheres in the presence of an electric field E_0 separated by the distance R . The radius of each hypersphere is a such that $\omega = a/R$ or $\bar{\omega} = R/a$.

derive an expression for the d -dimensional voltage using the method of images by firstly considering the contributions due to the point dipoles only, an exact result for $d = 2$ and in agreement with Djordjević *et al.* (1996), and then the full contributions that include the charges too. The special limit when the hyperspheres touch, $\omega = a/R = 1/2$, will be investigated due to the importance of nearest neighbour effects in closely-packed composites. Unfortunately as we shall see, in the case $d = 3$ when the limit of $\omega \rightarrow 1/2$ (spheres touching), the convergence is so slow that an enormous (approaching infinity) number of both dipole and charge contributions need to be calculated in order to show that $\Delta V \rightarrow 0$. This means that computationally at least, a numerical rather than a symbolic procedure must be favoured if we are to be more efficient.

5.6.1 Dipole contributions

Following the work of Djordjević *et al.* (1996), we consider two inclusions in the presence of a parallel and perpendicular component of an electric field E_0 , see Fig 5.5. We can write the voltage ΔV between the hyperspheres as

$$\Delta V = E_0 R + 2 \sum_{n=2}^{\infty} V_n^D, \quad (5.51)$$

where the factor 2 in eqn (5.51) represents the effect of the other hypersphere (symmetry) and V_n^D is the contribution from the dipoles *only*. We recall from previous sections that the positions of the dipoles (charges) are given by b_n , such that

$$b_n = \frac{a\omega}{1 - \omega\omega_{n-1}}, \quad (5.52)$$

and each dipole p_n is generated from the previous mapping as can be seen from the following expression

$$p_n = p_{n-1} \frac{\omega^d}{(1 - \omega\omega_{n-2})^d}. \quad (5.53)$$

Once again we can see that eqn (5.52) can be written as $b_n = a\omega_n$ because all the ω 's are generated by the continued fraction

$$\omega_n = \frac{\omega}{1 - \omega\omega_{n-1}}. \quad (5.54)$$

We can now write down the point-dipole only contribution to the voltage eqn (5.51) as

$$V_n^D = -\frac{1}{\Omega_d} \frac{b_{n-1}^{d-1}}{a^{2(d-1)}} p_{n-1}, \quad (5.55)$$

where a is the radius of each hypersphere and we use eqn (5.52) and eqn (5.53) to solve for ΔV :

$$\Delta V = E_0 R + 2 \sum_{n=2}^{\infty} \left[-\frac{1}{\Omega_d} \frac{b_{n-1}^{d-1}}{a^{2(d-1)}} p_{n-1} \right]. \quad (5.56)$$

Before proceeding any further, we will examine eqn (5.55) for the case $d = 2$ and study the all important leading terms. We will consider the leading terms given by $n = 2, 3, 4$ and note that $p_1 = \Omega_d E_0 a^d$ and $\Omega_d = 2^{d-1} \pi$. For $n = 2$, since $n = 1$ means that $V_1 = 0$, we have

$$V_2^D = -\frac{1}{\Omega_2} \frac{b_1}{a^2} p_1; \quad b_1 = \frac{a^2}{R}; \quad \Omega_2 = 2\pi,$$

so that

$$V_2^D = -\frac{1}{2\pi} \frac{p_1}{R}. \quad (5.57)$$

In a similar way we consider the $n = 3$ case and keep in mind that $\omega_0 = 0$ and $\omega_1 = \omega = a/R$:

$$V_3^D = -\frac{1}{2\pi} \frac{b_2}{a^2} p_2; \quad b_2 = \frac{a\omega}{1 - \omega^2}; \quad p_2 = p_1 \omega^2,$$

$$V_3^D = -\frac{1}{2\pi a} \frac{\omega}{(1 - \omega^2)} p_2.$$

By not writing out p_2 explicitly and after simplifying we finally have

$$V_3^D = -\frac{1}{2\pi} \frac{p_2}{(R - a^2/R)}. \quad (5.58)$$

The fourth order term $n = 4$ can be expanded in the same way as before so that the following expressions are obtained

$$V_4^D = -\frac{1}{2\pi} \frac{b_3}{a^2} p_3; \quad b_3 = \frac{a^2}{R - \frac{a^2}{R}}; \quad p_3 = p_2 \frac{\omega^2}{(1 - \omega^2)^2},$$

$$\omega_1 = \frac{a}{R}; \quad \omega_2 = \frac{\omega}{1 - \omega^2}; \quad \omega_3 = \frac{\omega}{1 - \frac{\omega^2}{1 - \omega^2}},$$

so that after all the ω 's have been replaced we arrive at the final result

$$V_4^D = -\frac{1}{2\pi} \frac{p_3}{\left(R - \frac{a^2}{R}\right)} \quad (5.59)$$

The terms given by eqn's (5.57), (5.58) and (5.59) are exactly the same as eqn (30) of the paper by Djordjević *et al.* (1996). In fact when we plot the result for ΔV as a function of ω we can see that the result is exactly that given by the ΔV obtained by Djordjević *et al.* (1996), who used hyperbolic series to arrive at their result. The reason why eqn (5.56) is exact in two dimensions is because the only contributions that exist are those that come from the point dipoles. For the case $d = 2$ all charge contributions vanish. However for other dimensions, the charges do not cancel so that we need to consider these in the next section.

5.6.2 Dipole and charge contributions

In two dimensions we expect the charges to disappear and the only contribution to the voltage comes from the point dipoles only. The expression for the latter can be used for the case $d = 3$, but the convergence is very slow especially when we consider the limit where the spheres are touching ($\omega = 1/2$). By the methods used previously and using the results for the charges, eqn's (5.47), (5.48) and (5.49), we write down the expression for the charge contributions, V_n^C :

$$V_n^C = -\frac{1}{\Omega_d} \sum_{k=1}^n \frac{Q_n^{(k)}}{\rho_{k-1}^{\frac{d-2}{2}}}, \quad (5.60)$$

where all symbols, b, a, p and so on, have the usual meaning as encountered before. We define the parameter ρ such that

$$\rho_{k-1}^{d-2} \equiv [R - b_{k-1}]^{d-2}. \quad (5.61)$$

As can be seen from eqn (5.61), when $d = 2$, $\rho = 1$ and the charges in eqn (5.60) cancel each other out. Thus the total voltage ΔV , which includes both point dipoles and charges can be written as:

$$\Delta V = E_0 a \left\{ \left(\frac{R}{a} \right) + \left(\frac{2}{E_0 a \Omega_d} \right) \sum_{n=2}^{\infty} \left[\sum_{k=1}^n \frac{Q_n^{(k)}}{\rho_{k-1}^{d-2}} - \frac{b_{n-1}^{d-1}}{a^{2(d-1)}} p_{n-1} \right] \right\}. \quad (5.62)$$

For three dimensions where the inclusions are spheres, eqn (5.62) gives us a slight improvement in convergence in the limit when the two spheres approach each other ($\omega \rightarrow 1/2$), as compared to when we consider the point dipole contributions only. The better convergence is due to the participation of the charges but unfortunately eqn (5.62) converges so slowly overall as $\omega \rightarrow 1/2$ that in order to improve upon this convergence an enormous number of terms needs to be considered which makes the whole procedure computationally difficult, especially as we are dealing with symbolic mathematical terms. Even so the method gives us a very powerful insight that could be used in conjunction with analytical methods to re-sum the terms appearing in say, the continued fractions, thus giving us the desired convergence without having to compute a vast amount of terms. While such a re-summation needs to be studied more carefully in great detail, something that is beyond the scope of this thesis, we will nevertheless illustrate the principle by considering the limit when the hyperspheres are touching, $\omega = 1/2$ or $\Delta V = 0$.²

To study the limit when the two hyperspheres touch, ie, when $\omega = 1/2$ (or $\bar{\omega} = 2$), we will consider the continued fraction w_n . We notice that for any large ω such that $n \rightarrow \infty$, the continued fraction has the form

$$w_{\infty} = \frac{\omega}{1 - \frac{\omega^2}{1 - \frac{\omega^2}{1 - \omega^2}}} \quad (5.63)$$

where for reasons we have talked about before, we are able to write such a continued fraction in ω alone. By evaluating such continued fractions at $\omega = 1/2$ we notice

²If we were to plot eqn (5.62) as a function of $\omega^{-1} = \bar{\omega} = R/a$, we find that when $\bar{\omega} = 2$, $\Delta V = 0$.

that we obtain the following pattern:

$$\{\omega_1, \omega_2, \omega_3, \omega_4, \dots\} = \left\{ \frac{1}{2}, \frac{2}{3}, \frac{3}{4}, \frac{4}{5}, \dots \right\}. \quad (5.64)$$

Now for any number x , we can expand it in a continued-fraction form such that

$$x = a_0 + \frac{1}{a_1 + \frac{1}{a_2 + \frac{1}{a_3 + \dots}}},$$

which can be represented in the following notation

$$x = \{a_0, a_1, a_2, a_3, \dots\}.$$

From eqn (5.64) we can surmise that for any w_n as $n \rightarrow \infty$, we obtain the formula

$$\omega_n = \{0, 1, n\} = \frac{1}{1 + \frac{1}{n}}, \quad (5.65)$$

so that by substituting values for n we derive

$$\begin{aligned} \omega_1 &= \{0, 1, 1\} = \frac{1}{1 + \frac{1}{1}} = \frac{1}{2}, \\ \omega_2 &= \{0, 1, 2\} = \frac{1}{1 + \frac{1}{2}} = \frac{2}{3}, \\ \omega_3 &= \{0, 1, 3\} = \frac{1}{1 + \frac{1}{3}} = \frac{3}{4}, \\ \omega_4 &= \{0, 1, 4\} = \frac{1}{1 + \frac{1}{4}} = \frac{4}{5}, \\ &\vdots \end{aligned} \quad (5.66)$$

and so forth. Thus for all n we can generate the ω 's in the simple form

$$\omega_n = \frac{n}{n+1}. \quad (5.67)$$

As the number of terms that need to be calculated increases considerably as the hyperspheres touch, eqn (5.67) reduces the otherwise complex terms to a form that is computationally more efficient.

At the same time eqn (5.67) gives us an idea as to how the voltage ΔV behaves at that limit. By taking the voltage due to the point dipoles only for brevity³, we can express it as:

$$V_{n+2}^D = -\frac{1}{\Omega_d} \frac{b_{n+1}^{d-1}}{a^{2(d-1)}} p_{n+1}, \quad (5.68)$$

³The same can be done with the voltage due to the charges, V_n^C , but it is more involved.

where we note that $n \geq 0$ and $p_1 = p_0 = \Omega_d E_0 a^d$. The dipoles are now obtained from

$$p_{n+1} = p_n \left[\frac{n}{n+1} \right]^d, \quad (5.69)$$

while the positions of the dipoles are given by

$$b_{n+1} = \frac{a(n+1)}{n+2}, \quad (5.70)$$

and by substituting eqn's (5.69) and (5.70) into eqn (5.68) we obtain

$$V_{n+2}^D = -\frac{1}{\Omega_d} \left[\frac{n+1}{a(n+2)} \right]^{d-1} \left[\frac{n}{n+1} \right]^d p_{n+1}. \quad (5.71)$$

When we take the limit $n \rightarrow \infty$ we see that eqn (5.71) simplifies to

$$\lim_{n \rightarrow \infty} V_{n+2}^D \equiv V_\infty^D = -\frac{1}{\Omega_d} \left[\frac{1}{a} \right]^{d-1} p_{\infty+1} \quad (5.72)$$

where we notice from eqn (5.69) that $p_{\infty+1} = p_\infty$ as $n \rightarrow \infty$. This means that $p_\infty \dots p_{100} = p_{99}, p_{99} = p_{98}, p_{98} = p_{97} \dots p_1$. Eqn (5.72) now becomes

$$V_\infty^D = -\frac{1}{\Omega_d} \left[\frac{1}{a} \right]^{d-1} p_1. \quad (5.73)$$

Substituting $p_1 = \Omega_d E_0 a^d$ we finally obtain

$$\frac{\Delta V}{V_0} = 2 + \frac{2}{V_0} \left(-\frac{1}{\Omega_d} \left[\frac{1}{a} \right]^{d-1} \Omega_d a^d E_0 \right) = 0, \quad (5.74)$$

where $V_0 = E_0 a$. Remarkably we see that for inclusions of any dimension d , the voltage ΔV becomes zero at $\omega = 1/2$, as expected.

Finally, a useful approximation for ΔV can be written down for all dimensions d , as a function of $\bar{\omega} = R/a$:

$$\frac{\Delta V}{V_0} = \left[\bar{\omega}^{(d-2)} (\bar{\omega}^d - 2^d) \right]^{\frac{1}{2(d-1)}}. \quad (5.75)$$

For $d = 2$ we obtain

$$\frac{\Delta V}{V_0} = \left[(\bar{\omega}^2 - 4) \right]^{\frac{1}{2}}. \quad (5.76)$$

This result is exact in two dimensions to that obtained by Djordjević *et al.* (1996), who obtained their version by the use of hyperbolic series. In three dimensions the voltage reduces to

$$\frac{\Delta V}{V_0} = \left[\bar{\omega} (\bar{\omega}^3 - 8) \right]^{\frac{1}{4}}. \quad (5.77)$$

When eqn (5.77) is plotted and compared against results obtained by others in the literature using techniques such as the finite element method, there is understandably an error associated with such an approximation. However eqn (5.77) can serve as a useful beginning to further investigate the behaviour of the voltage between two hyperspheres with a possible view to re-summing otherwise complex terms.

5.7 Weak-scattering approximation

We now return to the integral eqn (5.27) and study the behaviour for what we refer to as the *weak - scattering* limit, ie, $\alpha \rightarrow 1$. Now since the factor

$$\frac{\alpha - 1}{\alpha + 1} = \frac{\beta d}{2 + \beta(d - 2)}, \quad (5.78)$$

it follows that to $O(\beta^3)$ in κ we have the simple result

$$F_d(0) = d^2(d - 1) \int_0^{1/2} \frac{s^{d-1}}{(1 - s^2)^d} ds. \quad (5.79)$$

The integral eqn (5.79) is elementary and the values of $F_d(\beta)$ are easily calculated (see results Chapter). Using eqn (5.28) and eqn (5.79), we can write the coefficient κ of the c^2 term in the dielectric constant as

$$\kappa = d\beta^2 + \beta^3 d^2(d - 1) \int_0^{1/2} \frac{s^{d-1}}{(1 - s^2)^d} ds. \quad (5.80)$$

We can also easily expand the integrand in eqn (5.79); the first two terms upon integration yield $F_3(0) = 87/80$ in agreement with the β^3 terms of Jeffrey (1973). Note that the latter does not contain *all* the β^3 terms, as opposed to the image method presented here. This is an important observation and it maybe useful for the re-summation of the multipole series in Chapter 4. Finally, for *holes* where $\alpha \rightarrow 0$, the series eqn (5.29) can be easily summed to give the value of $\kappa = 7/12 = 0.583333\dots$, in good agreement with Jeffrey (1973) and the result using the multipole expansion method which gives the value $\kappa = 0.588277\dots$. The weak scattering approximation eqn (5.79) yields $\kappa = 0.591992\dots$ which in agreement to two significant figures. That this approximation is less good for the perfect conductor limit can also be seen

here, since eqn (5.79) predicts a value of $\kappa = 4.264061\dots$ to be compared with the known value $\kappa = 4.51\dots$ of Jeffrey (1973) and the result obtained using the multipole expansion method of Chapter 4.

5.8 A useful algebraic approximation

For some purposes it may be useful to have an analytic approximation for the pair term that is good to a few per cent for *all* dimensions d and for all values of α . This can be achieved by noting that the integral eqn (5.79) that occurs in the weak-scattering limit can be approximately evaluated to give

$$F_d(\beta) = d^2(d-1) \int_0^{1/2} \frac{s^{d-1}}{(1-s^2)^d} ds \approx d(d-1) \left(\frac{2}{3}\right)^{d+1}. \quad (5.81)$$

The agreement is reasonable at all d and with errors of less than 8 per cent for $d = 1$ up to 30. For very large d , an asymptotic evaluation of integral eqn (5.81) is larger by a factor of $3/2$, but this works less well in the range of d . Using this result and eqn (5.28), we have

$$\kappa = d\beta^2 + \beta^3 d(d-1) \left(\frac{2}{3}\right)^{d+1}. \quad (5.82)$$

Note that the second term is somewhat smaller than the first term in eqn (5.82), but nevertheless we find it convenient to display the results for κ rather than for F_d . The algebraic approximation eqn (5.82) is reasonable for all d and for all dielectric constants of host and inclusion, and leads to a dielectric constant

$$\epsilon = \epsilon_0 \left[1 + cd\beta + c^2 \left\{ d\beta^2 + \beta^3 d(d-1) \left(\frac{2}{3}\right)^{d+1} \right\} \right]. \quad (5.83)$$

This approximation leads to the exact results for κ both as $d \rightarrow 1$ and as $d \rightarrow \infty$, where $\beta = (\epsilon_1 - \epsilon_0)/(\epsilon_1 + (d-1)\epsilon_0)$. When $d = 1$, we have the exact expansion

$$\begin{aligned} \epsilon &= \epsilon_0(1 + c\beta + c^2\beta^2 + \dots) \\ &= \epsilon_0 \left[1 + c\left(1 - \frac{1}{\alpha}\right) + c^2\left(1 - \frac{1}{\alpha}\right)^2 + \dots \right], \end{aligned} \quad (5.84)$$

which can be obtained by noting that in one dimension $\kappa = \beta^2$ is an exact result, ie, the conductances which are equivalent to the dielectric constants add in parallel

to give $\alpha/\epsilon_0 = (1 - c\beta)^{-1}$, or equivalently $\alpha^{-1} = (1 - c)\epsilon_0^{-1} + c\epsilon_1^{-1}$. In the limit that $d \rightarrow \infty$, we have $\kappa = 0$ and we recover the virtual crystal approximation

$$\begin{aligned}\epsilon &= \epsilon_0 [1 + cd\beta] \\ &= \epsilon_0 [1 + c(\alpha - 1)] \\ &= (1 - c)\epsilon_0 + c\epsilon_1.\end{aligned}\tag{5.85}$$

This is equivalent to saying that the various pieces of the dielectric add up in parallel in one dimension and in series in infinite dimensions. In between, the situation is very complex, but the behaviour for a general d goes smoothly between these limits.

In concluding this Chapter, we note that we have presented an alternative study of the dielectric function to $O(c^2)$ using the method of images. By an extension of the Neumann image theory to d dimensions and to higher-order image dipoles, we have put the theory of images for the bispherical system into a unified framework. Numerical studies are consistent with that of Chapter 4, putting the multipole series expansion method in perspective (see results Chapter). We have found that the method of images for the dielectric bispherical system is rather difficult to implement in general and that analytical calculations beyond the fourth image sets $(\mathbf{p}_4^{\perp 0}, \rho_4^{\perp})$ and $(\mathbf{p}_4^{\parallel 0}, \rho_4^{\parallel})$ appear to be intractable. Nevertheless, the perfect conductor limit appears to be amenable to extensions beyond the fifth image sets $(\mathbf{p}_5^{\perp 0}, \rho_5^{\perp})$ and $(\mathbf{p}_5^{\parallel 0}, \rho_5^{\parallel})$. Our calculations for \mathbf{p}_5 , which is the third non-trivial term for the image series in this case, already converges to a value for $F_d(1)$ that is superior to the 20-term multipole series in Chapter 4 (see results later).

We have derived an expression for the voltage between two hyperspheres and looked at the important limit when they are touching ($\omega = 1/2$). Furthermore, two approximation methods were investigated in this Chapter. We studied the point-dipoles-only approximation, known to be exact for $d = 2$. We showed that for perfect conductors this approximation contains about 70 per cent of the result for $d = 3$. We have also investigated the weak-scattering limit. We have given a simple algebraic approximation for the pair term in the dielectric function, κ , that is exact in the limits $d = 1$ and $d \rightarrow \infty$, and shows the dimensional dependence of

κ explicitly. This should be useful in constructing affective medium theories that attempt to include the pair terms.

CHAPTER 6

Results and Beyond

6.1 Introduction

We have been interested in determining the dielectric function of a composite material by calculating κ in the virial expansion for the dielectric function ϵ :

$$\epsilon = \epsilon_0(1 + \eta c + \kappa c^2 + \dots) \quad (6.1)$$

where c is the volume fraction of inclusions. We have done this for a binary system of inclusions in a d -dimensional space using two alternative methods; the multipole expansion method and the images method. During all this we have considered how one-body effective medium theory can incorporate these two-body results to improve upon the results of Bruggeman and Maxwell-Garnett. That eqn (6.1) actually converges to known values in the appropriate limits is rather profound as no known proof, to the author's knowledge, exists that shows that indeed convergence occurs in this virial expansion as opposed to divergence. Even so eqn (6.1) is used widely in the literature and we have followed the example of others.

The calculations were arrived at using procedural programming in Mathematica. The primary reason for this was that the computations involved were mainly symbolic in nature. The disadvantage of using symbolic computations however is evident when we deal with memory considerations (swap files etc) as the enormous number of terms involved need to be dealt with efficiently. For example, in the multipole expansion method the $n = 200$ calculation involves a matrix of more than 40,000 unknowns and furthermore, for each unknown, there are series expansions involving hundreds of terms respectively. A typical calculation using the method of images may include computation of more than three hundred thousand terms. In the general dielectric case the multipole expansion method appears to converge

much faster to values for κ than the image method. However in the superconducting case for example, it is the other way around. The two different approaches agree with each other when values are compared to those of others in the field showing that there is at least a foundation to begin the next step of making improvements to EMIT in certain instances. At the same time, these methods can be used in different ways to solve problems of particular interest as was the case in the use of the image method in the solution of the d -dimensional voltage between two inclusions.

6.2 Results

In Chapter 4 we obtained d -dimensional solutions for the general dielectric case using the multipole expansion method. In particular we considered the bi-hyperspherical system with symmetry and the solutions generated by

$$(-1)^{(m-1)p} g_{m,n} + \beta_n \sum_{s=1}^{\infty} \binom{n+p+s-1}{n+p+m-1} p g_{m,s} \left(\frac{\alpha}{R}\right)^{n+p+s} = \beta_n \delta_{1,n}, \quad (6.2)$$

where $m = 0, 1$ corresponds to the parallel and perpendicular case respectively, $p = d - 2$ and d is the dimension. The generalized polarizability β_n is given by

$$\beta_n = \frac{n(\alpha - 1)}{n\alpha + n + p}, \quad (6.3)$$

and $\alpha = \epsilon_1/\epsilon_0$, with ϵ_1 is the dielectric constant of the inclusion and ϵ_0 is the dielectric constant of the host medium. Now by expanding the $g_{m,n}$ as a power series in the ratio $\xi = a/R$ in eqn (6.2), we can eventually write down the result for κ (see Chapter 4):

$$\kappa = d\beta \left[\beta + \sum_{s=2d} \frac{B_s - dA_s}{(s-d)2^{s-d}} \right]. \quad (6.4)$$

If we take the limit $d = 1$ in eqn (6.4), we see that $\kappa = \beta^2$ which is an exact result, all β_n become $1 - \frac{1}{\alpha}$ and only the parallel case survives in this limit with $g_1 = \beta$. The next logical step is to consider the $d = 2$ case and in Fig 6.1 we plot κ vs $\log_{10}(\alpha)$. The multipole expansion result is plotted against the result of Djordjević *et al.* (1996), whose results were obtained by expanding a series in β to $O(\beta^3)$. The convergence of the two methods can be seen given that the multipole

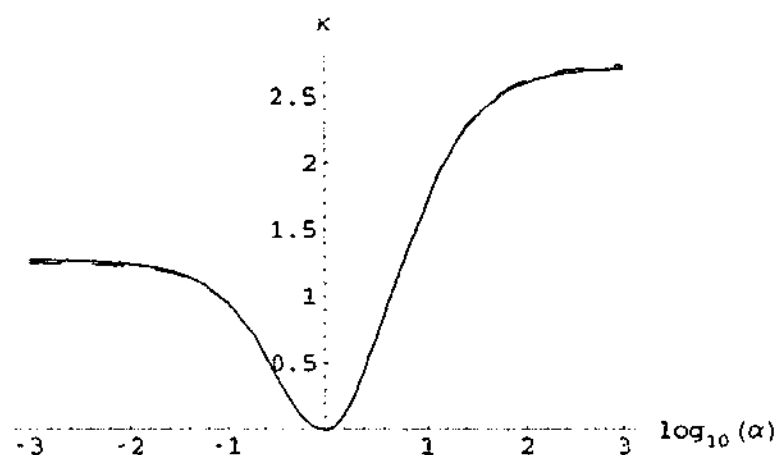


Figure 6.1: Plot of κ vs $\log_{10}(\alpha)$ for $d = 2$. The result of Djordjević *et al.* (1996) is shown as the dashed curve and has a slightly different convergence to that of the multipole expansion method due to the different number of terms calculated. Here $\alpha = \epsilon_i/\epsilon_0$ is the ratio of the dielectric constant of the inclusions ($i = 1, 2$) to that of the host medium.

expansion solution was evaluated to $O(\xi^{21})$ before averaging. In Fig 6.2 we consider the $d = 3$ case where the inclusions become spheres. The curve (solid line) for the multipole expansion method was calculated for all values of β_n in eqn (6.4) while Jeffrey (1973) calculated specific values for β each time separately and extrapolated his curve based on these results (see dots in Fig 6.2). In a similar way we can consider higher dimensions, particularly $d = 4$. There are no known results with which to compare the convergence of the $d = 4$ case here using the multipole expansion method. However the convergence for $d = 4$ is slower than that for the $d = 3$ case, especially in the perfect-conductor limit. In fact it is rather difficult to predict the correct behaviour for large d in the equations generated by eqn (6.2), but we expect the interaction between the hyperspheres to actually vanish. In Fig 6.3 we plot the different dimensions for comparison. Apart from the general dielectric case, two limits are of interest here: the perfect-conducting limit and the 'holes' limit. The perfect-conductor limit means that $\alpha \rightarrow \infty$ so that $\beta \rightarrow 1$. In Table 6.1 we consider the convergence properties for this case and show κ for different d . The very last row in Table 6.1 shows the known results published by Djordjević *et al.* (1996) for $d = 2$ and Jeffrey (1973) for $d = 3$ which shows that the value obtained by the multipole

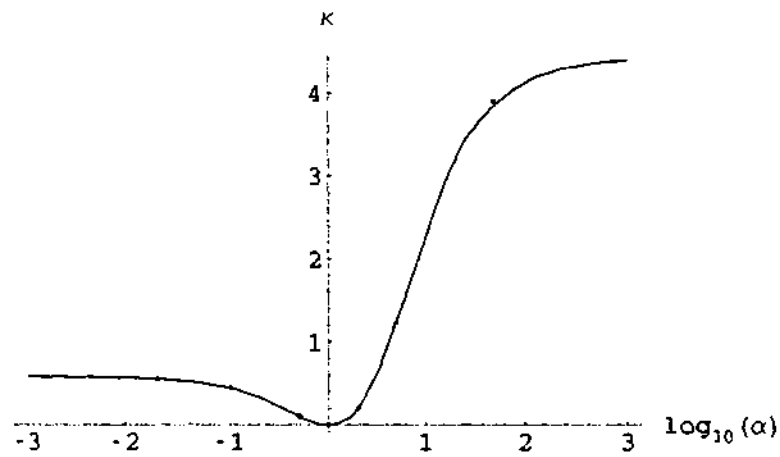


Figure 6.2: Plot of κ vs $\log_{10}(\alpha)$ for $d = 3$. The result using the multipole expansion method is compared to Jeffrey (1973), represented by the dots. Again $\alpha = \epsilon_i/\epsilon_0$ is the ratio of the dielectric constant of the inclusions to that of the host medium.

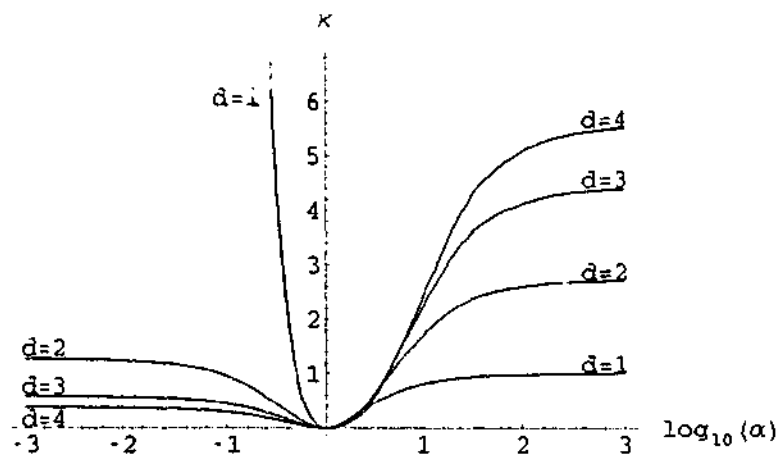


Figure 6.3: Plot of κ vs $\log_{10}(\alpha)$ for $d = 1, 2, 3, 4$. Again $\alpha = \epsilon_i/\epsilon_0$ has the same definition as in other figures.

Table 6.1: The coefficient κ to seven significant figures is tabulated for $d = 1, 2, 3, 4$ for the perfect-conductor, $\alpha \rightarrow \infty$.

n	$d = 1$	$d = 2$	$d = 3$	$d = 4$
20	1	2.722194	4.370400	5.566036
40	1	2.736795	4.454318	5.692201
60	1	2.740489	4.477818	5.724835
80	1	2.742055	4.488535	5.738464
100	1	2.742884	4.494546	5.745670
120	1	2.743385	4.498351	5.750006
140	1	2.743715	4.500958	5.752853
160	1	2.743945	4.502846	5.754840
180	1	2.744114	4.504271	5.756291
200	1	2.744241	4.505381	5.757389
220	1	2.744340	4.506268	5.758244
Extrapolated		2.7450	4.512	5.764
Known		2.744989	4.51	

expansion method agrees with Jeffrey to three significant figures. In fact we note that the series has not quite converged to the result of Jeffrey even for $n = 220$ but a $n^{-3/2}$ plot was made and the data was extrapolated to give $\kappa = 4.512$ which is consistent with Jeffrey's value of 4.51. The tabulated results for κ in $d = 1, 2, 3, 4$ were obtained by evaluating eqn (6.4) with the use of the expression:

$$\mathbf{S}(\mathbf{R}) = v^d \left[d\beta_1 \epsilon_0 \mathbf{E} - d\beta_1 \epsilon_0 \sum_{s=d}^{\infty} \frac{a^s}{R^s} \left(A_s \mathbf{E} - B_s \frac{\mathbf{E} \cdot \mathbf{R}}{R^2} \mathbf{R} \right) \right], \quad (6.5)$$

in the appropriate limit (see Chapter 4), up to $s = n + 1$, where n is given by the first column. The extrapolated value for $n \rightarrow \infty$ is also given and we can see the slow convergence towards the known results of Djordjević *et al.* (1996) for $d = 2$ and Jeffrey (1973) for $d = 3$. The other interesting limit is that for 'holes' where $\alpha \rightarrow 0$ which is a unique result for $d = 2$ as all $\beta_n \rightarrow -1$ giving a duality relation; $\kappa - 2$ for holes which is equal to $2 - \kappa$ for perfectly conducting inclusions giving the sum for κ as 4. This only applies for $d = 2$. Once again by considering eqn's (6.4) and (6.5) up to $s = n + 1$, in Table 6.2 we show the results for the quickly converging values for κ and compare them to the known values of Djordjević *et al.* (1996) for

Table 6.2: The coefficient κ to seven significant figures is tabulated for $d = 1, 2, 3, 4$ for the holes-limit, ie, when $\alpha \rightarrow 0$.

n	$d = 1$	$d = 2$	$d = 3$	$d = 4$
20	∞	1.277806	0.590254	0.381904
40	∞	1.263205	0.588277	0.381573
60	∞	1.259511	0.588023	0.381476
80	∞	1.257945	0.587937	0.381456
100	∞	1.257116	0.587901	0.381447
120	∞	1.256615	0.587883	0.381444
Extrapolated		1.2559	0.5878	0.3814
Known		1.255284	0.588	

$d = 2$ and Jeffrey (1973) for $d = 3$. The results encountered so far can be derived in the context of the image method (see the previous Chapter). The general dielectric case using the d -dimensional image method does not prove easy to solve beyond p_3 given the complexity of the dipole, line charge and charge density mappings. The region of integration in the equations is notably a problem as well as the involvement of non-elementary functions. We can however make comparison with the multipole expansion results via an expansion of a series in the ratio $\xi = a/R$. This can be done by averaging over angles and using a Clausius-Mossotti like formula. Thus we have found that κ up to the total averaged image \bar{p}_3 can be written as a sum

$$\kappa = d\beta^2 + \beta^3 F_d(\beta), \quad (6.6)$$

where

$$F_d(\beta) = d(d-1) \sum_{s=0}^{\infty} \left(\frac{1}{2}\right)^{d+2s} \binom{d+s-1}{s} \frac{\alpha+d-1}{\alpha(s+1)+d+s-1}. \quad (6.7)$$

The series in eqn (6.7) can be thought of as a partial resummation of eqn (6.4) of the multipole expansion method. When the two results are compared we find agreement up to the appropriate order in β . In Fig 6.4 we plot the graph of κ vs $\log_{10}(\alpha)$ where the dashed curves are the result of using the third order result from eqn (6.7), while the solid curves are due to the multipole expansion results. We now

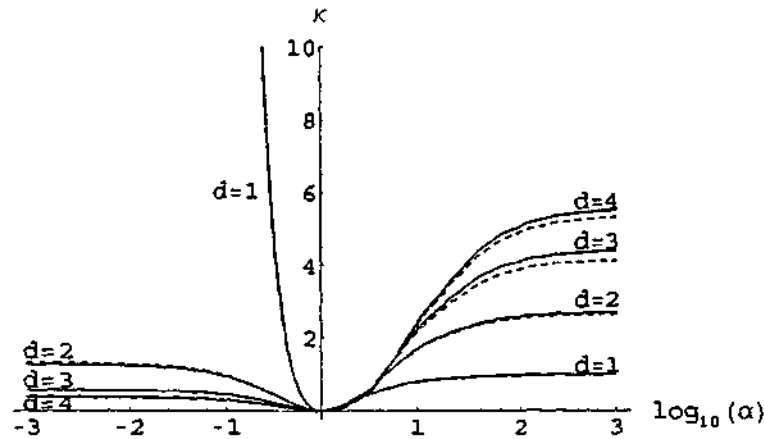


Figure 6.4: Plot of κ vs $\log_{10}(\alpha)$ for $d = 1, 2, 3, 4$, comparing the third order result (dashed lines), eqn (6.7), and the multipole expansion method results eqn (6.4). Note that the discrepancy in the convergence is due to the number of terms calculated in each case, which does not coincide in this graph.

return to the perfect-conductor limit ($\alpha \rightarrow \infty$). Only the $d = 2$ case can be solved easily using the general dielectric case. For other higher dimensions this is difficult, except for the limit of superconducting inclusions, ($\alpha \rightarrow \infty$). Even so, the perfect-conducting limit is still complicated by the parallel contributions of the field. This is because (except for $d = 2$) the point charges that are generated by the parallel configuration cannot be neglected. We have shown in Chapter 5 nevertheless, a method of mapping these higher order complex terms. Before investigating the total dipole moments that include the charge contributions we first examine the point-dipoles-only approximation. We recall that

$$\begin{aligned}
 F_d(1) &\approx \frac{2d(d-1)}{\omega_p E_0 a^{2d}} \int dR R^{d-1} \sum_{s=1}^{\infty} \bar{p}_{2s+1} \\
 &= \sum_{s=1}^{\infty} 2d(d-1) \int_0^{1/2} \frac{x^{2sd-d-1}}{\left[1 + \sum_{k=1}^s (-1)^k \binom{2s-k}{k} x^{2k} \right]^d} dx. \quad (6.8)
 \end{aligned}$$

By evaluating eqn (6.8), we can obtain the dipoles only contribution to any order¹. In Table 6.3 we have calculated the first eight contributions that converge very quickly in $d = 2$ because the charge contributions are zero. The next step is to

¹Note that $\beta = 1$ for the superconducting case so that $F_d(\beta) \rightarrow F_d(1)$

Table 6.3: The table below shows values for $F_d(1)$ for the perfect conductor limit $\alpha \rightarrow \infty$ for $d = 2, 3, 4$. Note that for the case $d=1$, the result is 0. Also note that $F_d(1)$ is related to κ by $\kappa = d + F_d(1)$.

s	$d = 2$	$d = 3$	$d = 4$
1	0.666666	0.842707	0.814815
2	0.722340	0.884733	0.839237
3	0.735509	0.891834	0.842187
4	0.740152	0.893781	0.842816
5	0.742196	0.894482	0.843002
6	0.743232	0.894783	0.843069
7	0.743813	0.894929	0.843098
8	0.744164	0.895007	0.843111

evaluate the contributions from both the dipoles and charges and in Table 6.4 the full total dipole moments to $n = 23$ have been tabulated that show the convergence to the known results in the various limits. It is possible to calculate the convergence to any order provided we can deal with computational limitations, one of which is the huge number of terms that have to be calculated symbolically, thus presenting us with memory limitations on any computing system. Another limit of interest is the so called *weak - scattering* limit when $\alpha \rightarrow 1$. To $O(\beta^3)$ in κ we obtained the result

$$F_d(0) = d^2(d-1) \int_0^{1/2} \frac{s^{d-1}}{(1-s^2)^d} ds, \quad (6.9)$$

where we have tabulated the results for eqn (6.9) in Table 6.5. We can write eqn (6.9) in terms of κ so that we have

$$\kappa = d\beta^2 + \beta^3 d^2(d-1) \int_0^{1/2} \frac{s^{d-1}}{(1-s^2)^d} ds. \quad (6.10)$$

In Fig 6.5 we compare eqn (6.10) for the weak-scattering limit (dashed curves) with the results obtained from the multipole expansion method. By expanding the integral in eqn (6.9) the first two terms upon integration give $F_3(0) = 87/80$ in agreement with the β^3 terms of Jeffrey (1973). As opposed to the method used here, Jeffrey's solutions do not contain all the terms for β which are important to have if we are considering a resummation of the multipole expansion series of

Table 6.4: The table below shows values for \bar{p}_n for the perfect conductor limit using higher order dipole images in d -dimensions. Values up to $n = 23$ are shown for $d = 2, 3, 4$. Note that for the case $d=1$, the result is 0. One can see from the results below that the convergence towards the known values is much faster when compared to the multipole expansion method. Also note that $F_d(1)$ is related to κ by $\kappa = d + F_d(1)$.

\bar{p}_n	$d = 2$	$d = 3$	$d = 4$
\bar{p}_3	0.666666	1.166666	1.370370
\bar{p}_4	0.666666	1.291666	1.550925
\bar{p}_5	0.722340	1.394103	1.652564
\bar{p}_6	0.722340	1.427576	1.691469
\bar{p}_7	0.735509	1.455031	1.716301
\bar{p}_8	0.735509	1.468273	1.729623
\bar{p}_9	0.740152	1.479289	1.738861
\bar{p}_{10}	0.740152	1.485755	1.744690
\bar{p}_{11}	0.742195	1.491220	1.748973
\bar{p}_{12}	0.742195	1.494825	1.751943
\bar{p}_{13}	0.743231	1.497916	1.754221
\bar{p}_{14}	0.743231	1.500118	1.755901
\bar{p}_{15}	0.743812	1.502030	1.757231
\bar{p}_{16}	0.743812	1.503469	1.758257
\bar{p}_{17}	0.744163	1.504731	1.759089
\bar{p}_{18}	0.744163	1.505717	1.759751
\bar{p}_{19}	0.744387	1.506592	1.760299
\bar{p}_{20}	0.744387	1.507297	1.760747
\bar{p}_{21}	0.744536	1.507927	1.761124
\bar{p}_{22}	0.744536	1.508447	1.761438
\bar{p}_{23}	0.744640	1.508915	1.761706

Known 0.744989...[1] 1.51...[2]

[1]The result for $d = 2$ is from Djordjevic *et al.* (1996)

[2]The result for $d = 3$ is from Jeffrey (1973)

Table 6.5: $F_d(\beta)$ in the weak-scattering limit to the leading order β .

d	$F_d(\beta)$
1	0.000000
2	0.666666
3	1.264061
4	1.629629
5	1.769689

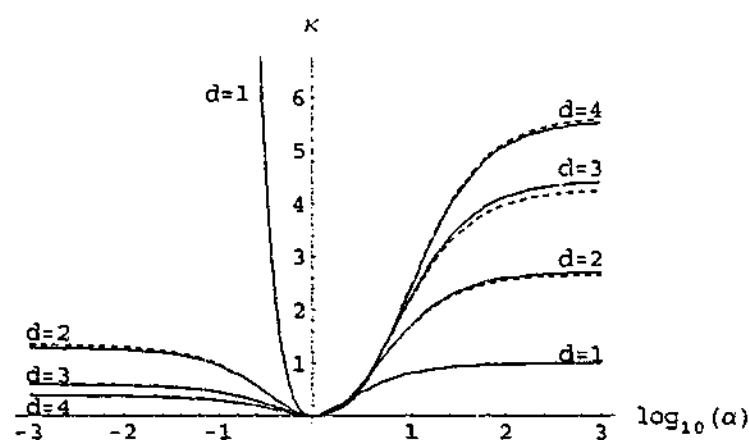


Figure 6.5: The graph of κ vs $\log_{10}(\alpha)$ for $d = 1, 2, 3, 4$. The weak-scattering limit eqn (6.10) is represented by the dashed curves and the solid curves represent the multipole expansion method eqn (6.4)

Chapter 4. Going back to eqn (6.7), for the limit of *holes* where $\alpha \rightarrow 0$, the series can be summed to give $\kappa = 0.583333\dots$, a value that is in good agreement with Jeffrey (1973) or the value $\kappa = 0.588277\dots$ obtained by the multipole expansion method. For the weak scattering approximation we find $\kappa = 0.591992\dots$ which is in agreement to two significant figures. On the other hand for the perfect-conducting case the weak scattering limit gives a value of $\kappa = 4.264061$ which does not quite converge to the known value of $\kappa = 4.51\dots$. We have derived a useful approximation for all d and all α from eqn (6.9). The agreement is good for all d with errors of less than 8%:

$$F_d(\beta) \approx d(d-1) \left(\frac{2}{3}\right)^{d+1} \quad (6.11)$$

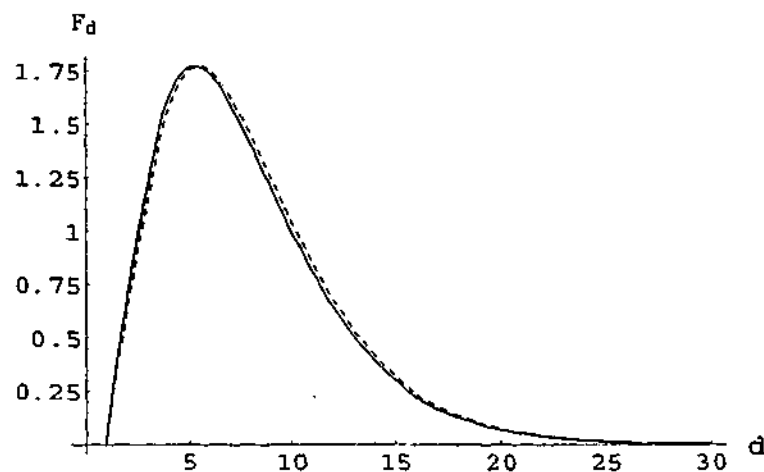


Figure 6.6: F_d vs d . The dashed line is eqn (6.11) and the solid line represents the weak-scattering limit eqn (6.9)

In Fig 6.6 we plot the weak-scattering limit eqn (6.9) together with eqn (6.11) and the dimensional dependence of F_d can be seen. More interestingly, in Fig 6.7 the algebraic approximation eqn (6.11) is compared to the results of the multipole expansion method for $d = 1, 2, 3, 4$. Notice that the exact asymptotic behaviour for $d = 4$ is as yet unknown. The results so far for the perfect-conductor case, $\alpha \rightarrow \infty$, allow us to plot the conductance σ against the low density of inclusions c . Fig 6.8 shows the behaviour of $\sigma = \epsilon/\epsilon_0$ of inclusions of varying dimension d . We now return to the problem of the voltage between two hyperspherical inclusions. In the previous Chapter we derived the voltage for any dimension in terms of both the dipole only *and* charge contributions respectively, see eqn (5.62). We also recall the approximation for the voltage ΔV

$$\frac{\Delta V}{V_0} = [\bar{w}^{(d-2)}(\bar{w}^d - 2^d)]^{\frac{1}{2(d-1)}}, \quad (6.12)$$

where V_0 is a constant and $\bar{w} = R/a$. In figure 6.9 we see a plot of $\frac{\Delta V}{V_0}$ vs \bar{w} for $d = 2$. As expected for $d = 2$ the charge contributions are zero and the only contributions are from the point dipoles only in eqn (5.62). Thus when we plot the results of Djordjević *et al.* (1996) vs eqn (5.62) we see that they are exact. Furthermore the approximation that we have derived eqn (6.12) is also exact and all

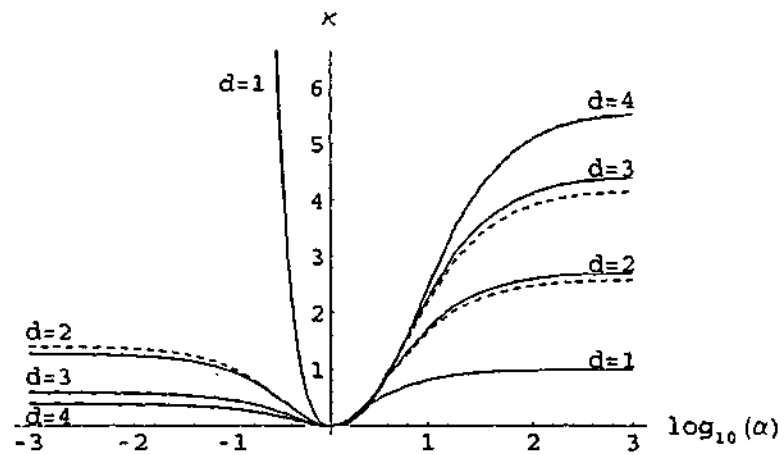


Figure 6.7: κ vs $\log_{10}(\alpha)$. The dashed lines come from eqn (6.11) and the solid lines are the result of the multipole expansion method.

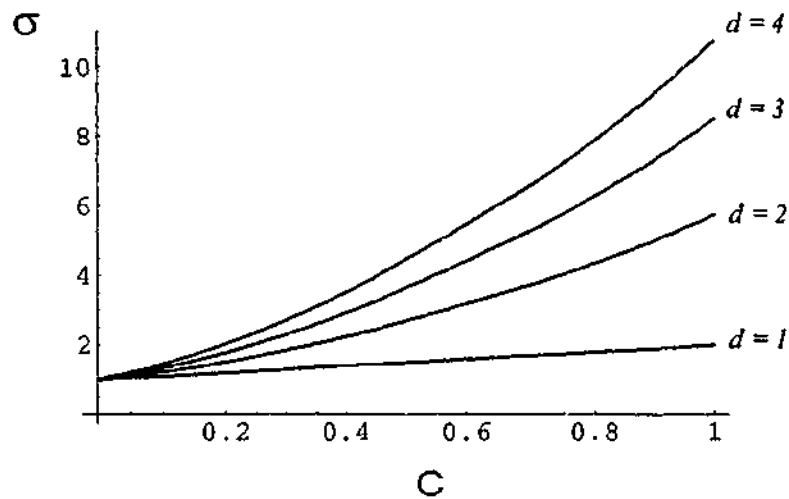


Figure 6.8: The conductance $\sigma = \epsilon/\epsilon_0$ has been plotted for $d = 1, 2, 3, 4$ in the low volume fraction of inclusions c , for perfect-conducting inclusions.

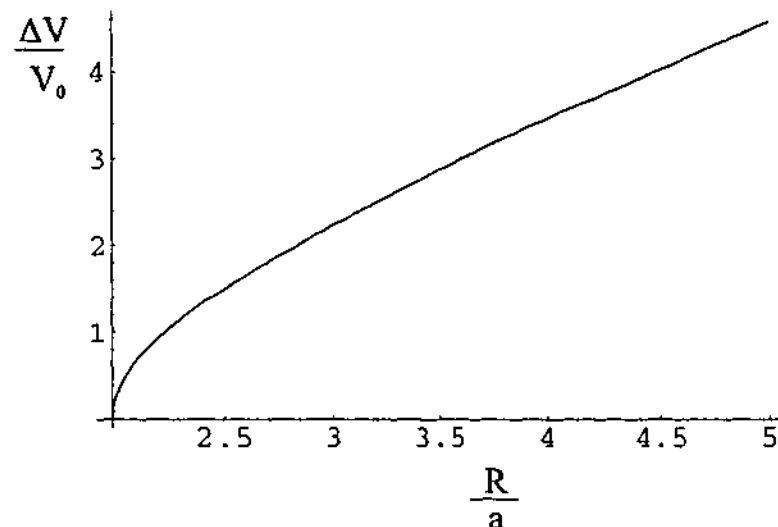


Figure 6.9: The voltage between two inclusions is shown for $d = 2$. Three results are actually shown (i) the case of the image method derived here eqn (5.62), (ii) the case of Djordjević *et al.* (1996) and (iii) the approximation eqn (6.12). All curves are exact and so lie on top of each other.

three curves coincide. These calculations require enormous computational power as was previously mentioned and unfortunately the author had limited facilities that could not allow calculations of higher orders. This is more evident when considering the voltage in $d = 3$ where apart from the dipoles-only contributions, we *must* include the contributions from the charges as well. Fig 6.10 shows the $d = 3$ case with the graphs corresponding to eqn (5.62)-without the charge contributions as well as the case where they are included. The approximation eqn (6.12) is also plotted for comparison. The true behaviour for the voltage should be close to the approximation eqn (6.12) within error considerations, however we observe that the convergence for both dipole only and dipole+charge contributions is painfully slow. Not surprising given that we require a very large number of terms in order to include all mappings of dipoles and charges. In Table 6.6 we see how slowly the convergence is for $d = 3$. The top part shows the convergence without the charges while the bottom two rows include the charges for comparison. Fig 6.10 shows that eqn (5.62) with both *dipoles – and – charges* only converges slightly more in comparison to eqn (5.62) without the *charges*. One way to avoid such computational complexity is to resum the terms and thus simplify calculations. For example when deriving

Table 6.6: Values obtained for ΔV showing very slow convergence for $d = 3$. The first four rows show convergence due to dipole-only interactions in eqn (5.62), while the last two rows include the image contributions also.

n	ΔV
10	1.29954
20	1.29233
150	1.28991
200	1.28989
10	1.24603
20	1.24408

eqn (6.12) two methods were used (i) inclusion of leading terms and (ii) a simple regression calculation in order to derive a 'fit' to the data.

6.3 Beyond

Throughout this thesis we have studied two methods that can be used in d -dimensions to study two body interactions, eg, the voltage between two inclusions. By studying these second order effects we can begin to consider extensions to existing 1-body EMT. One way of gaining further insight beyond the d -dimensional multipole expansion and image methods dealt with here is to solve the same problem using curvilinear coordinates for a binary system, which granted is not so easily done, but would check the validity of the previous two. Another consideration is to properly re-sum terms appearing in the complex mappings between the two inclusions, something that was done to a certain extent in this thesis with various approximations. Clearly these re-summations or approximations are also needed to deal with the huge amount of calculations that need to be performed computationally, a problem that unfortunately otherwise means the need to access high-end computer hardware and software. Such approximations or re-summations need to be investigated thoroughly before being seriously applied to extensions in current EMT.

We have investigated the dielectric function amongst other matters, which is based on electromagnetic considerations. The more complicated problem of deriving

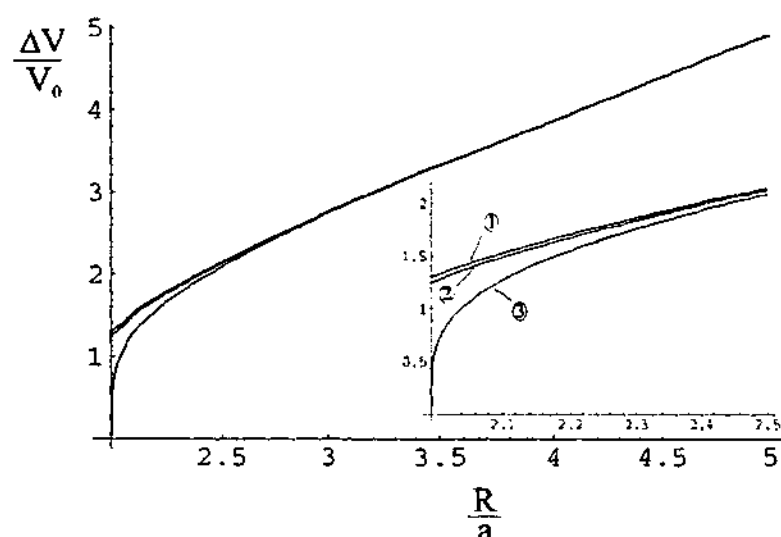


Figure 6.10: The voltage between two inclusions is shown for $d = 3$. Three results are actually shown (i) the case of the image method derived here eqn (5.62) *without* the charge contributions (curve 1), (ii) the case of eqn (5.62) *with* the charge contributions (curve 2) and (iii) the approximation eqn (6.12) (curve 3). The inset shows the interval $\tilde{\omega} \in [2, 2.5]$ so that the convergence can be better differentiated between each case.

a d -dimensional general solution for hydrodynamics in the same way should be pursued and properly understood, (founded by Einstein (1906)). The work presented here may be of use for such an investigation given that the underlying mathematical analysis can be easily used if symbols and equations are changed appropriately. In our treatment of the two-body problem we have dealt with the static case. Further expansions of the results here could come in the form of dynamical considerations. Moreover the real dielectric function was calculated for a composite material and it would be interesting to investigate the imaginary part of the dielectric function. The study of second order effects in EMT means improvements in various areas of condensed matter physics. For example, the study of optical properties of a dielectric host system embedded with a random distribution of metallic particles is of interest to many topics such as, doped semiconductors, colloids, metallic glasses as well as in areas involved in atmospheric pollution and remote sensing employing microwave radar instruments.

The application of the effective medium approach to the study of mechanical

properties of materials leads us to consider the elastic properties of solid systems (see solutions by Yamakawa (1962) of such a system). One interesting aspect is the combination of knowledge of fluid and mechanical properties to study sound propagation in a porous medium. However it is widely seen that the theories involved are inadequate due to the lack of self-consistency (see Harker and Temple (1988), thus leaving room for improvements using EMT techniques which of course might ultimately entail second-order corrections. Finally, one new area of research that has received much attention in recent years is that of non-linear composites. In the case of dielectrics, the inclusions are known to have a non-linear constitutive relation of the form (Landau, Lifshitz and Pitaevskii (1984))

$$\mathbf{D} = \epsilon \mathbf{E} + \chi |\mathbf{E}|^2 \mathbf{E}, \quad (6.13)$$

where the term non-linear susceptibility originated. The idea of course is similar to what we have been studying throughout in this thesis, that is, to find the effective coefficients σ_e , χ_e , ϵ_e , etc, and the various intrinsic coefficients. One would expect an analogy to the Bruggeman and Maxwell-Garnett formulae, but the one-body problem here is highly non-trivial, since Maxwell's equations lead us to non-linear partial differential equations. For weak non-linearities however, a perturbative solution using spherical harmonics can be obtained Yu *et al.* (1993), based on which an EMT theory can also be constructed. There are many areas of EMT that can be studied that might be improved by considering some of the methods that have been used here to solve for the two-body contributions. First however, these latter methods need to be investigated further in order to extend current understanding of the two-body problem. It is hoped that the work presented here in this thesis has contributed to that goal.

CHAPTER 7

Appendices

7.1 Appendix A: Spherical harmonics shift formula 1

Spherical harmonic shift formulae find applications in many areas of theoretical physics (Lord Rayleigh 1892; Kohn and Rostocker 1954). In this appendix we will be concerned with a classic formula attributed to Hobson (1931), which we will prove generalizes to arbitrary integer dimensions d . We begin with the geometrical configuration of Fig 7.1. With the usual definition whereby $z = x_0, x_1, x_2, \dots, x_{d-1}$ are the Cartesian coordinates, by Taylor's theorem the electrostatic potential in d dimensions can be expanded as

$$\begin{aligned} \frac{1}{[(z - \rho)^2 + x_1^2 + x_2^2 + \dots + x_{d-1}^2]^{p/2}} &= \sum_{l=0}^{\infty} \frac{(-1)^l}{l!} \rho^l \frac{\partial^l}{\partial z^l} \left(\frac{1}{r^p} \right) \\ &= \frac{1}{r^p} \left(1 - 2 \frac{z\rho}{r^2} + \frac{\rho^2}{r^2} \right)^{-p/2} \\ &= \frac{1}{r^p} \sum_{l=0}^{\infty} P_l \left(\frac{z}{r} \right) \left(\frac{\rho}{r} \right)^l \\ &= \sum_{l=0}^{\infty} \frac{\rho^l}{r^{l+p}} P_l(\cos \theta). \end{aligned} \quad (7.1)$$

We must remember that the P_l here are the p -Legendre polynomials. Therefore,

$$\frac{P_l(\cos \theta)}{r^{l+p}} = \frac{(-1)^l}{l!} \frac{\partial^l}{\partial z^l} \left(\frac{1}{r^p} \right). \quad (7.2)$$

Then by eqn (7.1) we have the following relation;

$$\begin{aligned} \frac{\partial^l}{\partial z^l} \left(\frac{1}{r^p} \right) &= \frac{\partial^l}{\partial z^l} \frac{1}{[x_1^2 + x_2^2 + \dots + (z + \rho)^2]^{p/2}} \\ &= \frac{\partial^l}{\partial \rho^l} \frac{1}{[r'^2 + 2z'\rho + \rho^2]^{p/2}} \\ &= \frac{\partial^l}{\partial \rho^l} \sum_{s=0}^{\infty} \frac{r'^s}{\rho^{p+s}} P_s(\cos \theta'') \end{aligned}$$

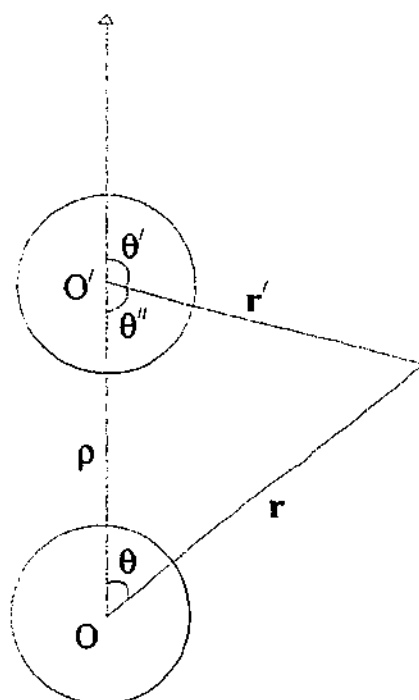


Figure 7.1: Reoriented twin spherical coordinates. The two polar angles θ and θ' are equivalent to θ_1 and θ_2 of Fig 4.1

$$= (-1)^l \sum_{s=0}^{\infty} \frac{(p+s+l-1)!}{(p+s-1)!} \frac{r'^s}{\rho^{p+s+l}} P_s(\cos \theta''). \quad (7.3)$$

Thus we have from eqn (7.2) that

$$\frac{P_l(\cos \theta)}{r^{l+p}} = \sum_{s=0}^{\infty} \binom{p+s+l-1}{p+s-1} \frac{r'^s}{\rho^{p+s+l}} P_s(\cos \theta''). \quad (7.4)$$

that proves the first shift formula in Chapter 4.

7.2 Appendix B: Spherical harmonics shift formula 2

This shift formula, as compared to the one above, is a little more involved. We first define complex coordinates: $\zeta = x + iy$, and $\eta = x - iy$. The main step requires the proof of the following properties of the raising operator:

$$\frac{1}{2} \left(\frac{\partial^m}{\partial \zeta^m} + \frac{\partial^m}{\partial \eta^m} \right) \frac{P_{l-m}(\mu)}{r^{l-m+p}} = \frac{1}{2^m} \frac{1}{r^{l+p}} P_l^m(\mu) \cos(m\phi). \quad (7.5)$$

Here $\mu = \cos \theta_{(1)} = \cos \theta$ and ϕ is equivalent to $\theta_{(2)}$, and the triplet $(x, y, z) = (x_1, x_2, x_0)$ now defines a three-dimensional subspace. This is an invariant subspace in the sense that the triplet can be rotated arbitrarily without affecting our results.

We also need,

$$\frac{1}{2} \left(\frac{\partial^m}{\partial \zeta^m} + \frac{\partial^m}{\partial \eta^m} \right) r^l P_l(\mu) = \frac{1}{2^m} r^{l-m} P_{l-m}^m(\mu) \cos(m\phi). \quad (7.6)$$

We suppress the subscript (1) of the appropriate angles for convenience as in Fig 7.1. We investigate the proof of these properties in a moment. First we will rewrite eqn (7.4) by changing $l \rightarrow (l - m)$ so that

$$\frac{P_{l-m}(\mu)}{r^{l-m+p}} = \sum_{s=0}^{\infty} \binom{p+s+l-m-1}{p+s-1} \frac{r'^s}{\rho^{p+s+l-m}} P_s(\cos \theta''). \quad (7.7)$$

Now by applying eqn's (7.5) and (7.6) we have

$$\frac{P_l^m(\mu)}{r^{l+p}} = \sum_{s=0}^{\infty} \binom{p+s+l-m-1}{p+s-1} \frac{r'^s}{\rho^{p+s+l-m}} P_{l-m}^m(\cos \theta''), \quad (7.8)$$

and the equation

$$\frac{P_l^m(\mu)}{r^{l+p}} = \sum_{s=m}^{\infty} \binom{p+s+l-1}{p+s+m-1} \frac{r'^s}{\rho^{p+s+l}} P_s^m(\cos \theta''), \quad (7.9)$$

thus proving the shift formula. It now remains to prove the relations eqn (7.5) and eqn (7.6). We only need to prove these relations for the case $m = 1$ as the general m case (which we don't require) follows a similar line which we will not present here.

We begin with

$$\begin{aligned} \left(\frac{\partial}{\partial x} + i \frac{\partial}{\partial y} \right) \frac{P_{l-1}(\mu)}{r^{p+l-1}} &= e^{i\phi} \left(\sin \theta \frac{\partial}{\partial r} + \frac{\cos \theta}{r} \frac{\partial}{\partial \theta} \right) \frac{P_{l-1}(\mu)}{r^{p+l-1}} \\ &= e^{i\phi} \left(-(p+l-1) \sin \theta \frac{P_{l-1}(\mu)}{r^{p+l}} + \frac{\cos \theta}{r^{p+l}} P_{l-1}'(\mu) \right), \end{aligned} \quad (7.10)$$

where we have defined $x = x_1$ and $y = x_2$ as above and use is made of the properties of the gradient operator in the invariant subspace. Recalling the definition of the p -Legendre polynomials: $P_l^1(\mu) = -\sin(\theta) P_l'(\mu)$, where the prime denotes derivative with respect to μ , we now have

$$\left(\frac{\partial}{\partial x} + i \frac{\partial}{\partial y} \right) \frac{P_{l-1}(\mu)}{r^{p+l-1}} = -\frac{e^{i\phi} \sin \theta}{r^{l+p}} \left[(p+l-1) P_{l-1}(\mu) + \mu P_{l-1}'(\mu) \right]. \quad (7.11)$$

Now from the generating function of our p -Legendre polynomials:

$$G(l, \mu) = \frac{1}{(1 - 2\mu t + t^2)^{p/2}} = \sum_0^{\infty} P_l(\mu) t^l, \quad (7.12)$$

we can derive numerous properties. Amongst them is the p -Legendre differential equation

$$(1 - \mu^2)P_l'' - (p + 1)\mu P_l' + l(l + p)P_l = 0, \quad (7.13)$$

and the relation

$$P_l' = (p + l - 1)P_{l-1} + \mu P_{l-1}', \quad (7.14)$$

where we have suppressed the arguments of the Legendre functions for convenience.

Using the latter relation in eqn (7.11) we finally obtain

$$\left(\frac{\partial}{\partial x} + i \frac{\partial}{\partial y} \right) \frac{P_{l-1}(\mu)}{r^{p+l-1}} = \frac{e^{i\phi} P_l^1(\mu)}{r^{l+p}}. \quad (7.15)$$

The extension of this theorem to $m > 1$ uses the same techniques. A final comment here is that our results are obviously connected with properties of the orthogonal group $O(p + 2)$ and that there may be shorter derivations than those presented here which use group theory methods.

7.3 Appendix C: Perpendicular flux formula

In this appendix we demonstrate that the flux formula can be deduced for any arbitrary perpendicular direction of the field. For this purpose, we will choose another perpendicular axis for the field. Since we have previously dealt with the axis $x_{(1)}$, let us now consider $x_{(2)}$. Thereafter the general result for $x_{(n)}$, where $n = 3, 4, \dots, (d - 1)$, can be obtained likewise.

For a perpendicular field in the $x_{(2)}$ -direction we now have the form

$$\Phi^{(i)} = E_0 x_{(2)} + \sum_{n=1}^{\infty} E_0 d_n \left(\frac{r_1}{a_1} \right)^n P_n^1(\cos \theta_{(1)}) \sin \theta_{(2)} \cos \theta_{(3)}, \quad (7.16)$$

where all angles and other quantities that refer to sphere 1 have their subscripts suppressed for convenience. We also suppress the arguments for the Legendre functions.

Now the gradient of this potential again looks like:

$$\begin{aligned}
\nabla\Phi^{(1)} = & E_0\hat{x}_{(2)} + \sum_{n=1}^{\infty} E_0d_n \left(\frac{nr_1^{n-1}}{a_1^n} \right) P_n^1(\cos\theta_{(1)}) \sin\theta_{(2)} \cos\theta_{(3)} \hat{r} \\
& + \sum_{n=1}^{\infty} E_0d_n \left(\frac{r_1^{n-1}}{a_1^n} \right) \frac{\partial P_n^1(\cos\theta_{(1)})}{\partial\theta_{(1)}} \sin\theta_{(2)} \cos\theta_{(3)} \hat{\theta}_{(1)} \\
& + \sum_{n=1}^{\infty} E_0d_n \left(\frac{r_1^{n-1}}{a_1^n} \right) P_n^1(\cos\theta_{(1)}) \frac{\cos\theta_{(2)} \cos\theta_{(3)}}{\sin\theta_{(1)}} \hat{\theta}_{(2)} \\
& - \sum_{n=1}^{\infty} E_0d_n \left(\frac{r_1^{n-1}}{a_1^n} \right) P_n^1(\cos\theta_{(1)}) \frac{\sin\theta_{(3)}}{\sin\theta_{(1)}} \hat{\theta}_{(3)}. \quad (7.17)
\end{aligned}$$

Once again the integral $\int dV$ projects out only the $\hat{x}_{(2)}$ terms and we have

$$\begin{aligned}
\int \nabla\Phi^{(1)} dV = & \frac{\omega_p a_i^d}{d} E_0\hat{x}_{(2)} + \int \sum_{n=1}^{\infty} E_0d_n^{(i)} \left(\frac{nr_i^{n-1}}{a_i^n} \right) P_n^1 \sin\theta_{(1)} \sin^2\theta_{(2)} \cos^2\theta_{(3)} dV \hat{x}_{(2)} \\
& + \int \sum_{n=1}^{\infty} E_0d_n^{(i)} \left(\frac{r_i^{n-1}}{a_i^n} \right) \frac{\partial P_n^1}{\partial\theta_{(1)}} \cos\theta_{(1)} \sin^2\theta_{(2)} \cos^2\theta_{(3)} dV \hat{x}_{(2)} \\
& + \int \sum_{n=1}^{\infty} E_0d_n^{(i)} \left(\frac{r_i^{n-1}}{a_i^n} \right) \frac{P_n^1}{\sin\theta_{(1)}} \cos^2\theta_{(2)} \cos^2\theta_{(3)} dV \hat{x}_{(2)} \\
& + \int \sum_{n=1}^{\infty} E_0d_n^{(i)} \left(\frac{r_i^{n-1}}{a_i^n} \right) \frac{P_n^1}{\sin\theta_{(1)}} \sin^2\theta_{(3)} dV \hat{x}_{(2)}. \quad (7.18)
\end{aligned}$$

We have to perform the $\theta_{(2)}$ and $\theta_{(3)}$ integrals at this stage. We use the formulae

$$\int \sin^p\theta_{(3)} d\theta_{(3)} = \frac{(p-1)}{p} \int \sin^{p-2}\theta_{(3)} d\theta_{(3)}, \quad (7.19)$$

and

$$\int \sin^{p-2}\theta_{(3)} \cos^2\theta_{(3)} d\theta_{(3)} = \frac{1}{p} \int \sin^{p-2}\theta_{(3)} d\theta_{(3)}. \quad (7.20)$$

Reabsorbing the integrals over $\theta_{(3)}$ back into dV we find the form:

$$\begin{aligned}
\int \nabla\Phi^{(1)} dV = & v^d E_0\hat{x}_{(2)} + \frac{1}{p} \int \sum_{n=1}^{\infty} E_0d_n \left(\frac{nr_1^{n-1}}{a_1^n} \right) P_n^1(\sin\theta_{(1)}) \sin^2\theta_{(2)} dV \hat{x}_{(2)} \\
& + \frac{1}{p} \int \sum_{n=1}^{\infty} E_0d_n \left(\frac{r_1^{n-1}}{a_1^n} \right) \frac{\partial P_n^1}{\partial\theta_{(1)}} \cos\theta_{(1)} \sin^2\theta_{(2)} dV \hat{x}_{(2)} \\
& + \frac{1}{p} \int \sum_{n=1}^{\infty} E_0d_n \left(\frac{r_1^{n-1}}{a_1^n} \right) \frac{P_n^1}{\sin\theta_{(1)}} \cos^2\theta_{(2)} dV \hat{x}_{(2)} \\
& + \frac{p-1}{p} \int \sum_{n=1}^{\infty} E_0d_n \left(\frac{r_1^{n-1}}{a_1^n} \right) \frac{P_n^1}{\sin\theta_{(1)}} dV \hat{x}_{(2)}. \quad (7.21)
\end{aligned}$$

Now in the case of the θ_2 integrals we have

$$\int \nabla\Phi^{(1)} dV = v^d E_0\hat{x}_{(2)} + \frac{1}{p+1} \int \sum_{n=1}^{\infty} E_0d_n \left(\frac{nr_1^{n-1}}{a_1^n} \right) P_n^1(\sin\theta_{(1)}) dV \hat{x}_{(2)}$$

$$\begin{aligned}
& + \frac{1}{p+1} \int \sum_{n=1}^{\infty} E_0 d_n \left(\frac{r_1^{n-1}}{a_1^n} \right) \frac{\partial P_n^1}{\partial \theta_{(1)}} \cos \theta_{(1)} dV \hat{x}_{(2)} \\
& + \frac{1}{p(p+1)} \int \sum_{n=1}^{\infty} E_0 d_n \left(\frac{r_1^{n-1}}{a_1^n} \right) \frac{P_n^1}{\sin \theta_{(1)}} dV \hat{x}_{(2)} \\
& + \frac{p-1}{p} \int \sum_{n=1}^{\infty} E_0 d_n \left(\frac{r_1^{n-1}}{a_1^n} \right) \frac{P_n^1}{\sin \theta_{(1)}} dV \hat{x}_{(2)}. \quad (7.22)
\end{aligned}$$

We can see that this reduction process will carry through in a similar way for any arbitrary perpendicular direction $x_{(n)}$, where $n = 3, 4, \dots, (d-1)$. This completes the proof.

7.4 Appendix D: Neumann image theory in d dimensions

We begin by considering the electrostatic potential in a d -dimensional space. In the geometrical configuration of Fig 7.2, remembering that $p = d - 2$, this is given by the expression

$$\frac{1}{|r'|^p} = \frac{1}{(r'^2 - 2ar \cos \theta + a^2)^{p/2}}. \quad (7.23)$$

Upon using the generating function for the Gegenbauer polynomials, C_n^p , defined by

$$\frac{1}{(1 - 2xt + t^2)^p} = \sum_{n=0}^{\infty} t^n C_n^p(x), \quad (7.24)$$

and eqn (7.23) can be written for the case $r > a$ as

$$\frac{1}{(r'^2 - 2ar \cos \theta + a^2)^{p/2}} = \frac{1}{r^p} \sum_{n=0}^{\infty} \left(\frac{a}{r} \right)^n C_n^{p/2}(\cos \theta), \quad (7.25)$$

or for the case $r < a$ as

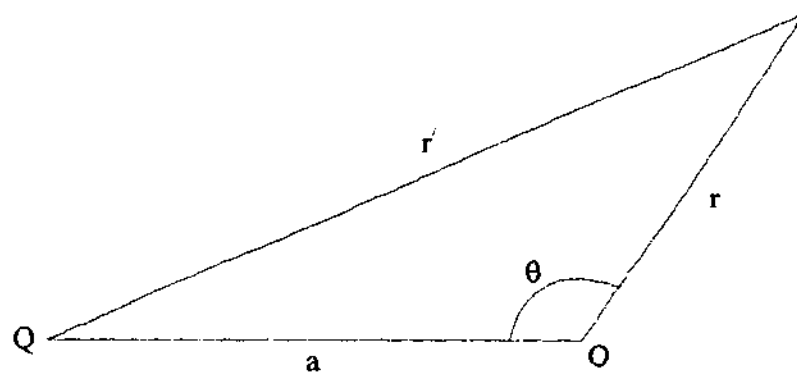
$$\frac{1}{(r'^2 - 2ar \cos \theta + a^2)^{p/2}} = \frac{1}{a^p} \sum_{n=0}^{\infty} \left(\frac{r}{a} \right)^n C_n^{p/2}(\cos \theta), \quad (7.26)$$

Thereafter, following Stratton (1941), we have for the potential inside a dielectric sphere in d dimensions due to a point charge

$$\phi^-(r, \theta) = \sum_{n=0}^{\infty} a_n r^n C_n^{p/2}(\cos \theta), \quad (7.27)$$

or for the potential outside

$$\phi^+(r, \theta) = \frac{Q}{\epsilon_0 r_2^p} + \sum_{n=0}^{\infty} b_n \frac{1}{r^{n+p}} C_n^{p/2}(\cos \theta). \quad (7.28)$$

Figure 7.2: The electrostatic potential in d -dimensions.

Upon using the standard boundary conditions

$$\begin{aligned}\phi^+(r, \theta) &= \phi^- \\ \epsilon_0 \frac{\partial \phi^+}{\partial r} &= \epsilon_1 \frac{\partial \phi^-}{\partial r},\end{aligned}\quad (7.29)$$

at the surface of the sphere $r = r_1$ and noting that

$$\frac{Q}{\epsilon_0 r_2^p} = \frac{Q}{\zeta^p} \sum_{n=0}^{\infty} \left(\frac{r}{\zeta}\right)^n C_n^p(\cos \theta), \quad (7.30)$$

where ζ is the distance of the charge from the centre of the sphere O , we easily obtain

$$a_n = \frac{Q}{\zeta^{p+n}} \frac{2n+p}{\epsilon_1 n + \epsilon_0(n+p)}, \quad (7.31)$$

and

$$b_n = \frac{Q n r_1^{2n+p}}{\epsilon_0 \zeta^{p+n}} \frac{\epsilon_0 - \epsilon_1}{\epsilon_1 n + \epsilon_0(n+p)}. \quad (7.32)$$

With the definition $\epsilon_1/\epsilon_0 = \alpha$ and $\zeta = d$, as well as reverting to $r_1 = a$, these potentials become

$$\phi^-(r, \theta) = \frac{Q}{\epsilon_1} \sum_{n=0}^{\infty} \frac{\alpha(2n+p)}{(\alpha+1)n+p} \frac{r^n}{d^{n+p}} C_n^{p/2}(\cos \theta), \quad (7.33)$$

and

$$\phi^+(r, \theta) = -Q \sum_{n=0}^{\infty} \frac{(\alpha-1)n}{(\alpha+1)n+p} \frac{a^{2n+p}}{d^{n+p}} \frac{1}{r^{n+p}} C_n^{p/2}(\cos \theta). \quad (7.34)$$

We can now use Neumann's trick (Bussemer 1994), which makes use of the identity

$$\begin{aligned}\frac{1}{(\alpha+1)n+p} &= \int_0^{\infty} dy e^{-[(\alpha+1)n+p]y} \\ &= \frac{1}{(\alpha+1)} \int_0^{\infty} d\xi e^{-n\xi} e^{-p\xi/(\alpha+1)}.\end{aligned}\quad (7.35)$$

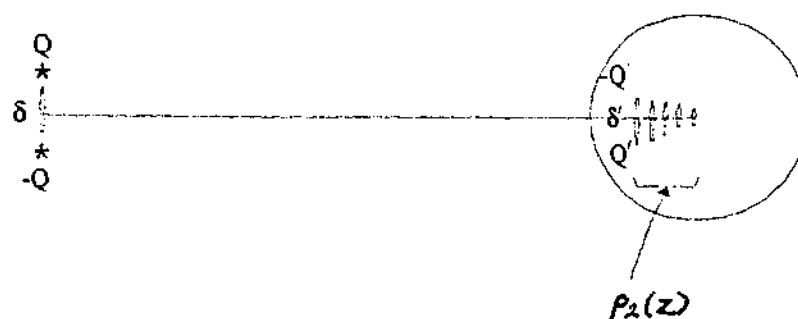


Figure 7.3: Derivation of the image set $(\mathbf{p}_2^{0\perp}, \rho_2^\perp)$.

Upon inserting this in eqn (7.34),

$$\phi^+(r, \theta) = -\frac{Q(\alpha - 1)}{(\alpha + 1)} \int_0^\infty d\xi e^{-p\xi/(\alpha+1)} \sum_{n=0}^{\infty} \frac{n}{(d d_K)^{(d/2)-1}} \left(\frac{d_K}{r}\right)^{n+p} C_n^{p/2}(\cos \theta), \quad (7.36)$$

where $d_K = a^2/d$ is the image point, and after suitable manipulations with the use of a partial integration (Bussemer 1994), the potential now becomes

$$\phi^+(r, \theta) = -\frac{Q(\alpha - 1)}{(\alpha + 1)} \left(\frac{d_K}{a}\right)^p \times \left[\frac{1}{|r - z' = d_K|^p} - \int_0^{d_K} dz' \left| \frac{1}{z'} \right|^p \left(\frac{z'}{d_K}\right)^{(d-2)/(\alpha+1)-1} \frac{d-2}{d_K(\alpha+1)} \right], \quad (7.37)$$

thereby completing the proof. We will conclude this derivation by pointing out that the limit $d \rightarrow 2$ or $p \rightarrow 0$ is in fact pathological. By suitable manipulations the electrostatic potential becomes a logarithmic function and the Gegenbauer polynomials can be shown to reduce to Chebyshev polynomials. However, all the results carry through by analytic continuation as $d \rightarrow 2$, thus the limit $p \rightarrow 0$ does not need further attention.

7.5 Appendix E: Point perpendicular dipole images

We derive the first perpendicular dipole images. We remind ourselves that from the electrostatic potential in d dimensions, the definition of a point dipole is given by $\mathbf{p}_1^\perp = Q(d-2)\delta$. Then from the geometry of Fig 7.3 we have $\delta'/\delta = b/R$. Using the result for the image point charge, the point dipole $\mathbf{p}_2^{0\perp}$ is derived:

$$\begin{aligned} \mathbf{p}_2^{0\perp} &= -Q \left(\frac{\alpha - 1}{\alpha + 1}\right) \left(\frac{a}{R}\right)^{d-2} (d-2)\delta' \\ &= -Q \left(\frac{\alpha - 1}{\alpha + 1}\right) \left(\frac{a}{R}\right)^{d-2} (d-2)\delta \frac{b_1}{R}, \end{aligned} \quad (7.38)$$

as required. In the same way as above, we can consider the two line image charges as forming a line dipole. The density of the line dipole is

$$\begin{aligned} \rho_2^\perp(z) &= \frac{Q}{a} \left(\frac{a}{R}\right)^{d-3} (d-2) \frac{\alpha-1}{(\alpha+1)^2} \left(\frac{z}{b_1}\right)^{(d-3-\alpha)/(\alpha+1)} \left(\frac{z}{R}\right) (d-2)\delta \\ &= \frac{p_1^\perp}{a} \left(\frac{a}{R}\right)^{d-1} (d-2) \frac{\alpha-1}{(\alpha+1)^2} \left(\frac{z}{b_1}\right)^{(d-2)/(\alpha+1)}, \end{aligned} \quad (7.39)$$

as required. We note that in the perpendicular configuration, the images are simple and charge neutrality is obvious from the geometrical structure. This is not the case for the parallel configuration which we will next examine.

7.6 Appendix F: Point parallel dipole images

A cursory examination of the geometrical configuration for the parallel case using our knowledge of Neumann images shows that there are several parts to consider. We begin by noting that from the binomial expansion of the electrostatic potential,

$$\left(\frac{1}{R+\delta}\right)^{d-2} \approx \frac{1}{R^{d-2}} \left[1 - (d-2)\frac{\delta}{R}\right]. \quad (7.40)$$

We have a residual image point charge at the image point given by

$$\begin{aligned} Q' &= -Q \left(\frac{\alpha-1}{\alpha+1}\right) \left(\frac{a}{R}\right)^{d-2} (d-2) \frac{\delta}{R} \\ &= -\frac{p_1^\parallel}{a} \left(\frac{\alpha-1}{\alpha+1}\right) \left(\frac{a}{R}\right)^{d-1}, \end{aligned} \quad (7.41)$$

with the last line following from the definition of the point dipole. Now the dipole length,

$$\delta' = \frac{a^2}{R} - \frac{a^2}{R+\delta} \approx \delta \frac{a^2}{R} \quad (7.42)$$

so that the point dipole image is given by

$$\begin{aligned} p_2^{0\parallel} &= Q \left(\frac{\alpha-1}{\alpha+1}\right) \left(\frac{a}{R}\right)^{d-2} (d-2)\delta' \\ &= Q \left(\frac{\alpha-1}{\alpha+1}\right) \left(\frac{a}{R}\right)^{d-2} (d-2)\delta \frac{b_1}{R}, \end{aligned} \quad (7.43)$$

which gives us the required result. Now we look at the line charges and we find that the R dependence goes as $R^{((d-2)\alpha)/(\alpha+1)}$, whereupon by the binomial expansion

$$\left(\frac{1}{R+\delta}\right)^{((d-2)\alpha)/(\alpha+1)} \approx \frac{1}{R^{((d-2)\alpha)/(\alpha+1)}} \left[1 - (d-2)\frac{\alpha}{\alpha+1} \frac{\delta}{R}\right]. \quad (7.44)$$

Thus we find the expected net line charge density as required. Finally, in view of the charge density, there is now an infinitesimal region of non-overlap of opposite charges given by the integral

$$\begin{aligned}
 Q'' &= \int_b^{b-\delta(a/R)^2} \frac{Q}{a} \left(\frac{a}{R}\right)^{d-3} (d-2) \frac{\alpha-1}{(\alpha+1)^2} \left(\frac{z}{b}\right)^{(d-3-\alpha)/(\alpha+1)} dz \frac{b}{b} \\
 &= \frac{p_1}{a} \left(\frac{a}{R}\right)^{d-1} \frac{\alpha-1}{(\alpha+1)^2}. \quad (7.45)
 \end{aligned}$$

Combining eqns (7.41) and (7.45), we are now left with a point charge as expected.

CHAPTER 8

Publications and References

PUBLICATIONS

- (1) Dipole tip model investigation of resonance effects in Scanning Tunneling Microscopy

T.M. Kalotas, A.R. Lee, J. Liesegang and A. Alexopoulos. Appl. Phys. Lett., 69 1710 (1996).

- (2) Dielectric function for a material containing hyperspherical inclusions to $O(c^2)$ -I. Multipole expansions

T.C. Choy, A. Alexopoulos, and M.F. Thorpe Proc. R. Soc. Lond. A, 454 1973 (1998)

- (3) Dielectric function for a material containing hyperspherical inclusions to $O(c^2)$ - II. Method of images

T.C. Choy, A. Alexopoulos, and M.F. Thorpe Proc. R. Soc. Lond. A, 454 1993 (1998)

- (4) Method of images in the determination of the dielectric properties of composite materials to $O(c^2)$

A. Alexopoulos, T.C. Choy, and M.F. Thorpe Proceedings of the 22nd ANZIP Condensed Matter Physics Meeting, (1998)

- (5) Dielectric properties of composite materials to $O(c^2)$ -Multipole moments method

T.C. Choy, A. Alexopoulos, and M.F. Thorpe Proceedings of the American Physical Society, Vol. 43, No. 1, 1-1048 (1998)

- (6) Dielectric properties of composite materials to $O(c^2)$ -Method of images

A. Alexopoulos, T.C. Choy, and M.F. Thorpe Proceedings of the American Physical Society, Vol. 43, No. 1, 1-1048 (1998)

(7) Second order interactions in a medium containing perfect-conducting hyperspherical inclusions

A. Alexopoulos, J. Phys. A: Math. Gen., 37, 11911-11933, (2004)

(8) I-V model of a two terminal device at the atomic level

A. Alexopoulos, IEEE Trans. Elect. Devices, in print, (2004)

References

- [1] Alexopoulos A., *J. Phys. A: Math. Gen.*, **37**, 11911-11933, (2004).
- [2] Arthurs A.M., *Complementary variational principles*. Second edition, Oxford, Clarendon Press (1980).
- [3] Ashcroft N. and Mermin N.D. *Solid State Physics*, 539-542.
- [4] Batchelor, G.K., *J. Fluid Mech.*, **52**, 245-268, (1972).
- [5] Batchelor, G.K., *A Rev. Fluid Mech.*, **6**, 227-255, (1974).
- [6] Batchelor, G.K., *J. Fluid Mech.*, **83**, 97-117, (1977).
- [7] Batchelor, G.K. and Green, J.T. *J. Fluid Mech.*, **56**, 201-427, (1972).
- [8] Batchelor G.K. and O'Brien R.W., *Proc. R. Soc.*, **A355**, 313, (1977).
- [9] Bedeaux, D. *J. Colloid Interface Sci.* **118(1)**, 80-6, (1987).
- [10] Benfatto, G. and Gallavotti, G., *Renormalisation group*, Physics Notes, (ed. P.W. Anderson, A.S. Wightman and S.B. Treiman). Princeton, NJ, Princeton University Press, (1995).
- [11] Bergman D.J., *Phys. Rev.* **B14**, 1531-42, (1976).
- [12] Bergman D.J., *Physics Report* **43** (9), 377-407, (1978).
- [13] Bergman D.J. and Stroud D., *Phys. Rev.* **B22(6)**, 3527-39, (1980).
- [14] Berryman J.G. in: *Elastic Wave Scattering and Propagation*, edited by Varadan V.K. and Varadan V.V., Ann Arbor Science, Michigan, pp 111-129, (1982)

- [15] Binns K.J., Lawrenson P.J., *Electric and magnetic field problems* . pp. 48-53, Oxford: Pergamon (1973).
- [16] Böttcher C.J.F., *Theory of electric polarisation*. Amsterdam, Elsevier (1952).
- [17] Böttcher C.J.F. and Bordewijk P., *Theory of Elastic Polarization* , Elsevier, New York, pp 476-491, (1978).
- [18] Bowman, J.J., Senior, T.B.A., and Uslenghi P.L.E. , *Electromagnetic scattering by simple shapes* . New York, Hemisphere, (1987).
- [19] Bragg W.L. and Pippard A.B., *Acta. Cryst.* 6, 865-7, (1953).
- [20] Brown Jr W.F., *J. Chem. Phys.* , 23 (8), 1514-17, (1955)
- [21] Bruggeman D.A.G., *Ann. Phys.* , 24, 636-679, (1935).
- [22] Brunning J.H. and Lo Y.T., *IEEE Trans. Antennas Propag.*, AP-19(3), 378-400, (1971).
- [23] Budiansky B., *J. Mech. Phys. Solids*, 13, 223-227, (1965)
- [24] Burkhart, T.W. and van Leeuwen, J.M.J., *Real space renormalisation*. Berlin, Springer-Verlag, (1982).
- [25] Bussemer P., *Am. J. Phys.* , 62, 657-658, (1994).
- [26] Chew W.C., Friedrich J.A. and Geiger R. , *IEEE Trans. Geosci. Remote Sensing* . 28(2), 207-14, (1990).
- [27] Choudhury N. and Ghosh S.K., *J. Chem. Phys.*, 110, p 8628, (1999)
- [28] Choy T.C. and Stoneham A.M., *J. Phys. Cond. Matter* 2, 939-51, (1990).
- [29] Choy T.C., *Physica A*221, 263-76, (1995).
- [30] Choy T.C., *Phys. Rev.* B55 (13), 16-20, (1997).

- [31] Choy T.C., Alexopoulos A. and Thorpe M.F. , Proc. R. Soc. Lond. A454, 1973-92, (1998a).
- [32] Choy T.C., Alexopoulos A. and Thorpe M.F. , Proc. R. Soc. Lond. A454, 1993-2013, (1998b).
- [33] Choy T.C., *Effective Medium Theory: Principles and Applications* , Clarendon Press, Oxford, (1999).
- [34] Cohen R.W., Cody G.D., Coutts M.D. and Abeles B., Phys. Rev.B8, 3689-701, (1973).
- [35] Cooper D.E., Wang D.S. and Kerker M., *Appl. Opt.*, **22**, 83-94, (1983).
- [36] Cruz L., Fonseca L.F. and Gomez M., *Phys. Rev. B*, **40**, 7491-7500, (1989).
- [37] Danos, M. and Maximon, L.C., *J. Math. Phys.* , **6**(5), 766-78, (1965).
- [38] Davidson A. and Tinkham M., Phys. Rev.B13, 3261-67, (1976).
- [39] Davis M.H., *Q. J. Mech. App. Math.* **17**, part 4, 499-511, (1964).
- [40] Debye, P., *Ann, Phys.* , Leipzig **30**, 59-62, (1909).
- [41] deGennes P.G., *Rev. Mod. Phys.*, **64**, p 645, (1992)
- [42] deGennes P.G., *Rev. Mod. Phys.*, **71**, p 5374, (1999)
- [43] den Hertog B.C. and Choy T.C., *J. Phys.: Condens. Matter* , **7**, 19-28, (1995).
- [44] Djordjević B.R., Hetherington J.H. and Thorpe M.F., Phys. Rev. B53(22), 14862-71, (1996).
- [45] Duraiswami R. and Prosperetti R., *J. Fluid Mech.*, **299**, pp. 187-215, (1995).
- [46] Einstein, A., *A. Phys.* , **19**, 289-306, (1906).
- [47] Elliot J.A., Krumhansl, J.A. and Leath P.L., *Rev. Mod. Phys.* **46**(3), 465-542, (1974).

- [48] Epton M.A. and Dembart B., *SIAM J. Sci. Comput.*, **4**, 865-897, (1995).
- [49] Erdélyi, A., *Higher order transcendental functions*, vol. 2, pp. 232-261, New York: McGraw-Hill, (1953).
- [50] Felderhof B.U., Ford G.W., and Cohen E.G.D., *J. Stat. Phys.* **28**, 649-672, (1982).
- [51] Gao L., Wan J.T.K., Yu K.W. and Li Z.Y., Karttunen M., Yu K.W., Dong L. and Gu G. Q., *Phys. Rev. E*, **61**(5), 6011-6014, (2000).
- [52] Gaunard G.C. and Huang H., *J. Acoust Soc. Am.*, **96**, 2526-2536, (1994).
- [53] Gaunard G.C., Huang H. and Strifors H., *J. Acoust Soc. Am.*, **98**(1), 495-507, (1995).
- [54] Gradshteyn I.S. and Ryzhik I.M., *Tables of integrals, series and products*, pp. 56-70, New York: Academic, (1980).
- [55] Gubernatis J.E. and Krumhansl J.A., *J. Appl. Phys.*, **46**, 1875-1883, (1975)
- [56] Gumerov N.A., Ivandaev A.L., and Nigmatulin R.I., *J. Fluid Mech.*, **193**, pp. 53-74, (1988).
- [57] Hadjipanayis G.C. and Siegel R.W., editors, *Nanophase materials: synthesis, properties, applications*. New York, Kluwer Academic Publishers, (1994).
- [58] Harker A.H. and Temple J.A.G., *J. Phys. D: Appl. Phys.*, **21**, 1576-88, (1988).
- [59] Hashin Z, Shtrikman S. and Franklin J., *Inst.*, **271**, 336-341, (1961)
- [60] Hashin Z. and Shtrikman S., *J. Appl. Phys.*, **33** (10), 3125-31, (1962a).
- [61] Hashin Z. and Shtrikman S., *J. Mech. Phys. Solids*, **10**, 343-52, (1962b).
- [62] Hashin Z. and Shtrikman S., *J. Mech. Phys. Solids*, **11** (10), 127-40, (1962c).
- [63] Hashin Z., *J. Composite Materials* **2**(3), 284-300, (1968).

- [64] Henderson D. (ed.), *Fundamentals of inhomogeneous fluids*, New York, Marcel Dekker, p 5374, (1992)
- [65] Hill R., *J. Mech. Phys. Solids*, **13**, 213-222, (1965).
- [66] Hobson E.W., *Spherical and ellipsoidal harmonics*. Cambridge University Press, (1931).
- [67] Huang J.P., Karttunen M., Yu K.W., Dong L. and Gu G. Q., *Phys. Rev. E*, **69**, 1539, (2004).
- [68] Huang J.P., Yu K.W. and Gu G.Q., *Phys. Rev. E*, **65**, 1063, (2002).
- [69] Hochstadt H., *The functions of mathematical physics*. pp. 168-189, New York: Wiley Interscience, (1971).
- [70] Iskander M.F., Lakhtakia A. and Durney C.H., *Proc. IEEE*, **70**, 1361-1362, (1982).
- [71] Iskander M.F., Lakhtakia A. and Durney C.H., *IEEE Trans. Anten. Propag.*, **AP-31**, 317-324, (1983).
- [72] Iskander M.F. and Lakhtakia A., *appl. Opt.*, **23**, 948-953, (1984).
- [73] Iskander M.F., Olsen S.C., Benner R.E. and Yoshida D., *Appl. Opt.*, **25**, 2514-2520, (1986).
- [74] Jackson J. D., *Classical Electrodynamics*. New York, Wiley, (1975).
- [75] Jeffrey., D.J., *Proc. R. Soc. Lond.* **A335**, 355-367, (1973).
- [76] Jeffrey D.J. and Onishi Y., *Proc. R. Soc. Lond.*, **A13**, 2847, (1980).
- [77] Jeffrey, G.B., *Proc. R. Soc. Lond.* **A87**, 109-120, (1912).
- [78] Kaelin B. and Johnson L.R., *J. Appl. Phys.*, **84**, 5451-5457, (1998a)
- [79] Kaelin B. and Johnson L.R., *J. Appl. Phys.*, **84**, 5458-5468, (1998b)

- [80] Kalotas T.M., Lee A.R., Liesegang J. and Alexopoulos A., *Appl. Phys. Lett.* **69**, 1710, (1996).
- [81] Kaplan T., Leath P.L., Gray L.J. and Diehl H.W., *Phys. Rev.* **B21**(10), 4230-46, (1980).
- [82] Kelvin Lord, 1884 Reprint of paper on electrostatics and magnetism, 2nd edn, pp. 52-85, London: Macmillan, (1848).
- [83] Kerker M., Cooke D., Chew H. and MacNulty P., *J. Opt. Soc. Am.*, **68**, 592-601, (1978)
- [84] Khinchin A.I., *Mathematical Foundations of Statistical Mechanics*. New York, Dover, (1949).
- [85] Kinoshita N. and Mura T., *Phys. Status. Solidi.*, 759-68, (1971).
- [86] Kohn W. and Sham L.J., *Phys. Rev.*, **140**, p A1133, (1965)
- [87] Kong J.A., *Electromagnetic Wave Theory*, John Wiley and Sons, New York, pp 557-563, (1986)
- [88] Korringa R., Brown J.S., Thompson D.D. and Runge R.J., *J. Geophys. Res.*, **84**, 5591-5598, (1979)
- [89] Kirkpatrick S., *Phys. Rev. Lett.* **27**, 1722-25, (1971).
- [90] Kirkpatrick S., *Rev. of Mod. Phys.* **45**, 574-88, (1973).
- [91] Kittel C., *Introduction to Solid State Physics* (fourth edition). New York, Wiley, (1971).
- [92] Klingenberg D.J., van Swol F. and Zukoski C.F., *Chem. Phys.*, **94**, 6170, (1990).
- [93] Koc S., Song J. and Chew W.C., *SIAM J. Numer. Anal.*, **36**, 906-921, (1999).
- [94] Kohn W. and Rostocker N., *Phys. Rev.*, **94**, 1111-1120, (1954).
- [95] Kong J.A., *Electromagnetic wave theory*. New York, Wiley, (1990).

- [96] Kristensson G. and Stroem S., *Radio Sci.*, **17**, 903-912, (1982).
- [97] Lakhtakia A., Varadan V.K. and Varadan V.V., *Appl. Opt.*, **24**, 4146-4154, (1985).
- [98] Lakhtakia A., *Optik*, **86**, 155-161, (1991).
- [99] Landau L.D. and Lifshitz E.M. and Pitaevskii, L.P., *Electrodynamics of continuous media*. Course of Theoretical Physics, Volume 8, Oxford, Pergamon Press, (1984).
- [100] Landau L.D. and Lifshitz E.M., *Quantum Mechanics (non relativistic theory)* third edition, Course of Theoretical Physics, Volume 3, Oxford, Pergamon Press, (1991).
- [101] Landauer R., *Electrical conductivity in inhomogeneous media* in Electrical transport and optical properties of inhomogeneous media (Ohio State University, 1977), AIP Conference Proceedings no. 40, pg 2-45, American Institute of Physics, New York (1978).
- [102] Langevin P., *J. Phys (4)* , (4), 678 (1905).
- [103] Lebedev N.N., Skalskaya I.P. and Uflyand Y.S., *Worked problems in applied mathematics* , New York, Dover, pp 242, (1965).
- [104] Lo C.K., Wan J.T.K. and Yu K.W., *Comp. Phys. Comm.*, **142**, 453-456, (2001).
- [105] Lei, L., Wan, J.T.K., Yu, K.W., Sun, H., *Phys. Rev. E* , **Vol63**, 12903, (2001).
- [106] Lindell I.V., *Am. J. Phys.* , **61**, 39-44, (1993).
- [107] Lorentz H.A., *Theory of Electrons* (reprint). New York, Dover, (1952).
- [108] Love, J.D., *Phil. Mag.* , **28**, 449, (1975).
- [109] Ma S.K., *Phys. Rev. Lett.* , **37**, 461-74, (1976).

- [110] Ma Y., Varadan V.V., Varadan V.K., *Appl. Opt.*, **27**, 2469-2477, (1988).
- [111] Mackowski, D.W., *Proc. Roy. Soc. Lond.*, **A433**, 599-603, (1991).
- [112] McLachlan D.S., Priou A., Chenerie I., Issac E. and Henry F., *J. EM Waves and Applications*, **9**, 1099-1131, (1992).
- [113] Manning R.M., *Stochastic Electromagnetic Image Propagation and Adaptive Compensation*. New York, McGrawHill, (1993).
- [114] Marnevsckaya L.A., *Sov. Phys. Acoust.*, **14(3)**, 356-360, (1969).
- [115] Maxwell, J.C., *Electricity and magnetism*. 1st edn, Oxford: Clarendon, (1873).
- [116] Mie, G., *Ann, Phys.*, Leipzig **25**, 377-81, (1908).
- [117] Mills R. and Ratanavararaksa P., *Phys. Rev.* **B18(10)**, 5291-308, (1978).
- [118] Milton G.W., *The Theory of Composites*, Chapter 7, Cambridge University Press, Cambridge, (2002).
- [119] Milton G.W., *Comm. Math. Phys.*, **99**, 463-500, (1985).
- [120] Mishchenko M.I., *J. Opt. Soc. Am. A*, **8**, 871-882, (1991).
- [121] Mishchenko M.I. and Travis L.D., *Opt. Comm.*, **109**, 16-21, (1994).
- [122] Mishchenko M.I. and Mackowski D.W., *Opt. Lett.*, **19**, 1604-1606, (1994).
- [123] Mishchenko M.I., Travis L.D. and Mackowski D.W., *T-matrix computation of light scattering by large nonspherical particles: recent advances in pasive infrared remote sensing of clouds and the atmosphere*. Ed. by Lynch D.K., *SPIE*, **2309**, 72-83, (1994).
- [124] Mishchenko M.I., Mackowski D.W. and Travis L.D., *Appl. Opt.*, **34**, 4589-4599, (1995).

- [125] Mishchenko M.I., Travis L.D. and Mackowski D.W., *J. Quant. Spectrosc. Radiat. Transf.*, **55**, 535-575, (1996).
- [126] Mishchenko M.I., Hovenier J.W. and Travis L.D. (editors), *Light scattering by nonspherical particles: theory, measurements, and applications*, San Diego, Academic Press, (2000).
- [127] Moon P.W., *Field Theory Handbook*. Berlin, Springer Verlag, (1986).
- [128] Moons P. and Spencer D.E., *Field theory handbook: including coordinate systems, differential equations and their solutions*. Springer, Berlin, (1988).
- [129] Morse P.M. and Feshbach H., *Methods of theoretical physics, vol 1*. New York: McGraw-Hill, (1953).
- [130] Moussiaux A. and Ronveaux J, *J. Phys.*, **A12**, 423, (1979).
- [131] Neumann C., *Hydrodynamische Untersuchungen nebst einem Anhang uber die Probleme der Elektrostatik und der magnetischen Induktion*, pp. 279-282, Leipzig: Teubner, (1883).
- [132] N'yuton R., *Mir*, Translated from Russian using Worldlingo: www.worldlingo.com, (1969).
- [133] Nickel B.G. and Butler W.H., *Phys. Rev. Lett.* **30**, 373-403, (1973).
- [134] O'Meara D.J. and Saville D.A., *Q. J. Mech. Appl. Math.*, **34**, 9, (1981).
- [135] Osborn J.A., *Phys. Rev.* **67**, 351-6, (1945).
- [136] Papas, C.H. *Theory of Electromagnetic Wave Propagation*. New York, Dover, (1998).
- [137] Pauling L. and Wilson E.B., *Introduction to Quantum Mechanics*. New York, McGrawHill, (1935).
- [138] Peterson B. and Stroem S., *Phys. Rev. D*, **8**, 3661-3678, (1973).

- [139] Peterson B. and Milford S., *Phys. Rev. D*, **10**, 3666-3677, (1973).
- [140] Peterson B. and Stroem S., *Phys. Rev. D*, **10**, 2670-2684, (1974).
- [141] Rayleigh Lord, *Phil. Mag.* **34**, 481-502, (1892).
- [142] Reitz J.R. and Milford F.J., *Foundations of Electromagnetic Theory* (second edition). Reading Massachusetts, Addison-Wesley, (1970).
- [143] Rickayzen G. and Augousti A., *Mol. Phys.*, **52**, p 1355, (1984)
- [144] Ross D.K., *Aust. J. Phys.* **21**, 817-822, (1968).
- [145] Rouleau F., *Astron. Astrophys.* , **310**, 686-98,(1996).
- [146] Shante V.K.S. and Kirkpatrick S., *Adv. Phys.* **20**, 325-57, (1971).
- [147] Sewell M.J., *Maximum and minimum principles: a unified approach with applications*. Cambridge, Cambridge University Press, (1992).
- [148] Shiff L.I., *Quantum Mechanics*. New York, McGraw-Hill, (1949).
- [149] Siu Y.L., Wan J.T.K. and Yu K.W., *Comp. Phys. Comm.*, **142**, 446-452, (2001).
- [150] Slater J.C., *Microwave transmission*. 1st edition, pp. 269-277, 281-288. New York, McGraw-Hill, (1942).
- [151] Stariolo D.A and Cannas S.A., *Phys. Rev. B* , **60**, 3013, (1999).
- [152] Stratton, J.A., *Electromagnetic Theory*. , New York, McGraw-Hill, (1941).
- [153] Stoner E.C., *Phil. Mag.* **36**, 803-06, (1945).
- [154] Stroem S., *Phys. Rev. D*, **10**, 2685-2690, (1974).
- [155] Stroud D., *Phys. Rev. B***12**(8) , 3368-73, (1975).
- [156] Thompson W., 1884 Reprint of paper on electrostatics and magnetism, 2nd edn, pp. 52-85, London: Macmillan, (1848).

- [157] Thorpe, M.F, *Proc. Roy. Soc. Lond.* , A437, 215-227, (1992).
- [158] Torquato S., *J. Chem. Phys.* 83(9), 4776-85, (1985).
- [159] Tsang L. and Kong J.A., *J. Appl. Phys.*, 53, 7162-7173, (1982).
- [160] Tsang L. and Kong J.A., *Radio Sci.*, 18, 1260-1272, (1983).
- [161] Tsang L., and Kong J.A. and Shin R.T., *Theory of microwave remote sensing* , New York, John Wiley, (1983).
- [162] Tsang L., *Radio Sci.*, 19, 1450-1460, (1984).
- [163] Van de Hulst, H.C., *Light scattering by small particles* , New York, Dover, (reprint), (1981).
- [164] Van Vleck J.H., *Electric and Magnetic Susceptibilities*. Oxford, Oxford University Press, (1932).
- [165] Varadan V.K., Bringi V.N. and Varadan V.V., *Phys. Rev. D*, 19, 2480-2489, (1979).
- [166] Varadan U.K. and Varadan V.V., *Acoustic, Electromagnetic and Elastic Wave Scattering: Focus on the T-matrix Approach* , Pergamon, New York, (1980).
- [167] Varadan V.K., Bringi V.N. and Varadan V.V., *Radio Sci.*, 18, 321-327, (1983).
- [168] Varadan V.K., Ma Y. and Varadan V.V., *Radio Sci.*, 19, 1445-1449, (1984).
- [169] Varadan V.V., Varadan V.K., Ma Y. and Steele W.A., *Radio Sci.*, 22, 491-498, (1987).
- [170] Wan J.T.K., Gu G.Q. and Yu K.W., *Phys. Rev. E* , 63, 1063, (2001a).
- [171] Wan J.T.K., Gu G.Q. and Yu K.W., *Comp. Phys. Comm.* , 142, 457-463, (2001b).
- [172] Waterman P.C. and Truell R., *J. Math. Phys.*, 2, 512-537, (1961).

- [173] Waterman P.C., *Proc. IEEE*, **53**, 805-812, (1965).
- [174] Waterman P.C., *Alta Freq.*, **38**, 348-352, (1969).
- [175] Waterman P.C., *Phys. Rev. D*, **3**, 825-839, (1971).
- [176] Waterman P.C., *J. Appl. Phys.*, **50**, 4550-4565, (1979).
- [177] Wang D.S. and Barker P.W., *Appl. Opt.*, **18**, 1190-1197, (1979).
- [178] Wu T.T., *Int. J. Solids Structures* **2**, 1-8, (1966).
- [179] Yan C.C., *Found. of Phys.* **25**(3) , 491-502, (1995).
- [180] Wiener O., *Abh. Math. Phys. Kl. Sachs. Akad. Wiss. Leipz* , **32**, 509, (1912).
- [181] Woodside W. and Messmer J.H. *J. Appl. Phys.* **32**, 1688-99, (1961).
- [182] Yamakawa N., *Geophys. Mag.* , **31**, 63-103, (1962).
- [183] Yu K.W., Wang Y.C., Hui P.M. and Gu G. Q., *Phys. Rev.* , **B47** (4), 1782-7, (1993).
- [184] Zardecki A. and Gerstl S.A.W., *Appl. Opt.*, **26**, 3000-2004, (1987).